**T·H·E
OHIO
STATE
UNIVERSITY**

RADIATION AND SCATTERING
FROM LOADED MICROSTRIP ANTENNAS
OVER A WIDE BANDWIDTH

D.P. Forrai

E.H. Newman

The Ohio State University

ElectroScience Laboratory

Department of Electrical Engineering
Columbus, Ohio   43212

NATIONAL AERONAUTICS AND SPACE ADMINISTRATION
Langley Research Center
Hampton, Virginia 23665

NOTICES

When Government drawings, specifications, or other data are
used for any purpose other than in connection with a definitely
related Government procurement operation, the United States
Government thereby incurs no responsibility nor any obligation
whatsoever, and the fact that the Government may have formulated,
furnished, or in any way supplied the said drawings, specifications,
or other data, is not to be regarded by implication or otherwise as
in any manner licensing the holder or any other person or corporation,
or conveying any rights or permission to manufacture, use, or sell
any patented invention that may in any way be related thereto.

50272-101

REPORT DOCUMENTATION PAGE	1. REPORT NO.	2.	3. Recipient's Accession No.

4. Title and Subtitle	5. Report Date
RADIATION AND SCATTERING FROM LOADED MICROSTRIP ANTENNAS OVER A WIDE BANDWIDTH	September 1988
	6.

7. Author(s)	8. Performing Organization Rept. No
D.P. Forrai and E.H. Newman	719493-1

9. Performing Organization Name and Address	10. Project/Task/Work Unit No.
The Ohio State University ElectroScience Laboratory 1320 Kinnear Road Columbus, Ohio 43212	11. Contract(C) or Grant(G) No (C) (G) NSG-1613

12. Sponsoring Organization Name and Address	13. Type of Report & Period Covered
National Aeronautics and Space Administration Langley Research Center Hampton, Virginia 23665	Technical
	14

15. Supplementary Notes

This report was also submitted as a thesis by D.P. Forrai.

16. Abstract (Limit 200 words)

The integral equation and moment method solution is developed for two different antennas in the presence of an infinite grounded dielectric substrate. The first antenna is a rectangular microstrip patch antenna. This antenna will be analyzed for excitation by an incident plane wave in free space and a vertical filament of uniform current in the dielectric. This antenna can be loaded by a lumped impedance in a vertical filament of uniform current extending from the patch through the dielectric to the ground plane. The radar cross section of the microstrip antenna is found from the plane wave excitation and shows good agreement to measurement for both an unloaded and loaded antenna. The input impedance is found from the current filament excitation. This is compared to the measured input impedance of a coaxially fed microstrip antenna and shows good agreement for both unloaded and loaded antennas when the dielectric substrate is much less than a wavelength. The second antenna antenna is a vertical thin wire monopole extending from the ground plane into or through the dielectric substrate. The mutual impedance between two imbedded monopoles is compared to a previous calculation.

17. Document Analysis   a. Descriptors

MICROSTRIP ANTENNAS
ANTENNA RADIATION PATTERNS
MONOPOLE ANTENNAS
IMPEDANCE
BANDWIDTH

PLANE WAVES
DIELECTRIC PROP.
RADAR CROSS SECTION
WAVE EQUATIONS
METHOD OF MOMENTS
INTEGRAL EQUATIONS

b. Identifiers/Open-Ended Terms

c. COSATI Field/Group

18. Availability Statement	19. Security Class (This Report) Unclassified	21. No. of Pages 94
	20. Security Class (This Page) Unclassified	22. Price

(See ANSI-Z39.18)   See Instructions on Reverse

OPTIONAL FORM 272 (4-77)
(Formerly NTIS-35)
Department of Commerce

TABLE OF CONTENTS

iv

LIST OF FIGURES

v

CHAPTER I

INTRODUCTION

A moment method (MM) [2] solution is applied to two different antennas in the presence of a grounded dielectric substrate. A grounded dielectric substrate is a dielectric substrate of thickness T on top of an infinite ground plane. The first antenna is a microstrip antenna consisting of a perfectly conducting rectangular patch lying horizontally on top of the dielectric substrate. Figure 1 in Chapter II shows the geometry of this antenna. The problems of interest for the microstrip antenna are plane wave scattering and the input impedance when the antenna is excited by a filament of uniform current. The antenna can be loaded by a lumped impedance in a filament of uniform current. The other antenna is a perfectly conducting vertical wire, or monopole antenna, extending from the ground plane, into or through the dielectric substrate. Figure 12 in Chapter III shows the geometry of this antenna. The problems of interest are the self impedance of a monopole and the mutual impedance between two monopoles.

The MM solution for the perfectly conducting rectangular patch is begun by considering the patch to be excited by an arbitrary source with currents $(\mathbf{J}^i, \mathbf{M}^i)$ located in either the dielectric substrate or the free space region above it. The surface equivalence theorem is used to replace the patch with an unknown surface current, $\mathbf{J}^S$. The boundary condition that the total tangential electric field on the patch surface must be zero is applied to yield the integral equation for the unknown

1

surface current $\mathbf{J}^S$. The unknown surface current $\mathbf{J}^S$ is expanded into a sum of N (known) entire domain expansion functions. The MM solution determines the N coefficients in this expansion. For plane wave scattering, the patch is excited by a uniform plane wave with an incident angle of (θ_i, ϕ_i). The scattered field is the sum of the field of each basis function multiplied by the strength of that basis function. To find the input impedance, the patch is excited by a vertical filament of uniform current extending from the ground plane to the patch. The input impedance is determined from the ratio of the voltage at the feed point and the current into the feed point. The effect of the load is determined from modeling the microstrip antenna as a two port device, where the excitation represents port 1 and the load represents port 2. The current through the load is determined from the unloaded case. The load current acts as a source and is added to the unloaded excitation to obtain the loaded result.

Many papers have been written on the rectangular patch microstrip antenna. Early work by Munson [3] and Derneryd [4] modeled the microstrip antenna as a transmission line that radiates from the open ends. This model does not include higher order modes and thus is valid only near the first resonance of the patch. Lo et al. [6] and Richards et al. [7] used a cavity model. This model assumes an admittance around the open edges of the patch to form a cavity. Higher order modes are supported by a cavity model. Agrawal and Bailey [5] performed a wire grid analysis of the microstrip patch. This was one of first solutions that attempted to model the microstrip patch by the currents on the patch. Newman and Tulyathan [8] employed a MM solution similar to that for plates. Bailey and Deshpande [9,10] and Pozar [15] used the Greens function for the grounded dielectric substrate in their MM solutions and used entire domain mode functions. Pozar compared the numerical efficiency of the entire domain modes and the piecewise

2

sinusoidal modes when solving for the impedance matrix. Most of the work up to this point was primarily concerned with the behavior of the microstrip patch in a narrow band around first resonance. Newman and Forrai [14] examined the wide band scattering of the microstrip patch. An impedance matrix interpolation scheme was employed to minimize the number of times the MM impedance matrix had to be computed. This report will examine the wide band scattering and the wide band input impedance of a loaded rectangular patch microstrip antenna. It will be shown that when the antenna is loaded by a vertical filament of uniform current that contains a lumped impedance, the results closely approximate the behavior of a microstrip antenna loaded through a coaxial port.

The MM solution for the perfectly conducting vertical thin wire is begun by considering the wire to be excited by an arbitrary source with currents $(\mathbf{J}^i, \mathbf{M}^i)$. The wire is replaced by a unknown surface current $\mathbf{J}^S$. Thin wire approximations are applied to this surface current. It is modeled as a vertical or $\hat{\mathbf{z}}$ directed filament of current [17]. This current is approximated by a sum of N (known) basis functions. The MM solution determines the unknown coefficients in this expansion for excitation by the so called delta gap generator [19]. The input impedance is determined from the ratio of the excitation voltage and the current on the wire at the point of excitation. The mutual impedance is determined from the ratio of the excitation voltage on one wire to the current on the other wire.

Collin and Zucker [18] analyzed a vertical electric current element inside a two layer earth. They modeled the earth as flat and therefore their analysis is similar to that of a vertical current element inside of a grounded dielectric substrate. Pinhas and Shtrikman [22] analyzed vertical currents in the dielectric region of a grounded dielectric substrate by modeling the vertical current as a horizontal surface current. One of their primary interests with this analysis was modeling the vertical current

for a coaxially fed microstrip antenna. Chi and Alexópoulos [21] performed an analysis of a vertical wire in a grounded dielectric substrate which is similar to the one presented in this report. Their excitation was a magnetic frill current in the aperture of the coaxial feed on the ground plane. This report will use the simpler so called delta gap generator for the excitation and compare the results to theirs. It is shown that the two different excitations produce nearly identical numerical results.

Chapter II describes the derivation of the integral equation and the MM solution for the microstrip antenna. Chapter III describes the same derivations for the vertical monopole antenna in the grounded dielectric substrate. Chapter IV contains the results for plane wave scattering and input impedance of an unloaded and loaded microstrip antenna. Data from both a MM computation and measurement is presented. Chapter IV also shows the mutual impedance between two vertical monopoles in a grounded dielectric substrate. Chapter V summarizes this report.

CHAPTER II

THE INTEGRAL EQUATION AND MOMENT METHOD
SOLUTION FOR THE RECTANGULAR PATCH MICROSTRIP
ANTENNA

2.1 Introduction

This chapter will describe the integral equation and the moment method [2] (MM) solution to the problem of plane wave scattering and input impedance of a rectangular patch microstrip antenna on an infinite microstrip slab. The basic geometry of this structure is shown in Figure 1. The antenna can be excited by either a filament of uniform current extending vertically through the dielectric substrate or by an incident plane wave. A load will be modeled by an uniform vertical current with fixed impedance.

The solution is begun by using the equivalence theorem to replace the perfectly conducting patch by an unknown surface current J^S. Then, the integral equation for J^S is obtained by requiring that the total electric field tangent to the patch surface be equal to zero. Finally, the integral equation is solved using the MM.

2.2 Derivation of the Integral Equation

This section describes the use of the surface equivalence theorem to derive the integral equation for the problem of radiation or scattering by a perfectly conducting rectangular patch on an infinite dielectric substrate on top of an infinite
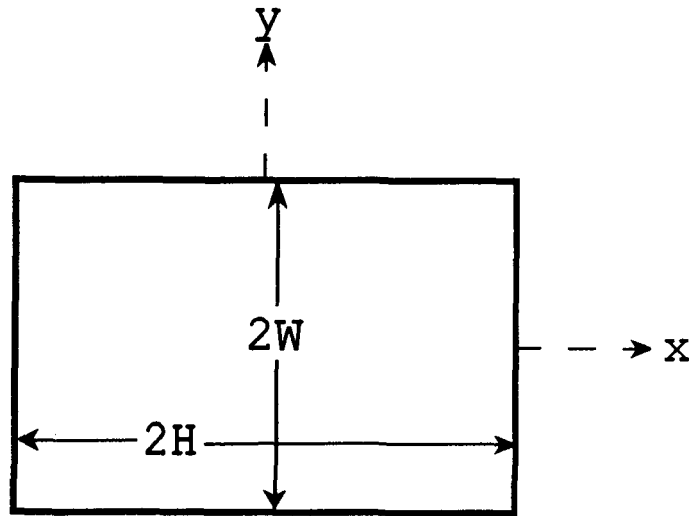
a) Top view of a perfectly conducting rectangular patch on top of a infinite dielectric slab.
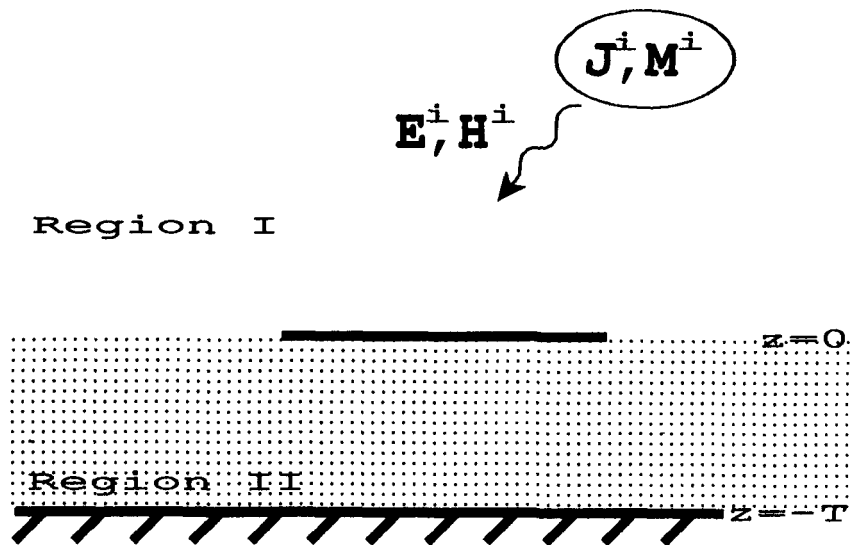
b) Side view of a perfectly conducting rectangular patch on an infinite dielectric substrate on a perfectly conducting ground plane. It is excited by an arbitrary source with electric and magnetic currents ($\mathbf{J}^i$,$\mathbf{M}^i$).

Figure 1: The basic geometry of a microstrip patch antenna.

perfectly conducting ground plane. The geometry of a dielectric substrate on top of a perfect conductor will be referred to as a grounded dielectric substrate. Figure 1 shows a perfectly conducting rectangular patch of length $2H$ in the $\hat{x}$ direction and width $2W$ in the $\hat{y}$ direction on a grounded dielectric substrate. The region above the dielectric substrate, referred to as Region I, is free space. The region inside the dielectric substrate, referred to as Region II, has a permittivity of ϵ_2, permeability of μ_0, and thickness T. The origin of the coordinate system is placed at the center of the rectangular patch. The normal to the rectangular patch surface is the $\hat{z}$ direction. An arbitrary source, which can be located in either Region I or Region II, has electric and magnetic currents $(\mathbf{J}^i, \mathbf{M}^i)$ that illuminate the patch with incident fields $(\mathbf{E}^i, \mathbf{H}^i)$. Note that $(\mathbf{E}^i, \mathbf{H}^i)$ are the fields of $(\mathbf{J}^i, \mathbf{M}^i)$ in the presence of the grounded dielectric substrate without the rectangular patch. Let $(\mathbf{E}, \mathbf{H})$ denote the electric and magnetic fields produced by $(\mathbf{J}^i, \mathbf{M}^i)$ in the presence of the grounded dielectric substrate with the rectangular patch.

Since the patch is a perfect conductor, the equivalent current on the rectangular patch surface will be

$$\mathbf{J}^S = \hat{z} \times \mathbf{H}. \tag{2.1}$$

Since the patch is infinitesimally thin, the surface current $\mathbf{J}^S$ actually represents the vector sum of the surface current on the top surface and of the surface current on the bottom surface of the patch [12]. The equivalent problem is illustrated in Figure 2. The total electric and magnetic fields in either region are

$$\mathbf{E} = \mathbf{E}^i + \mathbf{E}^S \tag{2.2}$$

$$\mathbf{H} = \mathbf{H}^i + \mathbf{H}^S \tag{2.3}$$

where $(\mathbf{E}^S, \mathbf{H}^S)$ are the fields radiated by the equivalent current $\mathbf{J}^S$ in the presence of the grounded dielectric substrate.
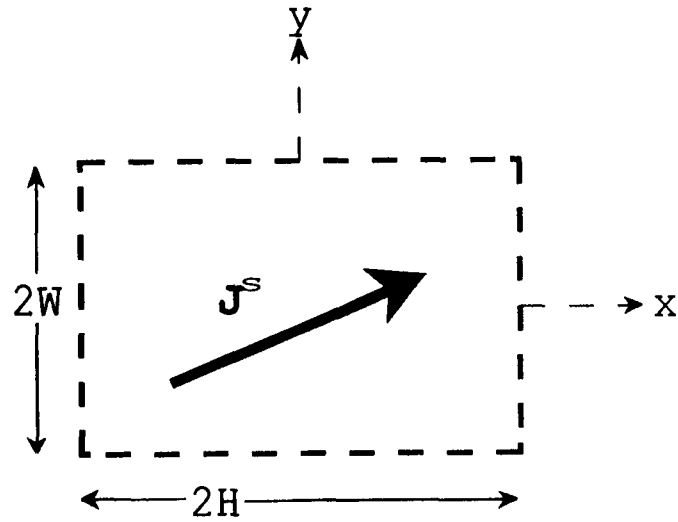
a) Top view of the equivalent surface current $\mathbf{J}^S$ replacing the perfectly conducting rectangular patch.
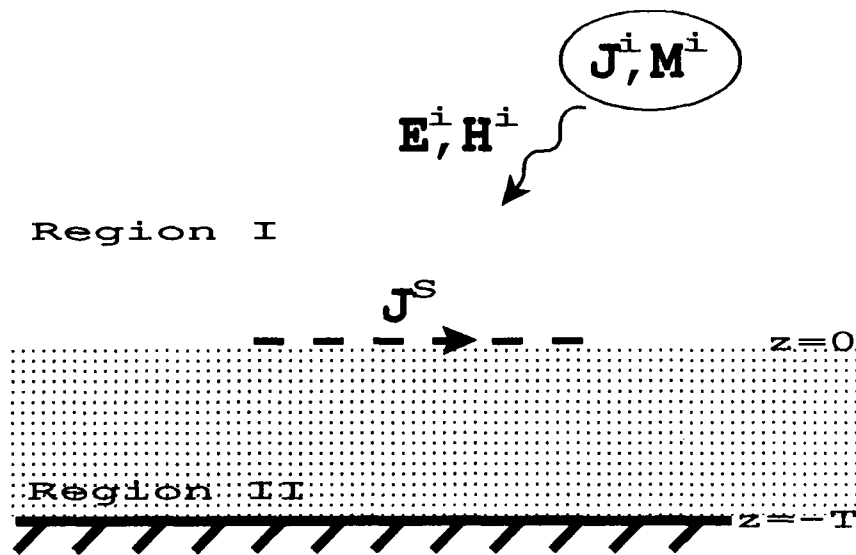
b) Side view of the equivalent surface current $\mathbf{J}^S$ replacing the perfectly conducting rectangular patch on a grounded dielectric substrate. It is in the presence source currents $(\mathbf{J}^i, \mathbf{M}^i)$.

Figure 2: The equivalent geometry of a microstrip patch antenna.

On the surface of the patch, the tangential components of the total electric field must equal zero. Then, from Equation (2.2)

$$(\mathbf{E}^i + \mathbf{E}^S) \times \hat{\mathbf{z}} = 0. \qquad (2.4)$$

This can also be written as

$$- \mathbf{E}^S_{tan} = \mathbf{E}^i_{tan}. \qquad (2.5)$$

This is the integral equation for $\mathbf{J}^S$ since

$$\mathbf{E}^S = \int_{-W}^{W} \int_{-H}^{H} \bar{\mathbf{G}}^2 \cdot \mathbf{J}^S \, dx' \, dy' \qquad (2.6)$$

where $\bar{\mathbf{G}}^2 = \bar{\mathbf{G}}^2(x', y' \mid x, y, z)$ is the dyadic Green's function for the grounded dielectric substrate. $\mathbf{E}^S$ is a function of (x, y, z), while $\mathbf{J}^S$ is a function of (x', y'). The dyadic Green's function $\bar{\mathbf{G}}^2$ is used only to show the integral form of an electric field and will not be used in the analysis.

2.3 The General Moment Method Solution

This section will use the integral equation developed in the preceding section to develop a general MM solution for the geometry of Figure 1. The unknown surface current in the integral equation will be replaced by a sum of N known vector expansion functions of unknown strengths. By taking an inner product between Equation (2.5) and a set of N vector weighting functions, a matrix equation is formed. A Galerkin solution will be used and expressions for the matrix elements will be given.

To begin the solution for the unknown equivalent surface current, $\mathbf{J}^S$ is represented as a sum of N known vector expansion functions

$$\mathbf{J}^S = \sum_{n=1}^{N} I_n \mathbf{J}_n^S \qquad (2.7)$$

9

where $\mathbf{J}_n^S$ are the expansion functions and I_n represents the unknown strength of each expansion function. Let $\mathbf{E}_n^S$ be the field radiated by the expansion function $\mathbf{J}_n^S$ in the presence of the grounded dielectric substrate. Then Equation (2.5) can be written as

$$-\sum_{n=1}^{N} I_n \mathbf{E}_{n\,tan}^S = \mathbf{E}_{tan}^i. \tag{2.8}$$

By taking the inner product of Equation (2.8) with a set of N known vector weighting functions defined on the surface of the patch, Equation (2.8) reduces to a $N \times N$ system of simultaneous linear equations. These equations can be written compactly in matrix form as

$$[Z][I] = [V] \tag{2.9}$$

where $[Z]$ is an $N \times N$ impedance matrix, $[I]$ is a N element current column array containing the unknown coefficients I_n of the expansion of $\mathbf{J}^S$ and $[V]$ is a N element voltage vector column array. Applying a Galerkin solution, which defines the vector weighting functions to be the same as the vector expansion functions, a typical element of $[Z]$ is

$$Z_{mn} = -\int_{-W}^{W} \int_{-H}^{H} \mathbf{E}_n^S \cdot \mathbf{J}_m^S \, dx \, dy \tag{2.10}$$

and a typical element of $[V]$ is

$$V_m = \int_{-W}^{W} \int_{-H}^{H} \mathbf{E}^i \cdot \mathbf{J}_m^S \, dx \, dy. \tag{2.11}$$

By applying reciprocity to Equation (2.11), the elements of the voltage vector can be expressed in terms of the electric field of $\mathbf{J}_m^S$ in the presence of the grounded dielectric substrate. The reciprocal expression is

$$V_m = \int \mathbf{E}_m^S \cdot \mathbf{J}^i \, dv \tag{2.12}$$

10

where the integral is over the volume of the impressed current and $\mathbf{E}_m^S$ is the electric field of $\mathbf{J}_m^S$. Now both the impedance matrix elements and the voltage vector elements are expressed in terms of the electric field of the expansion and weighting functions.

Note that in the preceding equations, the *tan* subscripts that appeared in Equation (2.8), from which the above were based, have been dropped. This can be done since the vector weighting functions have direction tangential to the patch surface.

2.4 Evaluation of the Impedance Matrix

In this section, exact integral expressions will be developed for the impedance matrix elements using the general expression developed in the preceding section. The expansion functions representing the unknown surface current will be restricted to having either $\hat{\mathbf{x}}$ or $\hat{\mathbf{y}}$ vector direction. Figure 3 shows an expansion function, $\mathbf{J}_n^S$, on the interface of Region I and Region II. The electric field for $\mathbf{J}_n^S$ in the presence of the grounded dielectric substrate will be developed using the plane wave expansion method [13]. Note that this electric field is used for evaluating both Equation (2.10) and Equation (2.12). Equation (2.10) will be evaluated to obtain the expressions for the impedance matrix elements.

Since the surface current exists on the interface of Region I and Region II, both regions can be considered source free. The fields in each region can be constructed from two scalar functions [1]. These scalar functions must satisfy the scalar wave equation. For Region I,

$$(\nabla^2 + \kappa_0^2) \begin{bmatrix} \Psi_{mI} \\ \Psi_{eI} \end{bmatrix} = 0 \qquad (2.13)$$

11
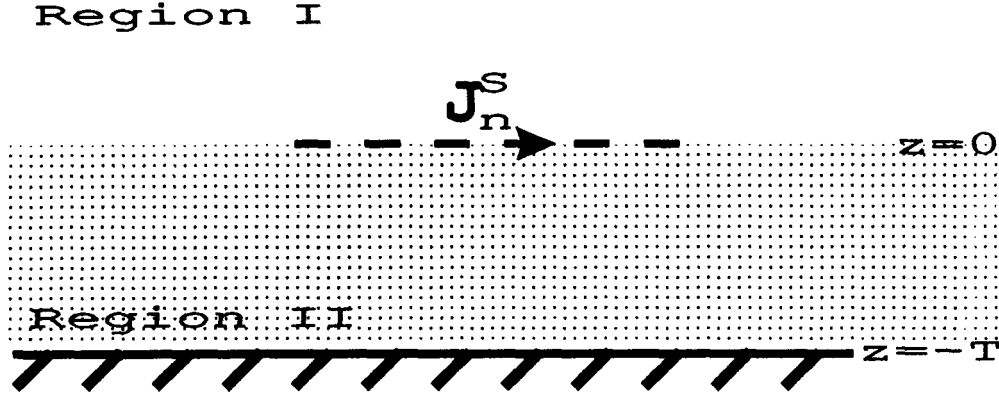
Region I

Figure 3: The MM expansion function, $\mathbf{J}_n^S$, at the dielectric interface.

and for Region *II*,

$$(\nabla^2 + \kappa_2^2) \begin{bmatrix} \Psi_{mII} \\ \Psi_{eII} \end{bmatrix} = 0 \qquad (2.14)$$

where,

$$\kappa_0 = \omega\sqrt{\epsilon_0\mu_0} \qquad (2.15)$$

$$\kappa_2 = \omega\sqrt{\epsilon_2\mu_0}. \qquad (2.16)$$

Ψ_m generates fields with a magnetic field tangent to the planar interface (TM) and Ψ_e generates fields with an electric field tangent to the planar interface (TE). The $\mathbf{E}$ and $\mathbf{H}$ fields of either region can be defined from the Ψ_m, Ψ_e, ϵ, and μ of the appropriate region using

$$\mathbf{E} = -\nabla \times (\hat{\mathbf{z}}\Psi_e) + \frac{1}{\jmath\omega\epsilon}\nabla \times \nabla \times (\hat{\mathbf{z}}\Psi_m) \qquad (2.17)$$

$$\mathbf{H} = \nabla \times (\hat{\mathbf{z}}\Psi_m) + \frac{1}{\jmath\omega\mu}\nabla \times \nabla \times (\hat{\mathbf{z}}\Psi_e). \qquad (2.18)$$

12

Using the plane wave expansion method [13], the scalar wave functions can be defined by their spectral functions. The equations to transform the spectral functions to the scalar wave functions are, in Region I,

$$\left[\begin{array}{c} \Psi_{mI} \\ \Psi_{eI} \end{array} \right] = \frac{1}{4\pi^2} \int_{-\infty}^{\infty} \int_{-\infty}^{\infty} \left[\begin{array}{c} \tilde{\Psi}_{mI} \\ \tilde{\Psi}_{eI} \end{array} \right] e^{-\jmath(\kappa_x x + \kappa_y y + \kappa_{z1} z)} \, d\kappa_x \, d\kappa_y \qquad (2.19)$$

where

$$\kappa_{z1} = \sqrt{\kappa_0^2 - \kappa_x^2 - \kappa_y^2} \qquad \mathrm{Re}(\kappa_{z1}) > 0, \ \mathrm{Im}(\kappa_{z1}) < 0 \qquad (2.20)$$

and in Region II,

$$\left[\begin{array}{c} \Psi_{mII} \\ \Psi_{eII} \end{array} \right] = \frac{1}{4\pi^2} \int_{-\infty}^{\infty} \int_{-\infty}^{\infty} \left[\begin{array}{c} \tilde{\Psi}_{mII} \cos(\kappa_{z2}[z+T]) \\ \tilde{\Psi}_{eII} \sin(\kappa_{z2}[z+T]) \end{array} \right] e^{-\jmath(\kappa_x x + \kappa_y y)} \, d\kappa_x \, d\kappa_y$$

$$(2.21)$$

where

$$\kappa_{z2} = \sqrt{\kappa_2^2 - \kappa_x^2 - \kappa_y^2} \qquad \mathrm{Re}(\kappa_{z2}) > 0, \ \mathrm{Im}(\kappa_{z2}) < 0. \qquad (2.22)$$

The conditions already satisfied are: the boundary condition on the ground plane ($\hat{z} \times \mathbf{E}_{II} = 0$) in Equation (2.21), the radiation condition as $r \to \infty$ in both Equation (2.19) and Equation (2.21), and the integrals in Equation (2.19) converge as $z \to \infty$. The following boundary conditions at the dielectric interface, $z = 0$, still need to be satisfied

$$\hat{z} \times (\mathbf{E}_{II} - \mathbf{E}_I) = 0 \qquad (2.23)$$

$$\hat{z} \times (\mathbf{H}_{II} - \mathbf{H}_I) = \mathbf{J}_n^S. \qquad (2.24)$$

$\mathbf{J}_n^S$ is assumed to be Fourier transformable and expressed in $\hat{x}$ and $\hat{y}$ components. The Fourier transform pair is

$$\mathbf{J}_n^S = \hat{x} J_{nx} + \hat{y} J_{ny}$$

13

$$= \frac{1}{4\pi^2} \int_{-\infty}^{\infty} \int_{-\infty}^{\infty} \left[\hat{\mathbf{x}} \tilde{J}_{nx}^+ + \hat{\mathbf{y}} \tilde{J}_{ny}^+ \right] e^{-\jmath(\kappa_x x + \kappa_y y)} \, d\kappa_x \, d\kappa_y \tag{2.25}$$

$$\tilde{\mathbf{J}}_n^S = \hat{\mathbf{x}} \tilde{J}_{nx}^+ + \hat{\mathbf{y}} \tilde{J}_{ny}^+$$

$$= \int_{-W}^{W} \int_{-H}^{H} \left[\hat{\mathbf{x}} J_{nx} + \hat{\mathbf{y}} J_{ny} \right] e^{\jmath(\kappa_x x + \kappa_y y)} \, dx \, dy \tag{2.26}$$

where $\tilde{J}_{nx}^+$ and $\tilde{J}_{ny}^+$ are the transforms of J_{nx} and J_{ny} respectively.

By substituting Equations (2.19) - (2.22) into Equations (2.17) - (2.18), the integral expressions for $\mathbf{E}_I, \mathbf{H}_I, \mathbf{E}_{II}$, and $\mathbf{H}_{II}$ are obtained. Applying the boundary conditions of Equations (2.23) - (2.24), with Equation (2.25) substituted into Equation (2.24), solves for $\Psi_{mI}, \Psi_{eI}, \Psi_{mII}$, and Ψ_{eII} in terms of $\tilde{J}_{nx}$ and $\tilde{J}_{ny}$. From this result, the total electric and magnetic fields of Region I and Region II [13] can be written in terms of $\tilde{J}_{nx}$ and $\tilde{J}_{ny}$ using Equations (2.17) - (2.18).

The tangential electric field components at the patch surface for a $\hat{\mathbf{x}}$ directed surface current is

$$\begin{bmatrix} E_{xn} \\ E_{yn} \end{bmatrix} = -\frac{\jmath}{4\pi^2} \int_{-\infty}^{\infty} \int_{-\infty}^{\infty} \begin{bmatrix} \left(\kappa_y^2 A_E + \kappa_x^2 A_M \right) \\ \kappa_x \kappa_y \left(A_E - A_M \right) \end{bmatrix} \tilde{J}_{nx}^{S+} e^{-\jmath(\kappa_x x + \kappa_y y)} \, d\kappa_x \, d\kappa_y, \tag{2.27}$$

and for a $\hat{\mathbf{y}}$ directed surface current

$$\begin{bmatrix} E_{xn} \\ E_{yn} \end{bmatrix} = -\frac{\jmath}{4\pi^2} \int_{-\infty}^{\infty} \int_{-\infty}^{\infty} \begin{bmatrix} \kappa_x \kappa_y \left(A_E - A_M \right) \\ \left(\kappa_y^2 A_E + \kappa_x^2 A_M \right) \end{bmatrix} \tilde{J}_{ny}^{S+} e^{-\jmath(\kappa_x x + \kappa_y y)} \, d\kappa_x \, d\kappa_y \tag{2.28}$$

where

$$A_E = \frac{\omega \mu_0 \sin \kappa_{z2} T}{\kappa^2 D_E} \tag{2.29}$$

$$A_M = \frac{\kappa_{z1} \kappa_{z2} \sin \kappa_{z2} T}{\omega \kappa^2 D_M} \tag{2.30}$$

$$\kappa^2 = \kappa_x^2 + \kappa_y^2 \tag{2.31}$$

$$D_E = \kappa_{z2} \cos \kappa_{z2} T + \jmath \kappa_{z1} \sin \kappa_{z2} T \tag{2.32}$$

$$D_M = \epsilon_2 \kappa_{z1} \cos \kappa_{z2} T + \jmath \epsilon_0 \kappa_{z2} \sin \kappa_{z2} T. \tag{2.33}$$

14

The elements in $[Z]$ are obtained by inserting Equations (2.27) and (2.28) into Equation (2.10) [13]. If mode n and mode m are $\hat{x}$ polarized, the mutual impedance is

$$Z_{mn} = \frac{j}{4\pi^2} \int_{-\infty}^{\infty} \int_{-\infty}^{\infty} \left[\kappa_y^2 A_E + \kappa_x^2 A_M\right] \tilde{J}_{mx}^+ \tilde{J}_{nx}^- \, d\kappa_x \, d\kappa_y \qquad (2.34)$$

If mode n is $\hat{x}$ polarized and mode m is $\hat{y}$ polarized, the mutual impedance is

$$Z_{mn} = \frac{j}{4\pi^2} \int_{-\infty}^{\infty} \int_{-\infty}^{\infty} \kappa_x \kappa_y \left[A_E - A_M\right] \tilde{J}_{nx}^+ \tilde{J}_{my}^- \, d\kappa_x \, d\kappa_y \qquad (2.35)$$

If mode n is $\hat{y}$ polarized and mode m is $\hat{x}$ polarized, the mutual impedance is

$$Z_{mn} = \frac{j}{4\pi^2} \int_{-\infty}^{\infty} \int_{-\infty}^{\infty} \kappa_x \kappa_y \left[A_E - A_M\right] \tilde{J}_{ny}^+ \tilde{J}_{mx}^- \, d\kappa_x \, d\kappa_y \qquad (2.36)$$

If mode n and mode m are $\hat{y}$ polarized, the mutual impedance is

$$Z_{mn} = \frac{j}{4\pi^2} \int_{-\infty}^{\infty} \int_{-\infty}^{\infty} \left[\kappa_y^2 A_E + \kappa_x^2 A_M\right] \tilde{J}_{ny}^+ \tilde{J}_{my}^- \, d\kappa_x \, d\kappa_y \qquad (2.37)$$

where, for example, $\tilde{J}_{nx}^+$ is the Fourier transform of J_{nx} (see Equations (2.25) and (2.26)) and

$$\tilde{J}_{nx}^- = \int_{-W}^{W} \int_{-H}^{H} J_{nx} e^{-j(\kappa_x x + \kappa_y y)} \, dx \, dy. \qquad (2.38)$$

Equation (2.39) shows the general form of an element of $[Z]$ and a transformation of the integral from (κ_x, κ_y) coordinates to (κ, α) coordinates. The transformation shown converts two integrals with infinite bounds to one integral with finite bounds and another integral with one infinite bound. This simplifies the application of the $[Z]$ element expressions since they are integrated numerically.

$$\begin{aligned} Z_{mn} &= \int_{-\infty}^{\infty} \int_{-\infty}^{\infty} F(\kappa_x, \kappa_y) \tilde{J}_m^+ \tilde{J}_n^- \, \kappa_x \, d\kappa_y \\ &= \int_0^{2\pi} \int_0^{\infty} F(\kappa, \alpha) \tilde{J}_m^+ \tilde{J}_n^- \, \kappa \, d\kappa \, d\alpha \end{aligned} \qquad (2.39)$$

where,

$$\kappa_x = \kappa \cos \alpha \qquad (2.40)$$

$$\kappa_y = \kappa \sin \alpha. \qquad (2.41)$$

15

2.5 Evaluation of the Voltage Vector

This section will obtain the general equations of the voltage vector of Equation (2.11) for an incident uniform plane wave in Region I and for a vertical filament of uniform current in Region II.

2.5.1 Voltage Vector for an Incident Plane Wave in Region I

This subsection will evaluate Equation (2.11) for the case of a uniform plane wave. Figure 4 shows the side view of a plane wave incident on a microstrip patch. A nonphysical impressed current that radiates a uniform plane wave in free space will be defined so that the voltage vector elements can be written in terms of the far zone electric field of a weighting mode in the presence of the grounded dielectric substrate. Finally, the far zone electric field of the weighting mode will be evaluated asymptotically so that the voltage vector elements can be computed analytically.

The electric field of a uniform incident plane wave in free space can be written as

$$\mathbf{E}_0^i = \mathbf{E}_0 e^{j\bar{\kappa} \cdot \mathbf{r}} \tag{2.42}$$

where

$$\bar{\kappa} = \hat{x}\kappa_0 \sin\theta \cos\phi + \hat{y}\kappa_0 \sin\theta \sin\phi + \hat{z}\kappa_0 \cos\phi \tag{2.43}$$

$$\mathbf{r} = \hat{x}r \sin\theta \cos\phi + \hat{y}r \sin\theta \sin\phi + \hat{z}r \cos\phi \tag{2.44}$$

with θ, ϕ defining the spherical angle of incidence. An infinitesimal dipole source in free space with current of amplitude $\frac{4\pi r}{j\omega\mu_0}\mathbf{E}_0$ will produce the plane wave described by Equation (2.42). Note that this source is physically unrealizable since the amplitude of the source is proportional to the distance r. Since an impressed current for a uniform plane wave in free space has been defined and the electric

16
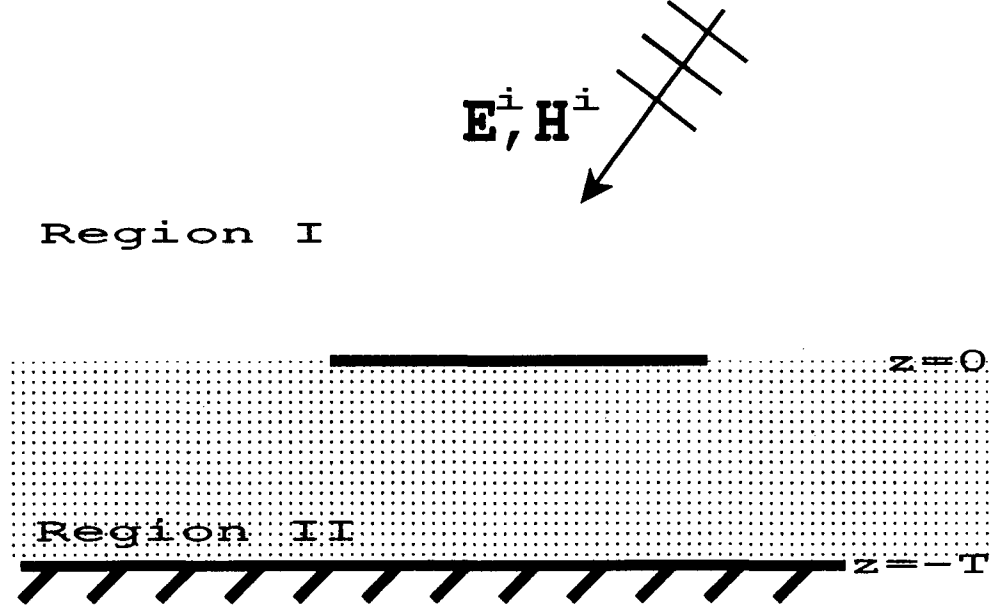
Figure 4: Plane wave incidence on a microstrip patch.

field of $\mathbf{J}_m^S$ in the presence of the grounded dielectric substrate was developed in the evaluation of the impedance matrix elements, Equation (2.12) can be used to express the elements of the voltage vector for a uniform plane wave in free space incident on the microstrip patch. Defining the impressed current to be in the far zone of the microstrip patch, let the far zone field of $\mathbf{J}_m^S$ be $\mathbf{e}_m$. Then, evaluating Equation (2.12), the voltage vector elements are written as

$$V_m = \frac{4\pi}{\jmath\omega\mu_0}\mathbf{e}_m \cdot \mathbf{E}_0. \tag{2.45}$$

Using the method of stationary phase [13], the far zone electric field of mode m can be evaluated asymptotically. With this evaluation, $\mathbf{e}_m$ can be written as

$$\mathbf{e}_m = \frac{\jmath\kappa_0}{2\pi}\left\{\hat{\phi}\left[\cos\phi\tilde{e}_y - \sin\phi\tilde{e}_x\right]\cos\theta + \hat{\theta}\left[\cos\phi\tilde{e}_y + \sin\phi\tilde{e}_x\right]\right\}\frac{e^{-\jmath\kappa_0 r}}{r} \tag{2.46}$$

where, for $\hat{x}$ polarized modes,

$$\tilde{e}_x = -C\left[(\epsilon_r\kappa_0^2 - \kappa_x^2\kappa_{z1}\cos\kappa_{z2}T + \jmath(\kappa_0^2 - \kappa_x^2)\kappa_{z2}\sin\kappa_{z2}T\right]\tilde{J}_{mx}^+ \tag{2.47}$$

17

$$\tilde{e}_y = C\kappa_x\kappa_y\left[\kappa_{z1}\cos\kappa_{z2}T + \jmath\sin\kappa_{z2}T\right]\tilde{J}_{mx}^+ \tag{2.48}$$

and for $\hat{y}$ polarized modes,

$$\tilde{e}_x = C\kappa_x\kappa_y\left[\kappa_{z1}\cos\kappa_{z2}T + \jmath\sin\kappa_{z2}T\right]\tilde{J}_{my}^+ \tag{2.49}$$

$$\tilde{e}_y = -C\left[(\epsilon_r\kappa_0^2 - \kappa_y^2\kappa_{z1}\cos\kappa_{z2}T + \jmath(\kappa_0^2 - \kappa_y^2)\kappa_{z2}\sin\kappa_{z2}T\right]\tilde{J}_{my}^+ \tag{2.50}$$

with

$$C = \frac{\jmath\sin\kappa_{z2}T}{\omega D_E D_M}. \tag{2.51}$$

When evaluating Equations (2.47) - (2.50), it is necessary to replace (κ_x, κ_y) by their values at the stationary phase point [14],

$$(\kappa_x, \kappa_y) \rightarrow (\kappa_0\sin\theta\cos\phi, \kappa_0\sin\theta\sin\phi) \tag{2.52}$$

2.5.2 Voltage Vector for a Vertical Uniform Filament of Current in Region II

This subsection will obtain the voltage vector elements for a uniform vertical current filament. Figure 5 shows a vertical filament of uniform current exciting the patch. Since the impressed current of this source is known and the electric field of $\mathbf{J}_m^S$ in the presence of the grounded dielectric substrate has been developed, the voltage vector elements will be obtained using Equation (2.12). For this problem, the electric field of $\mathbf{J}_m^S$ can not be simplified by a far zone asymptotic approximation. The voltage vector element for this excitation is obtained in integral form.

Starting with Equation (2.12) and letting

$$\mathbf{J}^i = \begin{cases} \hat{z}I_0\delta(x - x_f)\delta(y - y_f) & -T \leq z \leq 0 \\ 0 & \text{elsewhere} \end{cases} \tag{2.53}$$

18
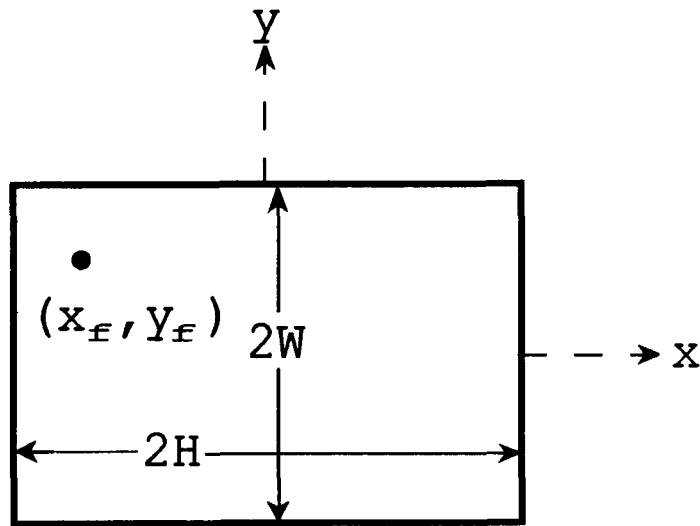
a) Top view of a microstrip patch excited by a current filament.

Region I
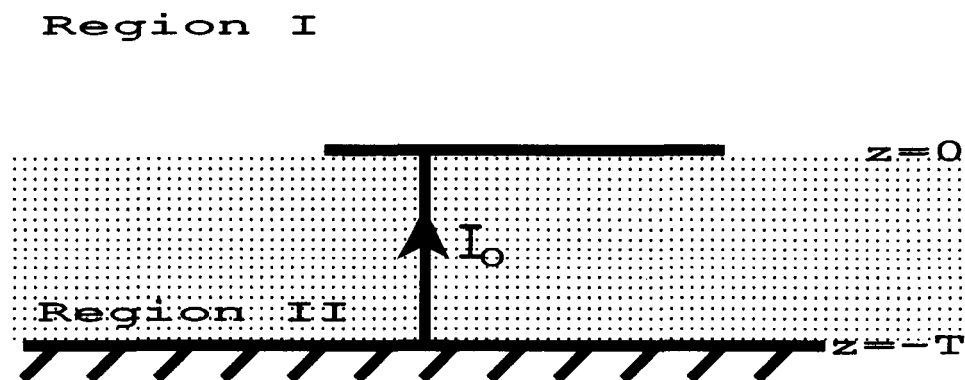
b) Side view of a microstrip patch excited by a current filament.

Figure 5: A rectangular patch microstrip antenna excited by a vertical current filament.

the voltage vector element becomes

$$V_m = \int_{-T}^{0} E_{zm} I_0 \, dz. \tag{2.54}$$

E_{zm} is

$$E_{zm} = -\frac{1}{4\pi^2} \int_{-\infty}^{\infty} \int_{-\infty}^{\infty} \frac{\kappa_{z1}}{\omega D_M} \kappa_x \tilde{J}_{mx} e^{-\jmath(\kappa_x x_f + \kappa_y y_f)} \cos \kappa_{z2}(z+T) \, d\kappa_x \, d\kappa_y \tag{2.55}$$

for $\hat{x}$ polarized modes and

$$E_{zm} = -\frac{1}{4\pi^2} \int_{-\infty}^{\infty} \int_{-\infty}^{\infty} \frac{\kappa_{z1}}{\omega D_M} \kappa_y \tilde{J}_{my} e^{-\jmath(\kappa_x x_f + \kappa_y y_f)} \cos \kappa_{z2}(z+T) \, d\kappa_x \, d\kappa_y. \tag{2.56}$$

for $\hat{y}$ polarized modes [13].

Substituting Equations (2.55) - (2.56) into Equation (2.54) and integrating over z defines the integral equation for the voltage vector element of a vertical uniform current. For $\hat{x}$ polarized modes,

$$V_m = -\frac{1}{4\pi^2} \int_{-\infty}^{\infty} \int_{-\infty}^{\infty} \frac{\kappa_{z1} \sin \kappa_{z2} T}{\omega \kappa_{z2} D_M} \kappa_x \tilde{J}_{mx} e^{-\jmath(\kappa_x x_f + \kappa_y y_f)} \, d\kappa_x \, d\kappa_y \tag{2.57}$$

and for $\hat{y}$ polarized modes,

$$V_m = -\frac{1}{4\pi^2} \int_{-\infty}^{\infty} \int_{-\infty}^{\infty} \frac{\kappa_{z1} \sin \kappa_{z2} T}{\omega \kappa_{z2} D_M} \kappa_y \tilde{J}_{my} e^{-\jmath(\kappa_x x_f + \kappa_y y_f)} \, d\kappa_x \, d\kappa_y \tag{2.58}$$

Equations (2.57) - (2.58) contain an exponential term dependant on the (x, y) location of the vertical current. This factor will produce an oscillatory convergence in the integration which will complicate its computation with respect to the computation of the impedance matrix elements.

Equation (2.59) shows the general form of the voltage vector element for the vertical uniform current. It also shows the transformation from (κ_x, κ_y) to (κ, α) coordinates used in the evaluation of the integral.

$$
\begin{aligned}
V_m &= \int_{-\infty}^{\infty} \int_{-\infty}^{\infty} G(\kappa_x, \kappa_y) \tilde{J}_m e^{-\jmath(\kappa_x x_f + \kappa_y y_f)} \, d\kappa_x \, d\kappa_y \\
&= \int_{0}^{2\pi} \int_{0}^{\infty} G(\kappa, \alpha) \tilde{J}_m e^{-\jmath(\kappa_x x_f + \kappa_y y_f)} \kappa \, d\kappa \, d\alpha
\end{aligned}
\tag{2.59}
$$

The V_m for a wire of radius a is easily developed from the solution for V_m of the filament if the wire is modeled as an infinite number of filaments as radius a around some point (x_c, y_c). Using Equation (2.59), the voltage vector of the wire is

$$V_m = \frac{1}{2\pi} \int_0^{2\pi} \int_0^{2\pi} \int_0^{\infty} G(\kappa, \alpha) \tilde{J}_m e^{-J(\kappa_x[x_c + a\cos\phi] + \kappa_y[y_c + a\sin\phi])} \kappa \, d\kappa \, d\alpha \, d\phi.$$

(2.60)

By evaluating the ϕ integral, Equation (2.60) becomes

$$V_m = \int_0^{2\pi} \int_0^{\infty} G(\kappa, \alpha) \tilde{J}_m e^{-J(\kappa_x x_c + \kappa_y y_c)} J_0(\kappa a) \kappa \, d\kappa \, d\alpha$$

(2.61)

where J_0 is the zero order Bessel function.

2.6 Loading of a Rectangular Microstrip Patch

This section will describe the procedure for modifying the voltage vector when a lumped load at an arbitrary position (x_L, y_L) is attached between the rectangular microstrip patch and the ground plane. The load is assumed to be in a vertical filament from $z = -T$ to $z = 0$ with a uniform current of magnitude I_L flowing through it from the patch to the ground plane. The load current is determined by modeling the microstrip antenna as a two port device.

Equation (2.9) describes the matrix equation for the MM solution of the unloaded microstrip patch. When a load Z_L is added, Equation (2.9) becomes

$$[Z][I] = \left[V^i\right] - I_L \left[V^L\right]$$

(2.62)

where $\left[V^i\right]$ is the excitation voltage vector, I_L is the magnitude of the uniform current through the load, and $\left[V^L\right]$ is the voltage vector for a 1 amp current filament at the load position, (x_L, y_L). Note that the 1 amp current from which $\left[V^L\right]$ is obtained is in direction opposite to the load current.

21
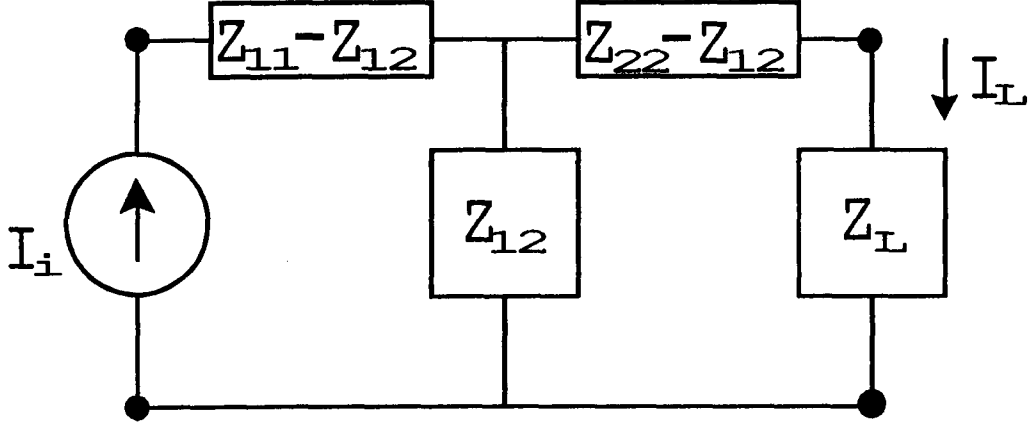
Figure 6: The equivalent circuit of a symmetric two port with an I_i current source at port 1 and a load Z_L at port 2.

In order to determine I_L, the microstrip antenna is modeled as a two port device. Figure 6 shows the equivalent circuit of a symmetric $(Z_{12} = Z_{21})$ two port device excited at port 1 by an I_i current source and with a load of impedance Z_L at port 2. From circuit theory, the current through Z_L is

$$I_L = \frac{Z_{12}}{Z_{22} + Z_L} I_i. \tag{2.63}$$

Since the product of Z_{12} and I_i is the voltage at port 2 with an open circuit at port 2, Equation (2.63) can be written as

$$I_L = \frac{V_{12}}{Z_{22} + Z_L} \tag{2.64}$$

where V_{12} is the open circuit voltage at port 2.

For the microstrip patch, V_{12} is equivalent to the voltage at (x_L, y_L) for an unloaded antenna. This voltage is called V_L^{oc} and can be found from

$$V_L^{oc} = -\int_{-T}^{0} E_z\, dz \tag{2.65}$$

where E_z is the $\hat{z}$ directed electric field at (x_L, y_L). This integral can also be expressed as

$$V_L^{oc} = - \sum_{m=1}^{N} I_m \int_{-T}^{0} E_{zm} \, dz. \tag{2.66}$$

where E_{zm} is the $\hat{z}$ directed field of patch mode m at (x_L, y_L) and I_m is the strength of mode m for the unloaded antenna. Since the elements of $\left[V^L\right]$ are obtained for a 1 amp $\hat{z}$ directed current filament at (x_L, y_L), Equation (2.12) can be written for $\left[V^L\right]$ as

$$\begin{aligned} V_m^L &= \int_{-T}^{0} \mathbf{E}_m \cdot \hat{z} \, dz \\ &= \int_{-T}^{0} E_{zm} \, dz \end{aligned} \tag{2.67}$$

where $\mathbf{E}_m$ is the total field of mode m at (x_L, y_L). From Equations (2.66) and (2.67), the matrix equation

$$V_L^{oc} = -[I]^t \left[V^L\right] \tag{2.68}$$

can be written where $[I]$ is the current column solution of Equation (2.9) for the unloaded antenna.

Z_{22} for the microstrip patch is obtained by solving for $[I]$ when the excitation voltage vector in Equation (2.9) is $\left[V^L\right]$. Using this $[I]$ in Equation (2.68) to solve for the voltage at the load port, Z_{22} is the ratio of the voltage at the load port to the input current at the load port (which is 1 amp). Note that the excitation voltage vector $\left[V^i\right]$ is not used in determining Z_{22}.

2.7 Expansion and Weighting Functions Used in the MM Solution

The expansion and weighting functions used in this MM analysis will now be defined. The weighting functions are chosen the same as the expansion functions, and thus a Galerkin solution is employed. The expansion functions chosen will

be entire domain, which implies that each mode exists over the entire rectangular patch surface. Each expansion function will be separable into a function of x and a function of y. These functions of x and y are Fourier transformable, as required in the derivation of the field equations for a surface current on the patch. Below the expansion functions and their transforms are presented. The advantages of choosing these expansion functions will also be discussed.

Starting with the $\hat{x}$ polarized expansion function, a mode n is defined to be

$$
\begin{aligned}
J_{nx} &= X_p(x, H) Y_q(y, W) \\
&= \sin \frac{p\pi}{2H}(x + H) \cos \frac{q\pi}{2W}(y + W)
\end{aligned}
\tag{2.69}
$$

where now mode n actually specifies an integer doublet pq where $p = 1, 2, 3, \ldots$ and $q = 0, 1, 2, \ldots$ are the bounds. When the Fourier transform, defined by Equation (2.26), is applied to Equation (2.69) the result is

$$
\tilde{J}_{nx}^{\pm} = \tilde{X}_p^{\pm}(\kappa_x, H) \tilde{Y}_q^{\pm}(\kappa_y, W)
\tag{2.70}
$$

where

$$
\begin{aligned}
\tilde{X}_p^{\pm} &= -\frac{\frac{p\pi}{H} \cos \kappa_x H}{\kappa_x^2 - (\frac{p\pi}{2H})^2} & p &= 1, 3, 5, \ldots \\
&= \pm \frac{\frac{jp\pi}{H} \sin \kappa_x H}{\kappa_x^2 - (\frac{p\pi}{2H})^2} & p &= 2, 4, 6, \ldots
\end{aligned}
\tag{2.71}
$$

$$
\begin{aligned}
\tilde{Y}_q^{\pm} &= \pm \frac{j2\kappa_y \cos \kappa_y W}{\kappa_y^2 - (\frac{q\pi}{2W})^2} & q &= 1, 3, 5, \ldots \\
&= \frac{2\kappa_y \sin \kappa_y W}{\kappa_y^2 - (\frac{q\pi}{2W})^2} & q &= 0, 2, 4, \ldots .
\end{aligned}
\tag{2.72}
$$

Similarily, the $\hat{y}$ polarized modes are

$$
\begin{aligned}
J_{my} &= X_{p'}(y, W) Y_{q'}(x, H) \\
&= \sin \frac{p'\pi}{2W}(y + W) \cos \frac{q'\pi}{2H}(x + H)
\end{aligned}
\tag{2.73}
$$

24

with the corresponding Fourier transform

$$\tilde{J}_{my}^{\pm} = \tilde{X}_{p'}^{\pm}(\kappa_y, W)\tilde{Y}_{q'}^{\pm}(\kappa_x, H). \tag{2.74}$$

Note that p', q' can be the same or different from p, q.

The transforms of the expansion and weighting functions are composed of even and odd functions of κ_x and κ_y. Realizing that the integral from $-\infty$ to ∞ of an odd function is zero, certain impedance matrix and voltage vector elements may be identically zero. As an example, consider the impedance matrix integral for an element where both modes n and m are $\hat{x}$ polarized. For this integral, the function $F(\kappa_x, \kappa_y)$ (refer to Equations (2.34) and (2.39)) is an even function of κ_x and κ_y. Using Equations (2.71) - (2.72), Figure 7 shows whether the expansion function $\tilde{J}_{nx}$ is even or odd with respect to κ_x and κ_y for all possible combinations of p and q being even or odd. Figure 8 shows whether the integrand is even or odd with respect to κ_x and κ_y for all possible even-odd combinations of $p_n, q_n, p_m,$ and q_m and whether the integral is non-zero or not. Only 1/4 of the elements in Figure 8 are non-zero. This allows a simplification of the general integral described by Equation (2.39). For the non-zero elements, the α integration is performed from 0 to $\pi/2$ and the result multiplied by 4. The zero elements are set to zero. Similar results are found with Equations (2.35)- (2.37).

With the voltage vector integrals of Equations (2.57) - (2.58), the exponential term can be separated into functions of κ_x and κ_y and these functions can be broken into a sum of an even function and an odd function. Equation (2.75) shows this process.

$$
\begin{aligned}
e^{-\jmath(\kappa_x x_f + \kappa_y y_f)} &= e^{-\jmath\kappa_x x_f}e^{-\jmath\kappa_y y_f} \\
&= (\cos\kappa_x x_f - \jmath\sin\kappa_x x_f)(\cos\kappa_y y_f - \jmath\sin\kappa_y y_f). \tag{2.75}
\end{aligned}
$$

p	q	$X_p(\kappa_x)$	$Y_q(\kappa_y)$
o	o	e	o
o	e	e	e
e	e	o	e
e	o	o	o

Figure 7: The κ_x and κ_y functions of $\tilde{J}_{nx}$ as even or odd functions with respect to p and q. Note: e is even, o is odd.

Expanding Equation (2.75), the integrand can be written as the sum of four terms, each separable into functions of κ_x and κ_y. By analyzing the even-odd functions in each of these terms, only one term is non-zero. Figure 9 shows the integrands of an $\hat{x}$ polarized mode voltage vector for all possible p and q even-odd combinations. For the voltage vector, none of the elements are zero in general, however, by having integrands that are even functions of κ_x and κ_y, the α integration can be performed from 0 to $\pi/2$ and multiplied by four.

One advantage of the entire domain expansion functions is that as the patch increases in electrical size, the width of the current transforms decreases. This results in more rapid convergence of the integrals involving the current transforms. The mode shapes also correspond to the resonant current distributions on the patch. This enables a simple physical interpretation of the magnitude of the elements in the current column vector.

2.8 Computation of the Scattered Field and Input Impedance

Once the impedance matrix elements and voltage vector elements are known, the current column array can be obtained using standard matrix algebra. Assuming the current column is known, this section will obtain expressions for the far

26

p_n	q_n	p_m	q_m	$FX_{p_n}X_{p_m}$	$FY_{q_n}Y_{q_m}$	Integral=0?
o	o	o	o	e	e	No
o	o	o	e	e	o	Yes
o	o	e	e	o	o	Yes
o	o	e	o	o	e	Yes
o	e	e	o	o	o	Yes
o	e	e	e	o	e	Yes
o	e	o	e	e	e	No
o	e	o	o	e	o	Yes
e	e	o	o	o	o	Yes
e	e	o	e	o	e	Yes
e	e	e	e	e	e	No
e	e	e	o	o	o	Yes
e	o	e	o	e	e	No
e	o	e	e	e	o	Yes
e	o	o	e	o	o	Yes
e	o	o	o	o	e	Yes

Figure 8: The κ_x and κ_y functions of the integrand ($F(\kappa_x, \kappa_y)$ is even for both κ_x and κ_y) as even or odd function with respect to p_n, q_n, p_m and q_m.

p	q	Integrand
o	o	$-G\tilde{J}_{mx}\kappa_x \sin\kappa_x x_f \sin\kappa_y y_f$
o	e	$-jG\tilde{J}_{mx}\kappa_x \sin\kappa_x x_f \cos\kappa_y y_f$
e	e	$G\tilde{J}_{mx}\kappa_x \cos\kappa_x x_f \cos\kappa_y y_f$
e	o	$-jG\tilde{J}_{mx}\kappa_x \cos\kappa_x x_f \sin\kappa_y y_f$

Figure 9: The integrands for a $\hat{x}$ polarized mode voltage vector with respect to p and q.

zone fields of the patch. These far zone fields are referred to as the radiated fields when the excitation is by the vertical current filament and as scattered fields when the excitation is by an incident plane wave. For excitation by the vertical uniform current, the input impedance of a mictrostrip antenna will be found.

The electric field of the patch is found from the sum of the field of each mode weighted by the strength of each mode,

$$\mathbf{E} = \sum_{n=1}^{N} I_n \mathbf{E}_n \tag{2.76}$$

where $\mathbf{E}_n$ is the radiated field of mode n as given by Equations (2.27) and (2.28). For the far zone electric field, Equation (2.76) reduces to

$$\mathbf{e}(\theta,\phi) = \sum_{n=1}^{N} I_n \mathbf{e}_n(\theta,\phi) \tag{2.77}$$

where $\mathbf{e}_n$ is the far zone asymptotically approximated field of mode n, defined in Subsection 2.5.1.

The input impedance of a microstrip antenna is the ratio of the voltage at the feed port to the input current. The voltage at a port on the microstrip patch for arbitrary excitation of the antenna is given by Equation (2.68) in the Section 2.6. When the excitation is a 1 amp uniform current at the port where the voltage is

28

desired, the input impedance can be written directly from Equation (2.68) as

$$Z_{in} = -[I]^t [V] \tag{2.78}$$

where $[I]$ is the current column solution and $[V]$ is the voltage vector at the input port. The probe itself tends to be inductive, and the reactance of this inductance can be modeled as [9]

$$X_L = \mu_0 T f_{MHz} \ln \left(\frac{2}{\kappa_2 T} \right) \tag{2.79}$$

where f_{MHz} is the frequency in megahertz. Using Equations (2.78) - (2.79), the input impedance becomes

$$Z_{in} = -[I]^t [V] + jX_L. \tag{2.80}$$

The input impedance of a microstrip patch excited by a vertical filament of uniform current shows good agreement to the input impedance of a coaxially fed microstrip antenna when the thickness of the substrate, T, is much smaller than one wavelength.

2.9 Numerical Difficulties

There are several numerical problems to overcome when computing the plane wave scattering or input impedance of a rectangular microstrip patch antenna. One problem is the CPU time to compute the impedance matrix. This problem is especially severe if one desires to compute the wideband scattering or input impedance of the antenna. Both the impedance matrix and voltage vector element integrands contain surface wave poles which produce singularities in the integration. Finally, there is the exponential term in the voltage vector element integral which produces an oscillatory behavior of that integral. Each of these problems will be discussed in the following subsections.

29

2.9.1 CPU Time Reduction for the Impedance Matrix Computation

Equation (2.39) shows the general form of an impedance matrix element integral expression and it is seen that the integrand is a separable function of $\tilde{J}_n^+$ and $\tilde{J}_n^-$. To generate all the elements of the impedance matrix, for every $\tilde{J}_n^+$ calculation there must be N calculations of $\tilde{J}_m^-$. Since there are N calculations of $\tilde{J}_n^+$, the total time to compute all the elements would be proportional to N^2. The impedance matrix is symmetric, therefore only $N^2/2$ elements need be calculated to generate all the elements.

Referring to Equations (2.71) - (2.72), the transforms $\tilde{J}_n^+$ and $\tilde{J}_n^-$ for the chosen expansion and weighting functions will either be equal or equal and opposite, depending on n. This indicates that when $\tilde{J}_n^+$ is calculated, $\tilde{J}_n^-$ is also known. When computing the elements of the impedance matrix, all N $\tilde{J}_n^+$ are calculated (which means that all N $\tilde{J}_n^-$ are obtained as well) within the integral expression of Equation (2.39). The impedance matrix elements are then obtained by multiplying $\tilde{J}_n^+$ and $\tilde{J}_m^-$ together for $n = 1, ..., N$ and $m = 1, ..., N$. Since the time required to multiply $\tilde{J}_n^+$ and $\tilde{J}_n^-$ together (which is proportional to $N^2/2$ when taking the symmetry into account) is significantly less than the time to compute $\tilde{J}_n^+$ and $\tilde{J}_n^-$ (which is proportional to N), the total time to compute all the elements of the impedance matrix tends to be proportional to N.

2.9.2 CPU Time for Wide Frequency Band Calculations

To make a broadband computation of the scattering or input impedance of a microstrip antenna, many frequency points are needed to show the behavior near resonance since microstrip antennas are narrow band. Thus, although the CPU time to evaluate the matrix elements at a single frequency may be tractable, the

CPU time required to evaluate the matrix elements at hundreds of frequencies over a wide bandwidth can be prohibitive.

A way to make broadband calculations of a microstrip antenna starts by analyzing the impedance matrix with respect to frequency. The elements in the impedance matrix are very slowly varying with frequency [16], which is quite different from the scattered field or input impedance data. An interpolation technique can be employed to approximate the impedance matrix elements at frequencies in between the frequencies at which the elements are calculated using Equations (2.34) - (2.37). Over the desired bandwidth, data points separated by a frequency interval of Δf_z are required to characterize the behavior of the microstrip antenna. The number of computations required to get data points every Δf_z would be impractical, so the impedance matrix elements are computed at intervals of Δf_c instead. Typically, $\Delta f_c \gg \Delta f_z$. Three of the points where the elements are calculated directly, f_{c1}, f_{c2}, f_{c3}, (with $f_{c1} < f_{c2} < f_{c3}$) will define a frequency band of width $2\Delta f_c$. A quadratic interpolation method can approximate the values of the elements every Δf_z in between f_{c1}, f_{c2} and f_{c2}, f_{c3}. By dividing the desired frequency band into sub-bands of width $2\Delta f_c$ and applying the quadratic interpolation method, data points for the impedance matrix elements at frequency intervals of Δf_z can be obtained for the entire desired bandwidth.

The CPU time to evaluate the integral expressions for the voltage vector of a uniform current filament, given by Equations (2.57) and (2.58), is similar to the CPU time required to evaluate the impedance matrix. Analysis of these voltage vector elements with frequency shows that they are slowly varying. For radiation problems and loaded antenna computations, this voltage vector is interpolated in the same manner as the impedance matrix.

31

2.9.3 Surface Wave Poles

The integrand for the Z_{mn} integrals are singular when D_E or D_M of Equations (2.32) and (2.33) equal zero and the integrand for the V_m integrals are singular when D_M equals zero. The D_E singularities are due to the TE surface waves and the D_M singularities due to the TM surface waves that exist on the grounded dielectric substrate. As the frequency increases, the number of surface wave poles can increase. For a lossless dielectric, these poles lie right on the $\text{Re}(\kappa)$ axis between κ_0, the propagation constant of Region I (in this problem, free space), and κ_2, the propagation constant of Region II. When the dielectric is lossy, the poles move into the fourth quadrant, but for low loss dielectrics, they are very close to the $\text{Re}(\kappa)$ axis. Figure 10 shows a map of the κ plane with poles near the $\text{Re}(\kappa)$ axis. To avoid these poles without having to compute their location and deforming the contour around them, the staggered contour in Figure 10 is used. This method has worked well with the imaginary stagger Δ on the order of $0.1\kappa_0$ and returning to the κ axis around $1.1\kappa_2$.

2.9.4 Oscillatory Behavior of the Voltage Vector

In Subsection 2.5.2, the integral expression for the voltage vector elements of a vertical filament of uniform current was derived. The integrand contains an exponential function where the argument is a function of (x_f, y_f). This exponential term contributes an oscillatory factor to the integral of Equation (2.59). Figure 11 is a typical integral with an oscillatory convergence factor. Note that the upper limit on this integral is x and the plot is comparing the value of the integral verses the upper limit of the integral. This integral oscillates around a converged limit, with the size of the oscillations decreasing as x increases. Since the integral of Equation (2.59) is evaluated numerically, the infinite upper limit on the κ integral
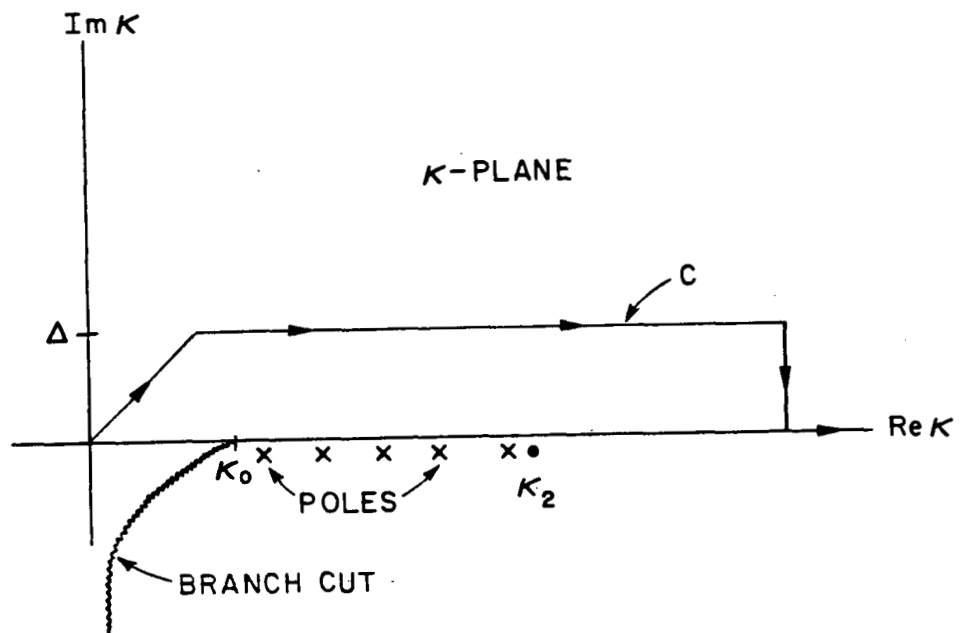
Figure 10: Contour of integration in the κ plane.
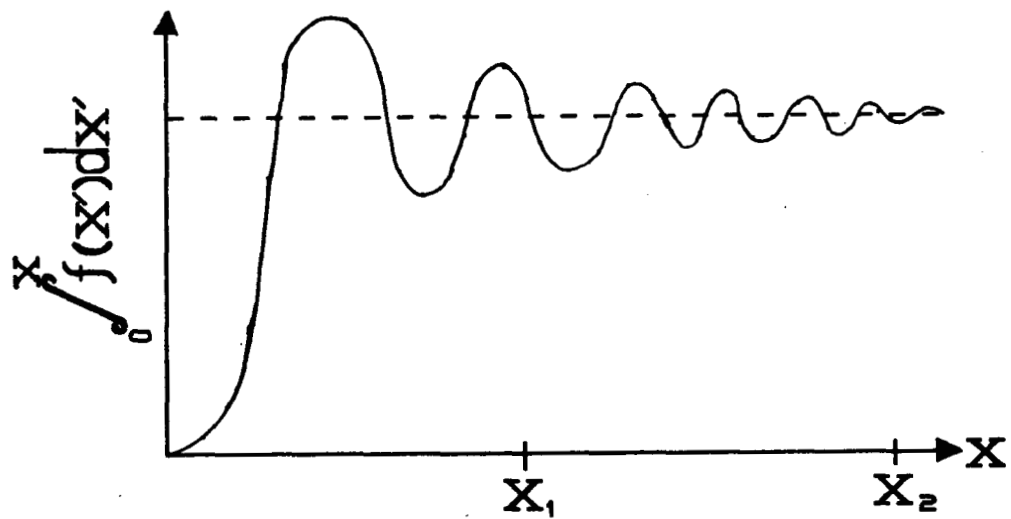
Figure 11: A plot of the integral from 0 to x of $f(x')$ verses x for an oscillatory convergent integral.

33

must be replaced by a finite limit (which is equivalent to x_2 in Figure 11) where the integral is well converged. This limit can be very large, so it would be desirable to determine the converged value before the oscillations around this limit become negligible. In Figure 11, x_1 represents a point where the converged limit of integral is apparent.

The way used to determine this converged limit is by incorporating a peak and valley detector in the numeric integration of the V_m integrals. The numeric integration computes the integral at discrete points. When a peak or valley is found between three integral points, a quadratic interpolation is performed on those three points to find the value of the peak or valley. Once a peak and a valley are found, the average value of the two is computed. With each new peak or valley, a new average is obtained. The integral is considered converged when the percent difference between two consecutive averages of a peak and a valley is less than a desired tolerance.

CHAPTER III

THE INTEGRAL EQUATION AND MOMENT METHOD
SOLUTION FOR A VERTICAL THIN WIRE THROUGH A
GROUNDED DIELECTRIC SUBSTRATE

3.1 Introduction

This chapter will describe the integral equation and the moment method [2] (MM) solutions to the problem of the self impedance of a vertical thin wire and mutual impedance between vertical thin wires on a grounded dielectric substrate. The basic geometry of this structure is shown in Figure 12.

The solution is begun by using the equivalence theorem to replace the perfectly conducting thin wire by an unknown surface current $\mathbf{J}^S$. Using the thin wire approximations, $\mathbf{J}^S$ is replaced by a vertical filament of current, $\hat{z}I^S$ [20,21]. Then, the integral equation for $\hat{z}I^S$ is obtained by requiring that the total tangential electric field along the filament be equal to zero. Finally, the integral equation is solved using the MM.

3.2 Derivation of the Integral Equation

This section describes the use of the surface equivalence theorem to derive the integral equation for the problem of radiation by a perfectly conducting vertical thin wire extending from an infinite perfectly conducting plane and through an infinite dielectric layer directly on top of the perfectly conducting plane. The

35
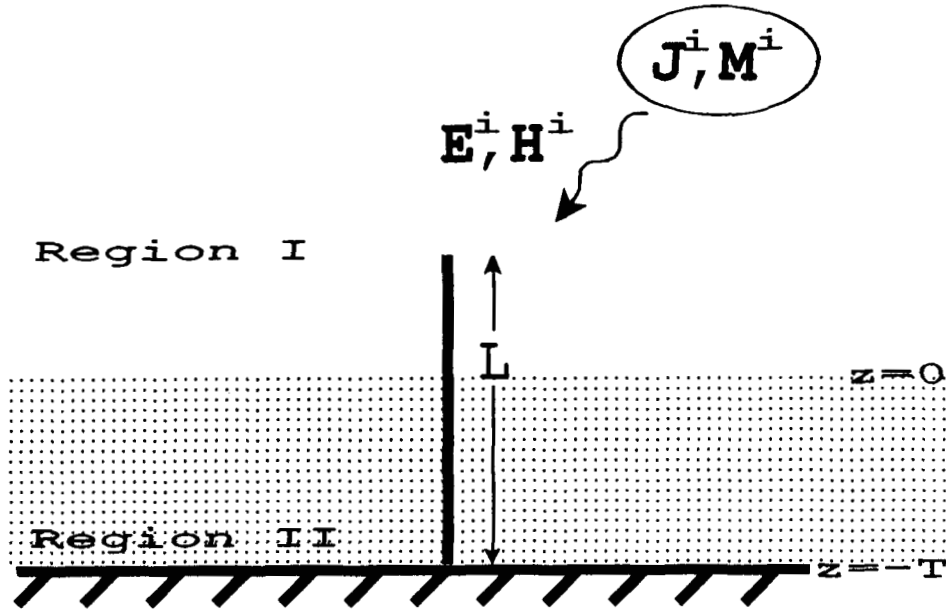
Figure 12: Side view of a vertical, perfectly conducting thin wire extending from a perfectly conducting ground plane through a dielectric layer. It is excited by an arbitrary source $(\mathbf{J}^i, \mathbf{M}^i)$ that can be located in either Region I or II.

geometry of a dielectric layer on top of a perfect conductor will be referred to as a dielectric coated ground plane. Figure 12 shows a perfectly conducting thin wire of length L in the $\hat{z}$ direction and radius a $(a \ll \lambda)$ extending from a grounded dielectric substrate. The region above the dielectric layer, referred to as Region I, is free space (permeability μ_0, permittivity ϵ_0). The region inside the dielectric layer, referred to as Region II, has a permittivity of ϵ_2, permeability of μ_0, and thickness T. The origin of the coordinate system is placed at the the point where the vertical wire intersects the planar interface of Region I and Region II. The wire is excited by source currents $(\mathbf{J}^i, \mathbf{M}^i)$ which illuminates the wire with fields $(\mathbf{E}^i, \mathbf{H}^i)$. Note that $(\mathbf{E}^i, \mathbf{H}^i)$ are the fields of $(\mathbf{J}^i, \mathbf{M}^i)$ in the presence of the grounded dielectric substrate without the wire. $(\mathbf{E}, \mathbf{H})$ denote the electric and magnetic fields from $(\mathbf{J}^i, \mathbf{M}^i)$ in the presence of the grounded dielectric substrate with wire.
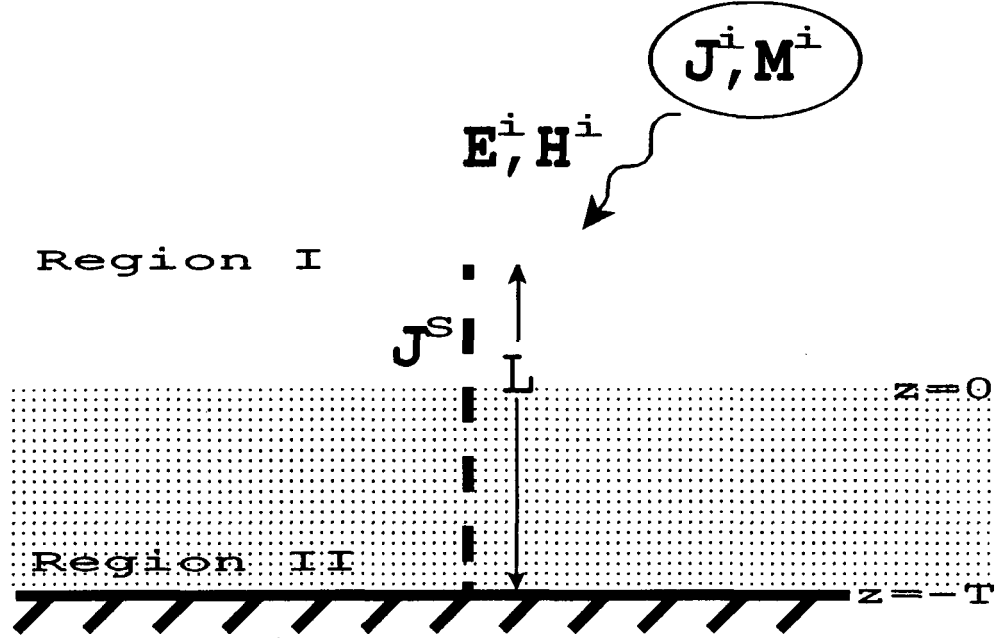
Figure 13: Side view of the equivalent vertical current $\mathbf{J}^S$ replacing the perfectly conducting thin wire on a dielectric coated ground plane. It is in the presence electric and magnetic currents ($\mathbf{J}^i, \mathbf{M}^i$).

Using the Equivalence theorem and ignoring the currents on the end cap, the equivalent surface current on the wire surface will be

$$\mathbf{J}^S = \hat{\rho} \times \mathbf{H} \tag{3.1}$$

Since the wire is thin, surface current on the wire surface is assumed to be $\hat{z}$ directed and uniform with respect to ϕ. So $\mathbf{J}^S$ can be written as

$$\mathbf{J}^S = \hat{z} I^S(z') \qquad \text{at } \rho' = a \tag{3.2}$$

where the wire current I^S is related to the wire surface current J^S by

$$J^S(z') = \frac{I^S(z')}{2\pi a} \tag{3.3}$$

The equivalent problem is illustrated in Figure 13. The total electric and magnetic fields in either region are

$$\mathbf{E} = \mathbf{E}^i + \mathbf{E}^S \tag{3.4}$$

37

$$\mathbf{H} = \mathbf{H}^i + \mathbf{H}^S \tag{3.5}$$

where $(\mathbf{E}^S, \mathbf{H}^S)$ are the fields radiated by the equivalent current $\mathbf{J}^S$ in the presence of the dielectric coated ground plane.

On the wire surface, the tangential components of the total electric field must equal zero. Then, from Equation (3.4)

$$(\mathbf{E}^i + \mathbf{E}^S) \times \hat{\rho} = 0 \tag{3.6}$$

For the $\hat{z}$ directed wire this can be written as

$$-\mathbf{E}_z^S = \mathbf{E}_z^i \tag{3.7}$$

Instead of enforcing the boundary condition on the wire surface, it will be enforced the center line of the wire. This technique is known as the filamentary test case.

3.3   The General Moment Method Solution

This section will use the integral equation developed in the preceding section to develop a general MM solution for the geometry of Figure 12. The unknown vertical current filament in the integral equation will be replaced by a sum of N known expansion functions of unknown strengths. An inner product between each side of integral equation and a sum of N known vector weighting functions will yield the matrix equation. The expressions for the impedance matrix and voltage vector elements will be given.

To begin the solution for the unknown equivalent vertical current, I^S is represented as a sum of N known expansion functions

$$I^S = \sum_{n=1}^{N} I_n I_n^S \tag{3.8}$$

where I_n^S is the n expansion function and I_n represents the unknown strength of the n expansion function. The superscript S is retained to distinguish the expansion

38

function from the unknown strength. Expansion function n is nonzero over the range $z_{n1} \leq z \leq z_{n2}$. Equation (3.7) can be written as

$$-\sum_{n=1}^{N} I_n E_{zn}^S = E_z^i. \tag{3.9}$$

E_{zn}^S is the $\hat{z}$ directed component of the electric field of expansion function n radiating in the presence of the grounded dielectric slab.

By taking the inner product of Equation (3.9) with a set of N known weighting functions located on the wire center line, Equation (3.9) is reduce to the matrix equation

$$[Z][I] = [V]. \tag{3.10}$$

where $[Z]$ is an $N \times N$ impedance matrix, $[I]$ is a N element current column array containing the unknown coefficients I_n of Equation (3.8) and $[V]$ is a N element voltage vector column array.

The scalar weighting functions employed in this solution will have the form

$$w_m = I_m^S(z) \qquad \text{at } \rho = 0 \tag{3.11}$$

and thus are chosen identical to the expansion functions.

Expressions for typical elements of $[Z]$ and $[V]$ are given by

$$Z_{mn} = -\int_{z_{m1}}^{z_{m2}} E_{zn}^S I_m^S \, dz \tag{3.12}$$

and

$$V_m = \int_{zm1}^{zm2} E_z^i I_m^S \, dz. \tag{3.13}$$

3.4 Evaluation of the Impedance Matrix

In this section, exact integral expressions will be developed for the impedance matrix elements using the general expression developed in the preceding section.

The equations will contain arbitrary expansion functions I_n^S and arbitrary weighting functions I_m^S. The electric field of a $\hat{\mathbf{z}}$ directed vertical current filament in either Region II or Region II is found in plane wave representation. This electric field is used in Equation (3.12) to obtain the impedance matrix elements.

The vector magnetic potential for an infinitesimal vertical current of strength I in free space at the origin is

$$\mathbf{A} = \hat{\mathbf{z}}\frac{I\,dz'}{4\pi}\frac{e^{-j\kappa_0 r}}{r} \tag{3.14}$$

where

$$\kappa_0 = \omega\sqrt{\epsilon_0\mu_0} \tag{3.15}$$

and dz is the infinitesimal length of the current element. The $\frac{e^{-j\kappa_0 r}}{r}$ term in Equation (3.14) can be represented as a spectrum of plane waves [20] by

$$\frac{e^{-j\kappa_0 r}}{r} = \int_0^\infty J_0(\beta\rho)\frac{e^{\mp j\gamma_z z}}{j\gamma_z}\,\beta\,d\beta \tag{3.16}$$

where J_0 is the Bessel function of order 0, the $\mp$ in the exponential term is $-$ for $z > 0$ and $+$ for $z < 0$ and γ_z is defined as

$$\gamma_z = \sqrt{\kappa_0^2 - \beta^2} \quad \text{with } \operatorname{Re}(\gamma_z) > 0 \text{ and } \operatorname{Im}(\gamma_z) < 0 \tag{3.17}$$

Substituting Equation (3.16) into Equation (3.14) yields

$$\mathbf{A} = \hat{\mathbf{z}}\frac{I\,dz'}{j4\pi}\int_0^\infty J_0(\beta\rho)\frac{e^{\mp j\gamma_z z}}{\gamma_z}\,\beta\,d\beta \tag{3.18}$$

If this infinitesimal vertical current element is placed in the dielectric layer of the dielectric coated ground plane (Region II) at $\rho' = 0$ and $z = z'$, the vector magnetic potential in Region II can be written as, for $-T \le z \le z'$,

$$A_z = \frac{I\,dz'}{j4\pi}\int_0^\infty \frac{J_0(\beta\rho)}{\gamma_{z2}}\left[e^{j\gamma_{z2}(z-z')} + R_0 e^{j\gamma_{z2}z} + R_{-T}e^{-j\gamma_{z2}(z+T)}\right]\beta\,d\beta \tag{3.19}$$

40

and for $z' \leq z \leq 0$,

$$A_z = \frac{I dz'}{j4\pi} \int_0^\infty \frac{J_0(\beta\rho)}{\gamma_{z2}} \left[e^{-j\gamma_{z2}(z-z')} + R_0 e^{j\gamma_{z2}z} + R_{-T} e^{-j\gamma_{z2}(z+T)} \right] \beta \, d\beta \quad (3.20)$$

and for $z \geq 0$,

$$A_z = \frac{I dz'}{j4\pi} \int_0^\infty \frac{J_0(\beta\rho)}{\gamma_{z2}} \left[T_0 e^{j\gamma_{z1}z} \right] \beta \, d\beta \quad (3.21)$$

where, from Equations (3.17) and (3.15),

$$\gamma_{z1} = \sqrt{\kappa_0^2 - \beta^2} \quad (3.22)$$

$$\gamma_{z2} = \sqrt{\kappa_2^2 - \beta^2} \quad (3.23)$$

$$\kappa_2 = \omega \sqrt{\epsilon_2 \mu_0} \quad (3.24)$$

and, the coefficients R_0, R_{-T}, T_0 are chosen to satisfy the boundary conditions

$$\mathbf{E}_{II} \times \hat{z} = 0 \qquad \text{at } z = -T \quad (3.25)$$

$$\mathbf{E}_{II} \times \hat{z} = \mathbf{E}_I \times \hat{n} \quad \text{at } z = 0 \quad (3.26)$$

$$\mathbf{H}_{II} \times \hat{z} = \mathbf{H}_I \times \hat{n} \quad \text{at } z = 0 \quad (3.27)$$

where the subscript denotes the region in which the field is defined. The **E** and **H** fields of the vector magnetic potential can be found from

$$\mathbf{H} = \nabla \times \mathbf{A} \quad (3.28)$$

$$\mathbf{E} = \frac{1}{j\omega\epsilon} \left(\nabla^2 + \kappa^2 \right) \mathbf{A} \quad (3.29)$$

where (ϵ, κ) are (ϵ_0, κ_0) for Region I and (ϵ_2, κ_2) for Region II. Substituting Equations (3.19) - (3.21) into Equations (3.28) - (3.29) and applying the boundary conditions defined by Equations (3.25) - (3.27), the vector magnetic potential of a vertical current of infinitesimal length located in Region II becomes, for $-T \leq z \leq z'$,

$$A_z = \frac{-I dz'}{j2\pi} \int_0^\infty \frac{J_0(\beta\rho)}{\gamma_{z2}} \left[e^{-j\gamma_{z2}z'} + X_M \cos \gamma_{z2}(z' + T) \right]$$
$$e^{-j\gamma_{z2}T} \cos \gamma_{z2}(z + T) \beta \, d\beta \quad (3.30)$$

41

and for $z' \leq z \leq 0$,

$$A_z = \frac{-Idz'}{j2\pi} \int_0^\infty \frac{J_0(\beta\rho)}{\gamma_{z2}} \left[e^{-J\gamma_{z2}z} + X_M \cos\gamma_{z2}(z+T) \right]$$
$$e^{-J\gamma_{z2}T} \cos\gamma_{z2}(z'+T)\beta \, d\beta \tag{3.31}$$

and for $z \geq 0$,

$$A_z = \frac{-Idz'}{j2\pi} \int_0^\infty J_0(\beta\rho)\frac{\epsilon_0}{D_M} \cos\gamma_{z2}(z'+T)e^{-J\gamma_{z1}z}\beta \, d\beta \tag{3.32}$$

where

$$X_M = \frac{\epsilon_0\gamma_{z2} - \epsilon_2\gamma_{z1}}{D_M} \tag{3.33}$$

$$D_M = \epsilon_2\gamma_{z1} \cos\gamma_{z2}T + J\epsilon_0\gamma_{z2} \sin\gamma_{z2}T. \tag{3.34}$$

If the vertical current of infinitesimal length is located in Region I at a point $(\rho = 0, z = z')$, the vector magnetic potential can be written as, for $-T \leq z \leq 0$,

$$A_z = \frac{Idz'}{j4\pi} \int_0^\infty \frac{J_0(\beta\rho)}{\gamma_{z1}} \left[T_0' e^{J\gamma_{z2}z} + R'_{-T}e^{-J\gamma_{z2}(z+T)} \right] \beta \, d\beta \tag{3.35}$$

and for $0 \leq z \leq z'$,

$$A_z = \frac{Idz'}{j4\pi} \int_0^\infty \frac{J_0(\beta\rho)}{\gamma_{z1}} \left[e^{J\gamma_{z1}(z-z')} + R_0'e^{-J\gamma_{z1}z} \right] \beta \, d\beta \tag{3.36}$$

and for $z' \leq z$,

$$A_z = \frac{Idz'}{j4\pi} \int_0^\infty \frac{J_0(\beta\rho)}{\gamma_{z1}} \left[e^{-J\gamma_{z1}(z-z')} + R_0'e^{-J\gamma_{z1}z} \right] \beta \, d\beta \tag{3.37}$$

where the coefficients R'_{-T}, R_0', and T_0' are solved for by substituting Equations (3.35) - (3.37) into Equations (3.28) - (3.29) and applying the boundary conditions of Equations (3.25) - (3.27). The vector magnetic potential for a infinitesimal vertical current element in Region I is, for $-T \leq z \leq 0$,

$$A_z = \frac{Idz'}{j2\pi} \int_0^\infty J_0(\beta\rho)\frac{\epsilon_2}{D_M} e^{-J\gamma_{z1}z'} \cos\gamma_{z2}(z+T)\beta \, d\beta \tag{3.38}$$

and for $0 \leq z \leq z'$,

$$A_z = \frac{Idz'}{j2\pi} \int_0^\infty \frac{J_0(\beta\rho)}{\gamma_{z1}D_M} [\epsilon_2\gamma_{z1} \cos \gamma_{z2}T \cos \gamma_{z1}z -$$

$$\epsilon_0\gamma_{z2} \sin \gamma_{z2}T \sin \gamma_{z2}z] e^{-j\gamma_{z1}z'} \beta \, d\beta \qquad (3.39)$$

and for $z' \leq z$,

$$A_z = \frac{Idz'}{j2\pi} \int_0^\infty \frac{J_0(\beta\rho)}{\gamma_{z1}D_M} \left[\epsilon_2\gamma_{z1} \cos \gamma_{z2}T \cos \gamma_{z1}z' -\right.$$

$$\left. \epsilon_0\gamma_{z2} \sin \gamma_{z2}T \sin \gamma_{z2}z'\right] e^{-j\gamma_{z1}z} \beta \, d\beta. \qquad (3.40)$$

In general, the vector magnetic potential of an infinitesimal vertical current element located in either Region I or Region II can be written as

$$A_z = \frac{Idz'}{j2\pi} \int_0^\infty h(\beta,\rho)f(\beta,z')g(\beta,z) \, d\beta. \qquad (3.41)$$

The functions f and g are harmonic functions of z' and z respectively. Their second derivative with respect to z' or z is

$$\frac{\partial^2}{\partial z'^2}f = -\gamma^2 f \qquad (3.42)$$

$$\frac{\partial^2}{\partial z^2}g = -\gamma^2 g \qquad (3.43)$$

where $\gamma = \gamma_{z1}$ for f or g in Region I and $\gamma = \gamma_{z2}$ for f or g in Region II.

Now that the vector magnetic potential for an infinitesimal vertical current element is known, the vector magnetic potential for a current of finite length can be found. If a filamentary vertical current $I(z')$ exists between z_1 and z_2, the vector magnetic potential is found by integrating the product of $I(z')$ and the appropriate vector magnetic potential for an infinitesimal current element with respect to z' between z_1 and z_2. Although the current can be continuous through the Region I - Region II interface, it will be analyzed in terms of the sections that wholly exist in either Region I or Region II. The expressions generated for the vector magnetic

potential of the vertical current will have both z_1 and z_2 lie in either Region I or Region II.

The general form of the vector magnetic potential of a vertical filamentary current is given by Equation (3.41). The form of the expression depends on the location of z. For $z \leq z_1 < z_2$, the general equation can be written as

$$A_z = \frac{1}{j2\pi} \int_0^\infty h(\beta,\rho) g_L(\beta,z) \int_{z_1}^{z_2} I(z') f_L(\beta,z') \, dz' \, d\beta \qquad (3.44)$$

and for $z_1 < z_2 \leq z$,

$$A_z = \frac{1}{j2\pi} \int_0^\infty h(\beta,\rho) g_U(\beta,z) \int_{z_1}^{z_2} I(z') f_U(\beta,z') \, dz' \, d\beta \qquad (3.45)$$

and for $z_1 \leq z \leq z_2$, the general equation is written as

$$
\begin{aligned}
A_z = \quad & \frac{1}{j2\pi} \int_0^\infty h(\beta,\rho) \left[g_U(\beta,z) \int_{z_1}^z I(z') f_U(\beta,z') \, dz' \right. \\
& + \left. g_L(\beta,z) \int_z^{z_2} I(z') f_L(\beta,z') \, dz' \right] d\beta.
\end{aligned}
\qquad (3.46)
$$

where the L subscript indicates that the f and g for $z \leq z'$ is used and the subscript U indicates that the f and g for $z \geq z'$ is used. With the restriction that z_1 and z_2 are both in the same region and by examining Equations (3.30) - (3.31) and (3.39) - (3.40) it is seen that the following relationship exists between $f_U, g_U, f_L,$ and g_L.

$$f_U(\beta,z') = g_L(\beta,z') = g(\beta,z') \qquad (3.47)$$

$$g_U(\beta,z) = f_L(\beta,z) = f(\beta,z) \cdot \qquad (3.48)$$

These relationships are a result of reciprocity and allow Equations (3.44) - (3.46) to be written as

$$A_z = \frac{1}{j2\pi} \int_0^\infty h(\beta,\rho) g(\beta,z) \int_{z_1}^{z_2} I(z') f(\beta,z') \, dz' \, d\beta \qquad (3.49)$$

44

$$A_z = \frac{1}{j2\pi} \int_0^\infty h(\beta,\rho) f(\beta,z) \int_{z_1}^{z_2} I(z')g(\beta,z')\,dz'\,d\beta \tag{3.50}$$

$$
\begin{aligned}
A_z &= \frac{1}{j2\pi} \int_0^\infty h(\beta,\rho) \left[f(\beta,z) \int_{z_1}^{z} I(z')g(\beta,z')\,dz' \right.\\
&\quad + \left. g(\beta,z) \int_{z}^{z_2} I(z')f(\beta,z')\,dz' \right] d\beta.
\end{aligned}
\tag{3.51}
$$

In order to find the impedance matrix elements for the thin vertical wire, the $\hat{z}$ directed electric field is needed. From Equation (3.29), the E_z field from $\hat{z}$ directed vector magnetic potential is

$$E_z = \frac{1}{j\omega\epsilon} \left(\frac{\partial^2}{\partial z^2} + \kappa^2 \right) A_z. \tag{3.52}$$

Using Equations (3.49) - (3.52), the general expressions for the E_z fields can be written. For $z \leq z_1 < z_2$,

$$E_z = \frac{-1}{2\pi\omega\epsilon} \int_0^\infty h(\beta,\rho) g(\beta,z) \int_{z_1}^{z_2} I(z')f(\beta,z')\,dz'\,\beta^3\,d\beta \tag{3.53}$$

and $z_1 < z_2 \leq z$

$$E_z = \frac{-1}{2\pi\omega\epsilon} \int_0^\infty h(\beta,\rho) f(\beta,z) \int_{z_1}^{z_2} I(z')g(\beta,z')\,dz'\,\beta^3\,d\beta \tag{3.54}$$

and for $z_1 \leq z \leq z_2$,

$$
\begin{aligned}
E_z &= \frac{-1}{2\pi\omega\epsilon} \int_0^\infty h(\beta,\rho) \left[\beta^2 \left(f(\beta,z) \int_{z_1}^{z} I(z')g(\beta,z')dz' \right.\right.\\
&\quad + \left. g(\beta,z) \int_{z}^{z_2} I(z')f(\beta,z')\,dz' \right) + \left(\frac{\partial f(\beta,z)}{\partial z} g(\beta,z) \right.\\
&\quad - \left.\left. \frac{\partial g(\beta,z)}{\partial z} f(\beta,z) \right) I(z) \right] \beta\,d\beta.
\end{aligned}
\tag{3.55}
$$

By examining Equations (3.30) - (3.32), the appropriate h, f, and g can be determined to write the E_{zn} field equations for a vertical filamentary wire located in Region II with mode current I_n^S and end points z_{n1} and z_{n2}. For $-T \leq z \leq z_{n1}$,

$$E_{zn} = \frac{-1}{2\pi\omega\epsilon_2} \int_0^\infty \frac{J_0(\beta\rho)}{\gamma_{z2}} e^{-j\gamma_{z2}T} \cos\gamma_{z2}(z+T)\tilde{F}_2(z_{n1},z_{n2},I_n^S)\beta^3\,d\beta \tag{3.56}$$

45

and for $z_{n1} \leq z \leq z_{n2}$,

$$E_{zn} = \frac{-1}{2\pi\omega\epsilon_2} \int_0^\infty \frac{J_0(\beta\rho)}{\gamma_{z2}} e^{-\jmath\gamma_{z2}T} \left[\beta^2 \left(e^{-\jmath\gamma_{z2}z} + X_M \cos\gamma_{z2}(z+T) \right) \right.$$
$$\tilde{G}_2(z_{n1}, z, I_n^S) + \beta^2 \cos\gamma_{z2}(z+T)\tilde{F}_2(z, z_{n2}, I_n^S)$$
$$\left. - \jmath\gamma_{z2}I_n^S \right] \beta \, d\beta \tag{3.57}$$

and for $z_{n1} \leq z_{n2} \leq z \leq 0$,

$$E_{zn} = \frac{-1}{2\pi\omega\epsilon_2} \int_0^\infty \frac{J_0(\beta\rho)}{\gamma_{z2}} e^{-\jmath\gamma_{z2}T} \left[e^{-\jmath\gamma_{z2}z} + X_M \cos\gamma_{z2}(z+T) \right]$$
$$\tilde{G}_2(z_{n1}, z_{n2}, I_n^S)\beta^3 \, d\beta \tag{3.58}$$

and for $z \geq 0$,

$$E_{zn} = \frac{-1}{2\pi\omega} \int_0^\infty \frac{J_0(\beta\rho)}{D_M} e^{-\jmath\gamma_{z1}z} \tilde{G}_2(z_{n1}, z_{n2}, I_n^S) \beta^3 \, d\beta \tag{3.59}$$

where

$$\tilde{F}_2(x_1, x_2, i) = \int_{x_1}^{x_2} \left[e^{-\jmath\gamma_{z2}x} + X_M \cos\gamma_{z2}(x+T) \right] i(x) \, dx \tag{3.60}$$

$$\tilde{G}_2(x_1, x_2, i) = \int_{x_1}^{x_2} \cos\gamma_{z2}(x+T)i(x) \, dx. \tag{3.61}$$

From Equations (3.38) - (3.40), the h, f, and g for a vertical filamentery current in Region I can be determined and the E_z can be written for a mode current I_n^S with endpoints at z_{n1} and z_{n2}. For $-T \leq z \leq 0$,

$$E_{zn} = \frac{-1}{2\pi\omega} \int_0^\infty \frac{J_0(\beta\rho)}{D_M} \cos\gamma_{z2}(z+T)\tilde{F}_1(z_{n1}, z_{n2}, I_n^S)\beta^3 \, d\beta \tag{3.62}$$

and for $0 \leq z \leq z_{n1} < z_{n2}$,

$$E_{zn} = \frac{-1}{2\pi\omega\epsilon_0} \int_0^\infty \frac{J_0(\beta\rho)}{\gamma_{z1}D_M} [\epsilon_2\gamma_{z1} \cos\gamma_{z2}T \cos\gamma_{z1}z$$
$$- \epsilon_0\gamma_{z2} \sin\gamma_{z2}T \sin\gamma_{z1}z] \tilde{F}_1(z_{n1}, z_{n2}, I_n^S)\beta^3 \, d\beta \tag{3.63}$$

46

and for $z_{n1} \leq z \leq z_{n2}$,

$$
\begin{aligned}
E_{zn} &= \frac{-1}{2\pi\omega\epsilon_0} \int_0^\infty \frac{J_0(\beta\rho)}{\gamma_{z1}D_M} \left(\beta^2 e^{-\jmath\gamma_{z1}z} \tilde{G}_1(z_{n1}, z, I_n^S) \right. \\
&\quad + \beta^2 [\epsilon_2\gamma_{z1} \cos\gamma_{z2}T \cos\gamma_{z1}z - \epsilon_0\gamma_{z2} \sin\gamma_{z2}T \sin\gamma_{z1}z] \\
&\quad \left. \tilde{F}_1(z, z_{n2}, I_n^S) - \jmath\gamma_{z1}D_M I_n^S(z) \right) \beta \, d\beta
\end{aligned}
\tag{3.64}
$$

and for $z_{n1} \leq z_{n2} \leq z$,

$$
E_{zn} = \frac{-1}{2\pi\omega\epsilon_0} \int_0^\infty \frac{J_0(\beta\rho)}{\gamma_{z1}D_M} e^{-\jmath\gamma_{z1}z} \tilde{G}_1(z_{n1}, z_{n2}, I_n^S) \beta^3 \, d\beta
\tag{3.65}
$$

where

$$
\tilde{F}_1(x_1, x_2, i) = \int_{x_1}^{x_2} e^{-\jmath\gamma_{z1}x} i(x) \, dx
\tag{3.66}
$$

$$
\begin{aligned}
\tilde{G}_1(x_1, x_2, i) = \int_{x_1}^{x_2} &[\epsilon_2\gamma_{z1} \cos\gamma_{z2}T \cos\gamma_{z1}x \\
&- \epsilon_0\gamma_{z2} \sin\gamma_{z2}T \sin\gamma_{z1}x] \, i(x) \, dx.
\end{aligned}
\tag{3.67}
$$

With the integral expressions for the E_{nz} field of a vertical filamentary modes in either Region I or Region II, the impedance matrix elements can be obtained using Equation (3.12). The self impedance of a thin wire of radius a will be modeled as the mutual impedance between two filaments of equal length separated by $\rho = a$. Therefore, the expressions for the impedance matrix elements will be given for two modes separated in the ρ dimension by the distance a. In order to simplify the expressions for the elements of the impedance matrix, an I_m^S mode will be required to exist entirely in either Region I or Region II. This is the same requirement placed on an I_n^S mode in the development of the E_{zn} expressions. The impedance matrix element expressions are given for the different locations that an I_n^S mode and an I_m^S mode can have in the z dimension. For an n mode and an m mode both located in Region II with $z_{m2} \leq z_{n1}$,

$$
Z_{mn} = \frac{1}{2\pi\omega\epsilon_2} \int_0^\infty \frac{J_0(\beta a)}{\gamma_{z2}} e^{-\jmath\gamma_{z2}T} \tilde{G}_2(z_{m1}, z_{m2}, I_m^S) \tilde{F}_2(z_{n1}, z_{n2}, I_n^S) \beta^3 \, d\beta
\tag{3.68}
$$

47

and for $z_{n1} = z_{m1}$ and $z_{n2} = z_{m2}$, both the n and m modes in Region II,

$$
\begin{aligned}
Z_{mn} = {} & \frac{1}{2\pi\omega\epsilon_2} \int_0^\infty \frac{J_0(\beta a)}{\gamma_{z2}} e^{-j\gamma_{z2}T} \int_{z_{m1}}^{z_{m2}} \Big[\beta^2 \left(e^{-j\gamma_{z2}z} + X_M \cos\gamma_{z2}(z+T) \right) \\
& \tilde{G}_2(z_{n1}, z, I_n^S) + \beta^2 \cos\gamma_{z2}(z+T) \tilde{F}_2(z, z_{n2}, I_n^S) \\
& - j\gamma_{z2}I_n^S \Big] I_m^S(z)\, dz\, \beta\, d\beta
\end{aligned}
\tag{3.69}
$$

and for $z_{n2} \leq z_{m1}$, the n and m modes in Region II,

$$
Z_{mn} = \frac{1}{2\pi\omega\epsilon_2} \int_0^\infty \frac{J_0(\beta a)}{\gamma_{z2}} e^{-j\gamma_{z2}T} \tilde{F}_2(z_{m1}, z_{m2}, I_m^S) \tilde{G}_2(z_{n1}, z_{n2}, I_n^S) \beta^3\, d\beta
\tag{3.70}
$$

and for mode n in Region II and mode m in Region I,

$$
Z_{mn} = \frac{1}{2\pi\omega} \int_0^\infty \frac{J_0(\beta a)}{D_M} \tilde{F}_1(z_{m1}, z_{m2}, I_m^S) \tilde{G}_2(z_{n1}, z_{n2}, I_n^S) \beta^3\, d\beta.
\tag{3.71}
$$

For mode n in Region I and mode m in Region II,

$$
Z_{mn} = \frac{1}{2\pi\omega} \int_0^\infty \frac{J_0(\beta a)}{D_M} \tilde{F}_1(z_{n1}, z_{n2}, I_n^S) \tilde{G}_2(z_{m1}, z_{m2}, I_m^S) \beta^3\, d\beta
\tag{3.72}
$$

and for both mode n and mode m in Region I with $z_{m2} \leq z_{n1}$,

$$
Z_{mn} = \frac{1}{2\pi\omega\epsilon_0} \int_0^\infty \frac{J_0(\beta a)}{\gamma_{z1}D_M} \tilde{F}_1(z_{n1}, z_{n2}, I_n^S) \tilde{G}_1(z_{m1}, z_{m2}, I_m^S) \beta^3\, d\beta
\tag{3.73}
$$

and for $z_{m1} = z_{n1}$ and $z_{m2} = z_{n2}$, both modes n and m in Region I,

$$
\begin{aligned}
Z_{mn} = {} & \frac{1}{2\pi\omega\epsilon_0} \int_0^\infty \frac{J_0(\beta a)}{\gamma_{z1}D_M} \int_{z_{m1}}^{z_{m2}} \Big(\beta^2 e^{-j\gamma_{z1}z} \tilde{G}_1(z_{n1}, z, I_n^S) \\
& + \beta^2 [\epsilon_2\gamma_{z1} \cos\gamma_{z2}T \cos\gamma_{z1}z - \epsilon_0\gamma_{z2} \sin\gamma_{z2}T \sin\gamma_{z1}z] \\
& \tilde{F}_1(z, z_{n1}, I_n^S) - j\gamma_{z1}D_M I_n^S(z) \Big) I_m^S(z)\, dz\, \beta\, d\beta
\end{aligned}
\tag{3.74}
$$

and for $z_{n2} \leq z_{m1}$, both modes n and m in Region I,

$$
Z_{mn} = \frac{1}{2\pi\omega\epsilon_0} \int_0^\infty \frac{J_0(\beta a)}{\gamma_{z1}D_M} \tilde{G}_1(z_{n1}, z_{n2}, I_n^S) \tilde{F}_1(z_{m1}, z_{m2}, I_m^S) \beta^3\, d\beta.
\tag{3.75}
$$

The impedance matrix elements of Equations (3.68) - (3.75) can also describe the mutual impedance between two filamentary vertical currents. If the distance

between the two filamentary currents is ρ_0, replacing the radius a with ρ_0 in the preceding impedance matrix element expressions will define the impedance matrix element expressions for the mutual impedance.

3.5   Evaluation for the Voltage Vector

The wire will be excited by the so-called delta gap generator [19] at $z = -T$. Using this model, the incident electric field of a V_0 volt delta gap generator is given by

$$\mathbf{E}^i = \hat{z} V_0 \delta(z + T). \tag{3.76}$$

Substituting Equation (3.76) into Equation (3.13) results in the expression for the voltage vector elements.

$$V_m = V_0 I_m^S(-T) \tag{3.77}$$

Equation (3.77) shows that V_m will be nonzero only if the weighting function I_m^S is nonzero at $z = -T$.

3.6   Expansion and Weighting Functions

Now that the general equations of the impedance matrix and voltage vector elements are defined, the expansion functions for I_n^S and the weighting functions for I_m^S will be defined. The wire will be broken into N segments called monopoles. Figure 14a shows a vertical wire divided into four segments. There will be N modes on the wire, all but one consisting of two monopoles to form a dipole. The monopole directly over the ground plane is one mode since its image in the ground plane makes it an equivalent dipole. Figure 14b shows the dipole modes formed by the four monopole segments on the wire. The functions $\tilde{F}$ and $\tilde{G}$ will be evaluated for each region using an arbitrary monopole. The expressions for the

49

electric field at a point between the endpoints of a monopole and the impedance matrix elements for overlapping monopoles will be evaluated.

The vertical wire is broken into a N segments. Figure 14a shows a vertical wire on a dielectric coated ground plane broken into four segments. These segments have a piecewise sinusoidal function associated with them and are referred to as monopoles. The piecewise sinusoidal function is described by

$$i_1(z) = \begin{cases} \frac{\sin \kappa_d(z_2 - z)}{\sin \kappa_d \Delta z} & \text{for } z_1 \leq z \leq z_2 \\ 0 & \text{elsewhere} \end{cases} \tag{3.78}$$

or

$$i_2(z) = \begin{cases} \frac{\sin \kappa_d(z - z_1)}{\sin \kappa_d \Delta z} & \text{for } z_1 \leq z \leq z_2 \\ 0 & \text{elsewhere} \end{cases} \tag{3.79}$$

where

$$\kappa_d = \begin{cases} \kappa_0 & \text{for Region } I \\ \kappa_2 & \text{for Region } II \end{cases} \tag{3.80}$$
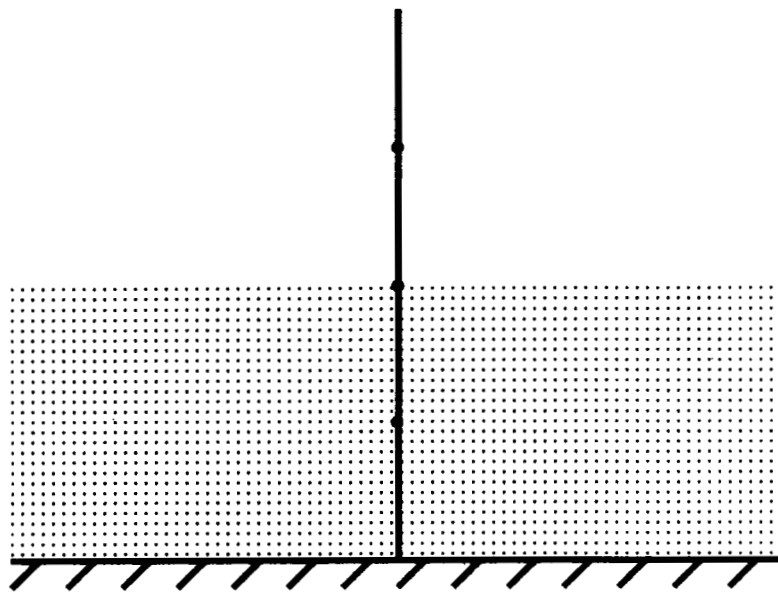
$$\Delta z = z_2 - z_1 \tag{3.81}$$

$$\kappa_d \Delta z \leq \frac{\pi}{2}. \tag{3.82}$$

The $\tilde{F}$ and $\tilde{G}$ functions shown in the integrands of Equations (3.56), (3.58), (3.59), (3.62), (3.63), and (3.65) are obtained for the monopoles of Equations (3.78) and (3.79) between points z_1 and z_2. For the i_1 function,

$$\tilde{F}_1 = \frac{1}{\beta^2 \sin \kappa_0 \Delta z} \left(\kappa_0 e^{-J\gamma_{z1} z_2} - [-J\gamma_{z1} \sin \kappa_0 \Delta z + \kappa_0 \cos \kappa_0 \Delta z] e^{-J\gamma_{z1} z_1} \right) \tag{3.83}$$

$$\tilde{G}_1 = \frac{1}{\beta^2 \sin \kappa_0 \Delta z} \left(\epsilon_2 \gamma_{z2} \cos \gamma_{z2} T \left[\kappa_0 \left(\cos \gamma_{z1} z_2 - \cos \gamma_{z1} z_1 \cos \kappa_0 \Delta z \right) \right.\right.$$

$$+ \left. \gamma_{z1} \sin \gamma_{z1} z_1 \sin \kappa_0 \Delta z \right]$$

$$+ \epsilon_0 \gamma_{z2} \sin \gamma_{z2} T \left[\kappa_0 \left(\sin \gamma_{z1} z_2 - \sin \gamma_{z1} z_1 \cos \kappa_0 \Delta z \right) \right.$$

a) A vertical wire through a grounded dielectric substrate broken into four segments.
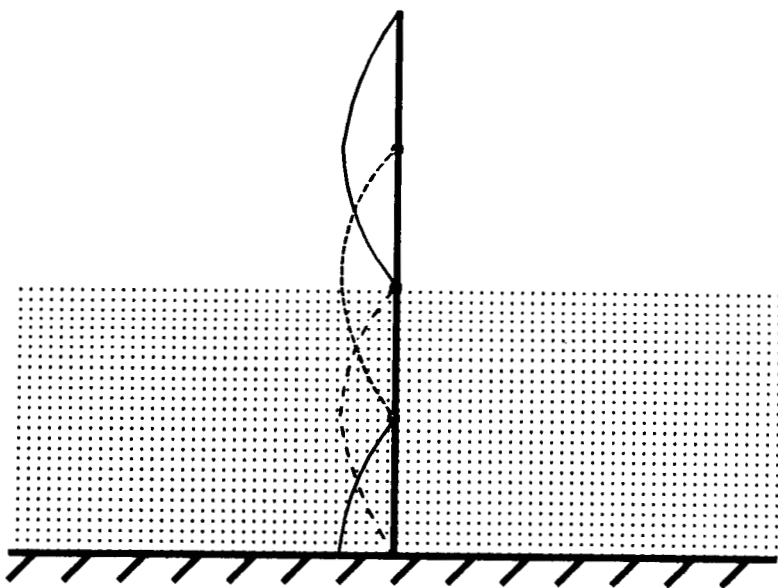
b) The piecewise sinusoidal functions on each segment to construct the MM modes.

Figure 14: An example of a MM modal model for a vertical wire through a grounded dielectric substrate.

51

$$- \quad \gamma_{z1} \cos \gamma_{z1} z_1 \sin \kappa_0 \Delta z]) \qquad (3.84)$$

$$\begin{aligned}
\bar{F}_2 &= \frac{1}{\beta^2 \sin \kappa_2 \Delta z} \left(\kappa_2 \left[e^{-J\gamma_{z2} z_2} - \cos \kappa_2 \Delta z e^{-J\gamma_{z2} z_1} \right] \right. \\
&\quad - \quad J\gamma_{z2} \sin \kappa_2 \Delta z e^{-J\gamma_{z2} z_1} \\
&\quad + \quad X_M \left[\kappa_2 \left(\cos \gamma_{z2}(z_2 + T) - \cos \kappa_2 \Delta z \cos \gamma_{z2}(z_1 + T) \right) \right. \\
&\quad + \quad \left. \left. \gamma_{z2} \sin \kappa_2 \Delta z \sin \gamma_{z2}(z_1 + T) \right] \right) \qquad (3.85)
\end{aligned}$$

$$\begin{aligned}
\bar{G}_2 &= \frac{1}{\beta^2 \sin \kappa_2 \Delta z} \left(\kappa_2 \left[\cos \gamma_{z2}(z_2 + T) - \cos \kappa_2 \Delta z \cos \gamma_{z2}(z_1 + T) \right] \right. \\
&\quad + \quad \left. \gamma_{z2} \sin \kappa_2 \Delta z \sin \gamma_{z2}(z_1 + T) \right) \qquad (3.86)
\end{aligned}$$

and for the i_2 segment function,

$$\bar{F}_1 = \frac{1}{\beta^2 \sin \kappa_0 \Delta z} \left(\kappa_0 e^{-J\gamma_{z1} z_1} - [J\gamma_{z1} \sin \kappa_0 \Delta z + \kappa_0 \cos \kappa_0 \Delta z] e^{-J\gamma_{z1} z_2} \right) \quad (3.87)$$

$$\begin{aligned}
\bar{G}_1 &= \frac{1}{\beta^2 \sin \kappa_0 \Delta z} \left(\epsilon_2 \gamma_{z1} \cos \gamma_{z2} T \left[\kappa_0 \left(\cos \gamma_{z1} z_1 - \cos \gamma_{z1} z_2 \cos \kappa_0 \Delta z \right) \right. \right. \\
&\quad - \quad \left. \gamma_{z1} \sin \gamma_{z1} z_2 \sin \kappa_0 \Delta z \right] \\
&\quad + \quad \epsilon_0 \gamma_{z2} \sin \gamma_{z2} T \left[\kappa_0 \left(\sin \gamma_{z1} z_1 - \sin \gamma_{z1} z_2 \cos \kappa_0 \Delta z \right) \right. \\
&\quad + \quad \left. \left. \gamma_{z1} \cos \gamma_{z1} z_2 \sin \kappa_0 \Delta z \right] \right) \qquad (3.88)
\end{aligned}$$

$$\begin{aligned}
\bar{F}_2 &= \frac{1}{\beta^2 \sin \kappa_2 \Delta z} \left(\kappa_2 \left[e^{-J\gamma_{z2} z_1} - \cos \kappa_2 \Delta z e^{-J\gamma_{z2} z_2} \right] \right. \\
&\quad + \quad J\gamma_{z2} \sin \kappa_2 \Delta z e^{-J\gamma_{z2} z_2} \\
&\quad + \quad X_M \left[\kappa_2 \left(\cos \gamma_{z2}(z_1 + T) - \cos \kappa_2 \Delta z \cos \gamma_{z2}(z_2 + T) \right) \right. \\
&\quad - \quad \left. \left. \gamma_{z2} \sin \kappa_2 \Delta z \sin \gamma_{z2}(z_2 + T) \right] \right) \qquad (3.89)
\end{aligned}$$

$$\begin{aligned}
\bar{G}_2 &= \frac{1}{\beta^2 \sin \kappa_2 \Delta z} \left(\kappa_2 \left[\cos \gamma_{z2}(z_1 + T) - \cos \kappa_2 \Delta z \cos \gamma_{z2}(z_2 + T) \right] \right. \\
&\quad - \quad \left. \gamma_{z2} \sin \kappa_2 \Delta z \sin \gamma_{z2}(z_2 + T) \right) . \qquad (3.90)
\end{aligned}$$

When a dipole is constructed from two monopoles, some terms in the $\bar{F}$ and $\bar{G}$ will cancel. These terms are due to the discontinuous current in the monopole. The first step for identifying terms that cancel is to determine the $\hat{z}$ directed electric field of a dipole. For this step the terms that cancel are called charge terms, since

the physical representation is a charge at the end of the monopole where the current is non zero. The integrand of the spectral integral for the E_z field of a $\hat{z}$ directed monopole consists of terms that have a $\beta^{-\frac{1}{2}}$ dependance and a $\beta^{\frac{1}{2}}$ dependance. When two monopoles are combined to form a dipole, all $\beta^{\frac{1}{2}}$ dependent terms are charge terms and cancel regardless of the position of the monopoles or the field point. Without removing the charge terms, the integrals of the monopole are non convergent. All of the charge terms are products with either γ_{z1} and $\sin \kappa_0 \Delta z$ in them for Region I or γ_{z2} and $\sin \kappa_2 \Delta z$ in them for Region II. As an example, for $\tilde{F}_1$ of the i_1 function, the charge term is $-j\gamma_{z1} \sin \kappa_0 \Delta z e^{-j\gamma_{z1} z_1}$ when $\tilde{F}_1$ is in the integral equation for the $\hat{z}$ directed electric field.

The last step in identifying terms that cancel requires the determination of the dipole to dipole impedance matrix element integral expressions. The terms that cancel from these expressions are of similar algebraic form as charge terms, and are called current discontinuity terms. Although the integrals will converge with the current discontinuity terms, removing them can decrease the convergence time of the numerical integration. The identification of the current discontinuity terms involves examining all possible dipole to dipole configurations. These configurations are dependent upon the z location of the monopoles.

In Equations (3.57) and (3.64), the $\tilde{F}$ and $\tilde{G}$ are functions of the z component of the field point. Evaluating $\tilde{F}$ and $\tilde{G}$ for the piecewise sinusoidal expansion function and expanding the part of the integrands in Equations (3.57) and (3.64) which are a function of z, the integrands can be simplified. For (3.57), the part of the integrand that contains the functions of z is

$$\beta^2 \left(e^{-j\gamma_{z2} z} + X_M \cos \gamma_{z2}(z + T) \right) \tilde{G}_2(z_{n1}, z, I_n^S)$$
$$+\beta^2 \cos \gamma_{z2}(z + T)\tilde{F}_2(z, z_{n2}, I_n^S) - j\gamma_{z2} I_n^S \tag{3.91}$$

Letting $I_n^S = i_1$, evaluating $\tilde{F}$ and $\tilde{G}$, and simplifying the result, Equation (3.91) becomes

$$\frac{1}{\sin \kappa_2 \Delta z} \left(e^{-J\gamma_{z2}z} \left[\gamma_{z2} \sin \gamma_{z2}(z_{n2} + T) - \kappa_2 \cos \gamma_{z2}(z_{n1} + T) \cos \kappa_2 \Delta z \right] \right.$$
$$\cos \gamma_{z2}(z + T) \left[\kappa_2 e^{-J\gamma_{z2}z_{n2}} + X_M \left(\kappa_2 \cos \gamma_{z2}(z_{n2} + T) \right. \right. \tag{3.92}$$
$$\left. \left. \left. + \gamma_{z2} \sin \gamma_{z2}(z_{n1} + T) \sin \kappa_2 \Delta z - \kappa_2 \cos \gamma_{z2}(z_{n1} + T) \cos \kappa_2 \Delta z \right) \right] \right)$$

Doing the same with $I_n^S = i_2$, Equation (3.91) becomes

$$\frac{1}{\sin \kappa_2 \Delta z} \left(e^{-J\gamma_{z2}z} \left[\kappa_2 \cos \gamma_{z2}(z_{n1} + T) \right] + \cos \gamma_{z2}(z + T) \left[(-J\gamma_{z2} \sin \kappa_2 \Delta z \right. \right.$$
$$\left. - \kappa_2 \cos \kappa_2 \Delta z \right) e^{-J\gamma_{z2}z_{n2}} + X_M \left(-\gamma_{z2} \sin \gamma_{z2}(z_{n2} + T) \sin \kappa_2 \Delta z \right.$$
$$\left. \left. \left. - \kappa_2 \cos \gamma_{z2}(z_{n2} + T) \cos \kappa_2 \Delta z + \kappa_2 \cos \gamma_{z2}(z_{n1} + T) \right) \right] \right)$$

$$\tag{3.93}$$

For Equation (3.64), the part of the integrand which contains functions of z is

$$\beta^2 e^{-J\gamma_{z1}z} \tilde{G}_1(z_{n1}, z, I_n^S) + \beta^2 \left[\epsilon_2 \gamma_{z1} \cos \gamma_{z2} T \cos \gamma_{z1} z \right.$$
$$\left. - \epsilon_0 \gamma_{z2} \sin \gamma_{z2} T \sin \gamma_{z1} z \right] \tilde{F}_1(z, z_{n2}, I_n^S) - J\gamma_{z1} D_M I_n^S \tag{3.94}$$

Letting $I_n^S = i_1$ and evaluating, Equation (3.94) becomes

$$\frac{1}{\sin \kappa_0 \Delta z} \left(e^{-J\gamma_{z1}z} \left[\epsilon_2 \gamma_{z1} \cos \gamma_{z2} T \left(-\kappa_0 \cos \gamma_{z1} z_{n1} \cos \kappa_0 \Delta z \right. \right. \right.$$
$$\left. + \gamma_{z1} \sin \gamma_{z1} z_{n1} \sin \kappa_0 \Delta z \right) - \epsilon_0 \gamma_{z2} \sin \gamma_{z2} T \left(-\kappa_0 \sin \gamma_{z1} z_{n1} \cos \kappa_0 \Delta z \right.$$
$$\left. \left. - \gamma_{z1} \cos \gamma_{z1} z_{n1} \sin \kappa_0 \Delta z \right) \right] + \left[\epsilon_2 \gamma_{z1} \cos \gamma_{z1} z \right. \tag{3.95}$$
$$\left. \left. - \epsilon_0 \gamma_{z2} \sin \gamma_{z1} z \right] \kappa_0 e^{-J\gamma_{z1}z_{n2}} \right)$$

Letting $I_n^S = i_2$, Equation (3.94) becomes

$$\frac{1}{\sin \kappa_0 \Delta z} \left(\kappa_0 e^{-J\gamma_{z1}z} \left[\epsilon_2 \gamma_{z1} \cos \gamma_{z2} T \cos \gamma_{z1} z_{n1} - \epsilon_0 \gamma_{z2} \sin \gamma_{z2} T \sin \gamma_{z1} z_{n1} \right] \right.$$
$$- \left[\epsilon_2 \gamma_{z1} \cos \gamma_{z2} T \cos \gamma_{z1} z - \epsilon_0 \gamma_{z2} \sin \gamma_{z2} T \sin \gamma_{z1} z \right] \left[\kappa_0 e^{-J\gamma_{z1}z_{n2}} \cos \kappa_0 \Delta z \right.$$
$$\left. \left. + J\gamma_{z1} e^{-J\gamma_{z1}z_{n2}} \sin \kappa_0 \Delta z \right] \right)$$

$$\tag{3.96}$$

Note that the charge terms in the above expressions are the terms that contain γ_{z1} and $\sin \kappa_0 \Delta z$ or or γ_{z2} and $\sin \kappa_2 \Delta z$.

By using Equations (3.92) - (3.93) in Equation (3.57) and applying this result to Equation (3.12), the integral expression for an impedance matrix element of overlapping piecewise sinusoidal monopoles with expansion mode I_n^S and weighting mode I_m^S can be written. For the monopoles in Region II and with $I_n^S = i_1$,

$$
\begin{aligned}
Z_{mn} = \ & \frac{1}{2\pi\omega\epsilon_2} \int_0^\infty \frac{J_0(\beta a)}{\gamma_{z2}\sin\kappa_2\Delta z} e^{-\jmath\gamma_{z2}T} \Big(\tilde{F}_0(z_{m1}, z_{m2}, I_m^S) \left[\gamma_{z2}\sin\gamma_{z2}(z_{n1}+T) \right. \\
& - \left. \kappa_2\cos\gamma_{z2}(z_{n1}+T)\cos\kappa_2\Delta z\right] + \tilde{G}_2(z_{m1}, z_{m2}, I_m^S) \left[\kappa_2 e^{-\jmath\gamma_{z2}z_{n2}}\right. \\
& + X_M \left(\kappa_2\cos\gamma_{z2}(z_{n2}+T) + \gamma_{z2}\sin\gamma_{z2}(z_{n1}+T)\sin\kappa_2\Delta z \right. \\
& - \left.\left.\kappa_2\cos\gamma_{z2}(z_{n1}+T)\cos\kappa_2\Delta z\right)\right] \Big)\, \beta\, d\beta.
\end{aligned}
\tag{3.97}
$$

For the monopoles in Region II with $I_n^S = i_2$,

$$
\begin{aligned}
Z_{mn} = \ & \frac{1}{2\pi\omega\epsilon_2} \int_0^\infty \frac{J_0(\beta a)}{\gamma_{z2}\sin\kappa_2\Delta z} e^{-\jmath\gamma_{z2}T} \Big(\tilde{F}_0(z_{m1}, z_{m2}, I_m^S) \left[\kappa_2\cos\gamma_{z2}(z_{n2}+T)\right] \\
& + \tilde{G}_2(z_{m1}, z_{m2}, I_m^S) \left[\left(-\jmath\gamma_{z2}\sin\kappa_2\Delta z - \kappa_2\cos\kappa_2\Delta z\right)e^{-\jmath\gamma_{z2}z_{n2}}\right. \\
& + X_M \left(\kappa_2\cos\gamma_{z2}(z_{n1}+T) - \gamma_{z2}\sin\gamma_{z2}(z_{n2}+T)\sin\kappa_2\Delta z \right. \\
& - \left.\left.\kappa_2\cos\gamma_{z2}(z_{n2}+T)\cos\kappa_2\Delta z\right)\right] \Big)\, \beta\, d\beta
\end{aligned}
\tag{3.98}
$$

where

$$
\tilde{F}_0(x_1, x_2, i) = \int_{x_1}^{x_2} e^{-\jmath\gamma_{z2}x} i(x)\, dx.
\tag{3.99}
$$

Note that $\tilde{F}_0$ is the same as $\tilde{F}_1$ with γ_{z1} replaced by γ_{z2}. For a piecewise sinusoidal monopole, the integral in Equation (3.99) can be obtained from Equations (3.83) and (3.87) by replacing γ_{z1} by γ_{z2} and κ_0 by κ_2. Using Equations (3.64) and (3.95) - (3.96) the impedance matrix element for overlapping monopoles in Region I becomes, with $I_n^S = i_1$,

$$
\begin{aligned}
Z_{mn} = \ & \frac{1}{2\pi\omega\epsilon_0} \int_0^\infty \frac{J_0(\beta a)}{\gamma_{z1}\sin\kappa_0\Delta z} \big(\left[\epsilon_0\gamma_{z2}\cos\gamma_{z2}T\left(\gamma_{z1}\sin\gamma_{z1}z_{n1}\sin\kappa_0\Delta z\right.\right. \\
& - \left.\kappa_0\cos\gamma_{z1}z_{n1}\cos\kappa_0\Delta z\right) + \epsilon_0\gamma_{z2}\sin\gamma_{z2}T\left(\kappa_0\sin\gamma_{z1}z_{n1}\cos\kappa_0\Delta z\right. \\
& + \left.\left.\gamma_{z1}\cos\gamma_{z1}z_{n1}\sin\kappa_0\Delta z\right)\right] \tilde{F}_1(z_{m1}, z_{m2}, I_m^S)
\end{aligned}
$$

$$+ \quad \kappa_0 \tilde{G}_1(z_{m1}, z_{m2}, I_m^S) e^{-J\gamma_{z1}z_{n2}} \Big) \beta \, d\beta. \tag{3.100}$$

For the monopoles in Region I with $I_n^S = i_2$,

$$
\begin{aligned}
Z_{mn} &= \frac{1}{2\pi\omega\epsilon_0} \int_0^\infty \frac{J_0(\beta a)}{\gamma_{z1} \sin \kappa_0 \Delta z} \Big(\tilde{F}_1(z_{m1}, z_{m2}, I_m^S) \kappa_0 \left[\epsilon_0 \gamma_{z2} \cos \gamma_{z2} T \cos \gamma_{z1} z_{n1} \right. \\
&\quad - \left. \epsilon_0 \gamma_{z2} \sin \gamma_{z2} T \sin \gamma_{z1} z_{n1} \right] + \tilde{G}_1(z_{m1}, z_{m2}, I_m^S) \left[\kappa_0 e^{-J\gamma_{z1}z_{n2}} \cos \kappa_0 \Delta z \right. \\
&\quad + \left. J\gamma_{z1} e^{-J\gamma_{z1}z_{n2}} \sin \kappa_0 \Delta z \right] \Big) \beta \, d\beta. \tag{3.101}
\end{aligned}
$$

3.7 Numerical Difficulties

The integrand for the Z_{mn} integrals are singular when D_M equals zero. The D_M singularities is due to the TM surface waves that exist on the dielectric coated ground plane. As the frequency increases, the number of surface wave poles can increase. For a lossless dielectric, these poles lie right on the $\text{Re}(\kappa)$ axis between κ_0, the propagation constant of Region I (in this problem, free space), and κ_2, the propagation constant of Region II. When the dielectric is lossy, the poles move into the fourth quadrant, but for low loss dielectrics, they are very close to the $\text{Re}(\kappa)$ axis. Figure 10 in Subsection 2.9.3 shows a map of the κ plane near the $\text{Re}(\kappa)$ axis, including a staggered contour which avoids the surface wave poles.

CHAPTER IV

NUMERICAL RESULTS

4.1 Introduction

This chapter compares calculated and measured input impedance and radar cross section (RCS) of unloaded and loaded rectangular patch microstrip antennas. The mutual impedance of vertical wires in a grounded dielectric substrate is compared to previously calculated data [21]. The first section will compare calculations to a compact range measurement of the RCS of a rectangular patch on a grounded dielectric substrate. A calculation will be made for input impedance of this patch when corner fed in order to show the modal relationship between RCS peaks and input impedance resonances. The patch will then be loaded near the corner with a 50 ohm load. The RCS measurement and calculation for the loaded microstrip patch will be compared. The next section will compare the calculation to the measurement for the input impedance of a microstrip antenna. This will include a wide band comparison and near resonance narrow band comparisons. The antenna will be loaded with a 50 ohm load near the corner and the input impedance calculation and measurement compared. Next, the calculation of the mutual impedance between two vertical thin wires imbedded in a grounded dielectric substrate will be compared to previously calculated data [21].
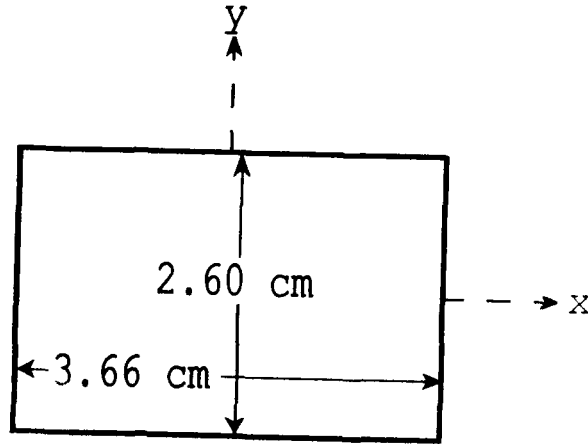
Figure 15: The rectangular microstrip antenna used for RCS calculation and measurement.

4.2 Plane Wave Scattering Results

This section will compare the MM computation for the radar cross section (RCS) of a microstrip patch to measurement. Figure 15 shows the geometry of the microstrip patch used for the unloaded RCS data. Figure 16 shows the geometry of the same patch with location of the vertical filament of current used for an input impedance calculation. Figure 17 shows the same patch used for loaded RCS data. The patch is loaded with 50 ohms for a comparison of calculated and measured RCS data. The measured patch was loaded through a coaxial feed.

The patch has dimensions of $2H = 3.66$ cm and $2W = 2.60$ cm. The substrate has thickness $T = 0.158$ cm, relative permittivity $\epsilon_r = 2.17$, and a loss tangent of 0.001. The incident plane wave has an angle of incidence of $(\theta_i, \phi_i) = (60°, 45°)$ and its electric field is $\hat{\theta}$ polarized. Figure 18 shows the RCS of the patch from 2 to 10 GHz. Figures 19 and 20 show the calculated real and imaginary parts of the input impedance of this patch over the same frequency range when excited by

58
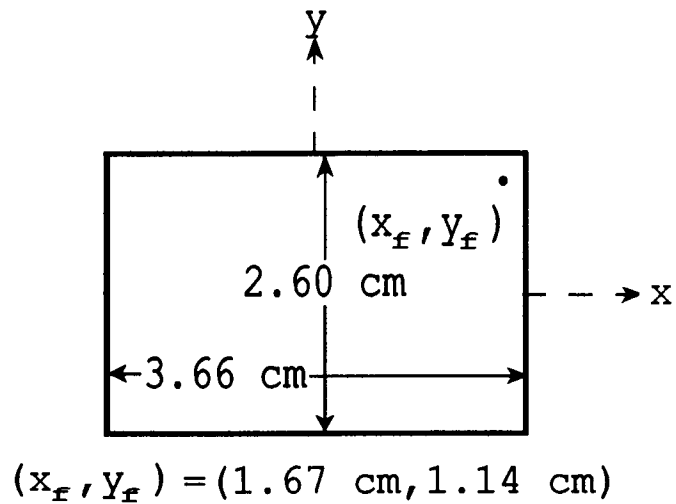
Figure 16: The rectangular microstrip antenna of Figure 15 with a feed port for input impedance calculation.
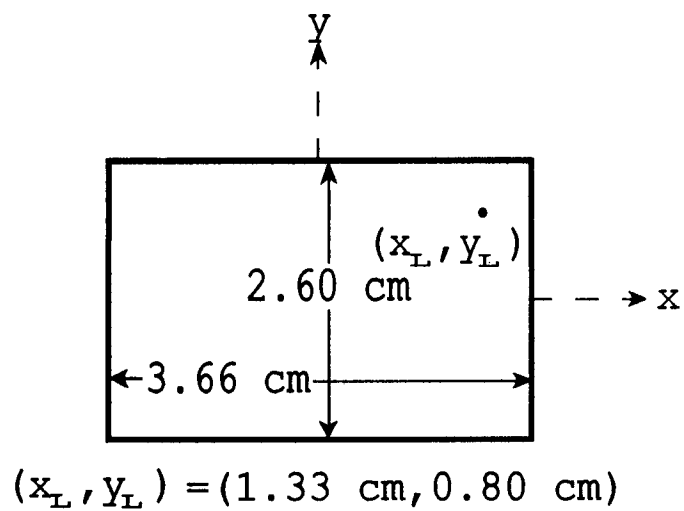
Figure 17: The rectangular microstrip antenna of Figure 15 loaded for RCS calculation and measurement.

a vertical current located at (x_f, y_f)=(1.60 cm,1.10 cm), which is very close to a corner of the patch. Figure 21 compares the wideband RCS of the same patch when loaded by 50 ohms at (x_L, y_L)=(1.33 cm,0.80 cm).

The MM computations of Figures 18 - 21 were made with $\Delta f_c = 400$ MHz (the frequency interval for impedance matrix and wire voltage vector computation) and $\Delta f_z = 5$ MHz (the frequency interval for the MM solution) [14]. The solid curves are the calculated data with the dots on Figure 18 representing the points where the impedance matrix has been calculated. The number of modes used to calculate the data of Figures 18 - 20 were 17 for the frequency range of 2 to 6 GHz and 31 from 6 to 10 GHz. Note that the changing of the number of modes causes a discontinuity at 6 GHZ for some of the calculated data. To test for convergence, the MM solution was run for 84 modes. The data was virtually the same. The total CPU time to calculate the data in Figure 18 was about 27 minutes on a VAX 11/780. The computation of the data in Figures 19 - 20 took about 30 minutes on a VAX 8550. For Figure 21, 4 modes were used to calculate the curve from 2 to 5 GHz, 12 modes from 5 to 7.5 GHz, and 24 modes from 7.5 GHz to 10 GHz. Discontinuities in the calculated data at 5 GHz and 7.5 GHz are due to changing the number of modes. The total CPU time to compute the data of Figure 21 was about 30 minutes on a VAX 8550.

Comparing Figures 18 - 20 shows that the same modes can be excited by both sources. The edge feed location was chosen to excite all modes in the displayed frequency range. Some of the peaks in the RCS and resonances in the input impedance are caused by a resonance of a single patch mode, others are caused by the mutual coupling between patch modes. This will be analyzed in more detail in Section 4.3.

60
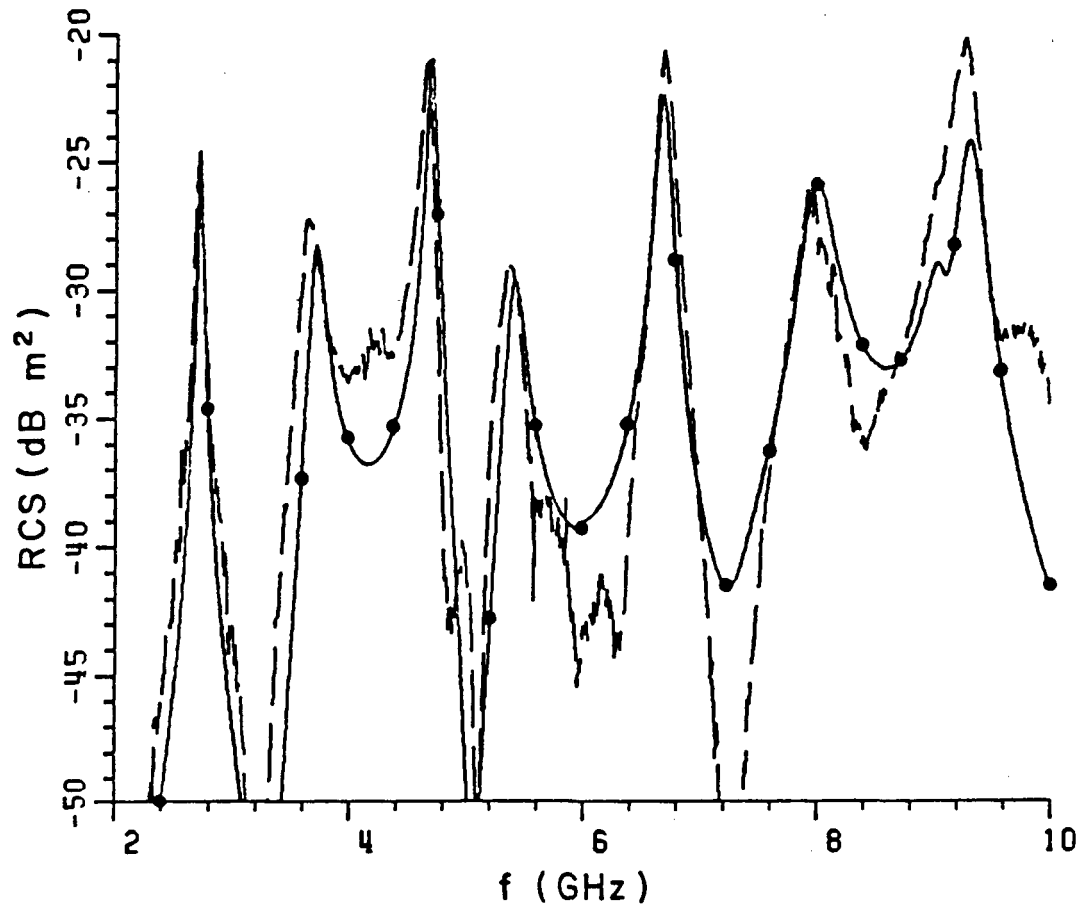
Figure 18: A comparison of the computed and measured theta polarized RCS of a rectangular patch on a grounded dielectric substrate.

2H=3.66cm 2W=2.60cm
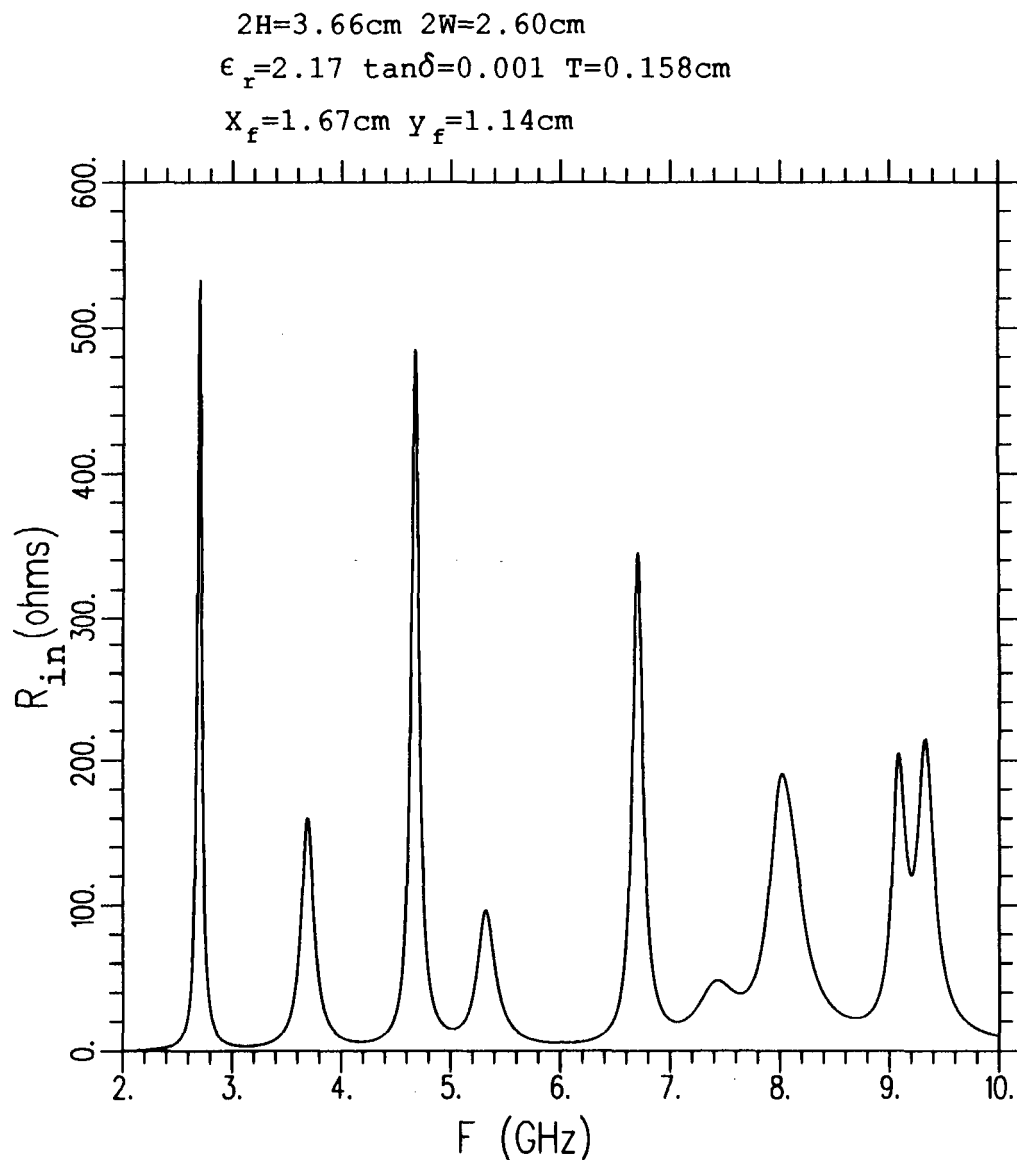
ϵ_r=2.17 tanδ=0.001 T=0.158cm

X_f=1.67cm y_f=1.14cm

Figure 19: A calculation of the real part of the input impedance for the microstrip antenna of Figure 16.

$2H=3.66cm$ $2W=2.6cm$
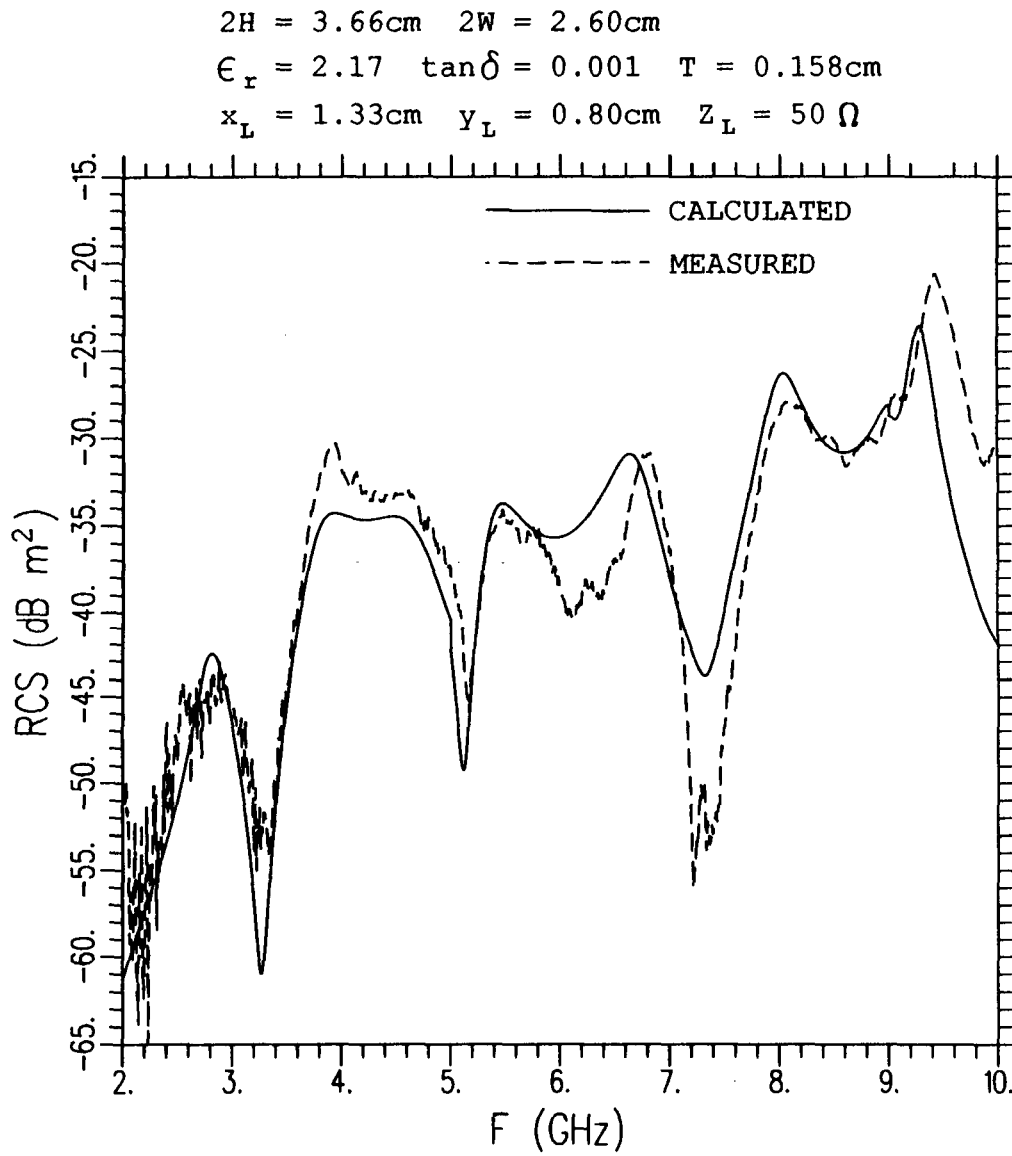$\epsilon_r=2.17$ $\tan\delta=0.001$ $T=0.158cm$
$x_f=1.67cm$ $y_f=1.14cm$
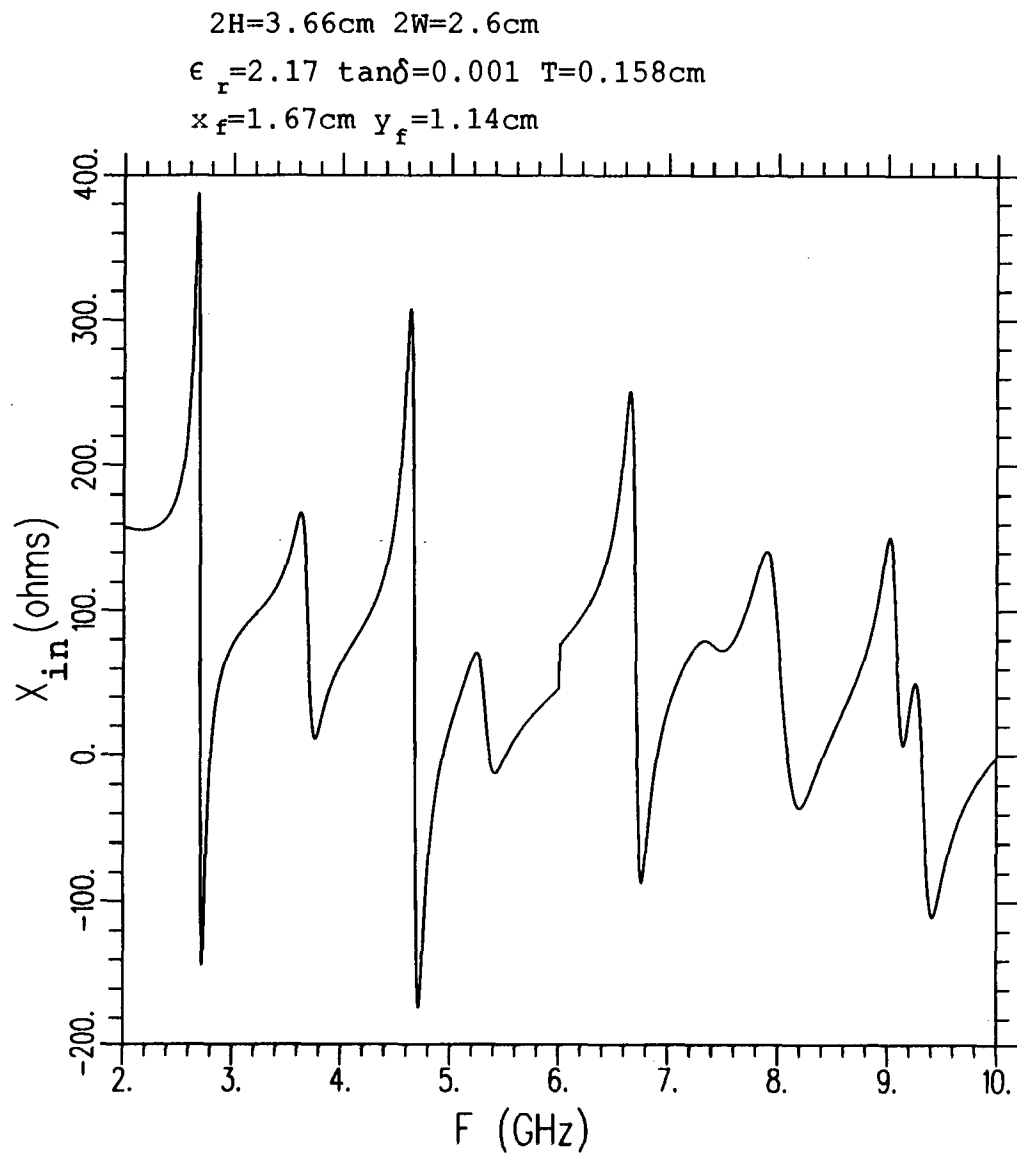
Figure 20: A calculation of the imaginary part of the input impedance for the microstrip antenna of Figure 16.

63

$2H = 3.66cm$ $2W = 2.60cm$
$\epsilon_r = 2.17$ $\tan\delta = 0.001$ $T = 0.158cm$
$x_L = 1.33cm$ $y_L = 0.80cm$ $Z_L = 50\ \Omega$

Figure 21: A comparison of the computed and measured theta polarized RCS of a loaded rectangular patch on a grounded dielectric substrate.

4.3 Input Impedance Results

This section will compare the calculated input impedance of a microstrip antenna excited by a filament of uniform current to the input impedance of a coaxially fed microstrip antenna. The measured antenna is loaded through a coaxial feed. Note that the current filament is not a model for the coaxial feed since it does not account for the aperture in the ground plane and the current on the outer conductor of the coax. Figure 22 shows the geometry of the unloaded microstrip antenna used to generate Figures 25 to 31. Figure 23 shows the geometry of the edge loaded microstrip antenna used to generate Figures 32 and 33. Figure 24 shows the geometry of the corner loaded microstrip antenna used to generate Figures 34 and 35. The thickness of the substrate was measured to be 0.088 cm. The loaded antenna had a load impedance of 50 ohms. The relative permittivity and loss tangent, as supplied with the substrate, are 2.17 and 0.0015 respectively. Referring to Figure 5a, the feed is located at $(x_f, y_f) = (0.85$ cm,1.22 cm). Figure 25 shows the wide band input resistance and Figure 26 shows the wide band input reactance of this microstrip antenna. Figures 27 - 31 show the calculated and measured narrow band input impedance plotted on a Smith Chart for each resonance between 1 and 7 GHz. Figure 34 shows loaded input impedance from 1 to 4 GHz with the load located at (x_L, y_L)=(1.53 cm,1.1 cm). Figure 35 shows the loaded input reactance.

For the calculated data of Figures 25 and 26, Δf_c was chosen to be 400 MHz and Δf_z was chosen to be 5 MHz. Twelve modes were used in the MM solution to compute the curve between 1 and 3.5 GHz, 24 modes were used for the calculation between 3.5 and 6.4 GHz, and 50 modes were used for the calculation of the curve between 6.4 and 8.0 GHz. The convergence of this data was tested by using 24
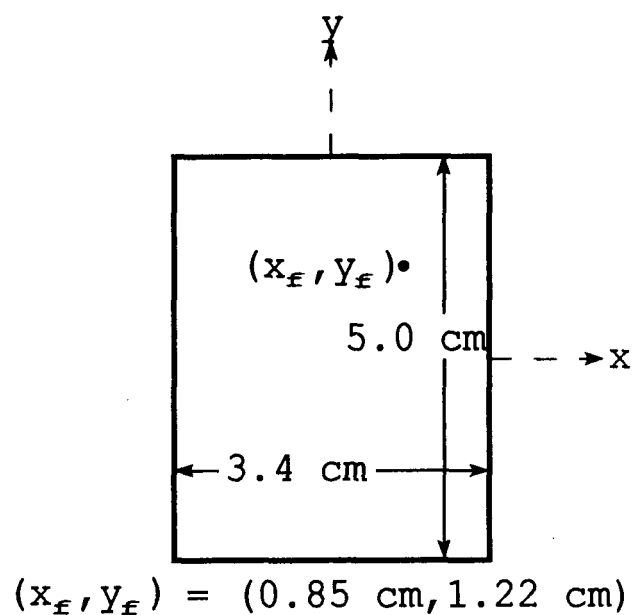
$$(x_f, y_f) = (0.85 \text{ cm}, 1.22 \text{ cm})$$

Figure 22: The rectangular microstrip antenna used for input impedance
calculation and measurement.

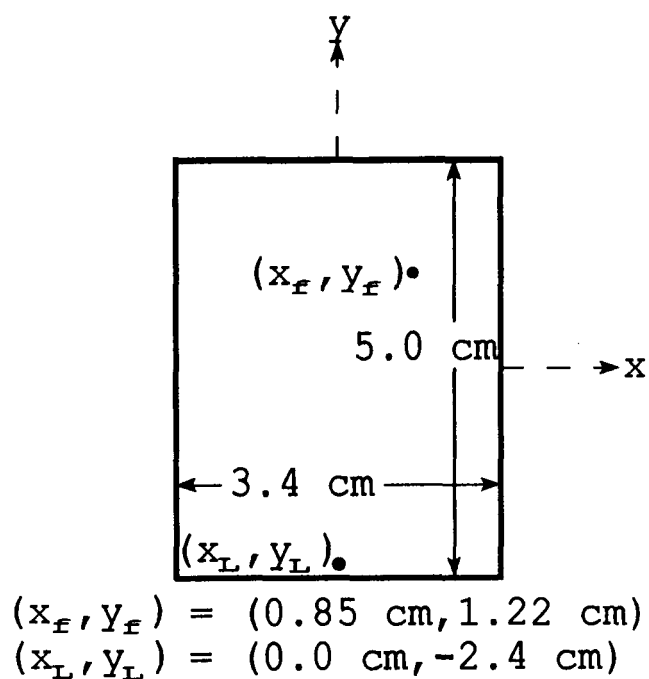$$(x_f, y_f) = (0.85 \text{ cm}, 1.22 \text{ cm})$$
$$(x_L, y_L) = (0.0 \text{ cm}, -2.4 \text{ cm})$$

Figure 23: The rectangular microstrip antenna of Figure 22 loaded at the edge
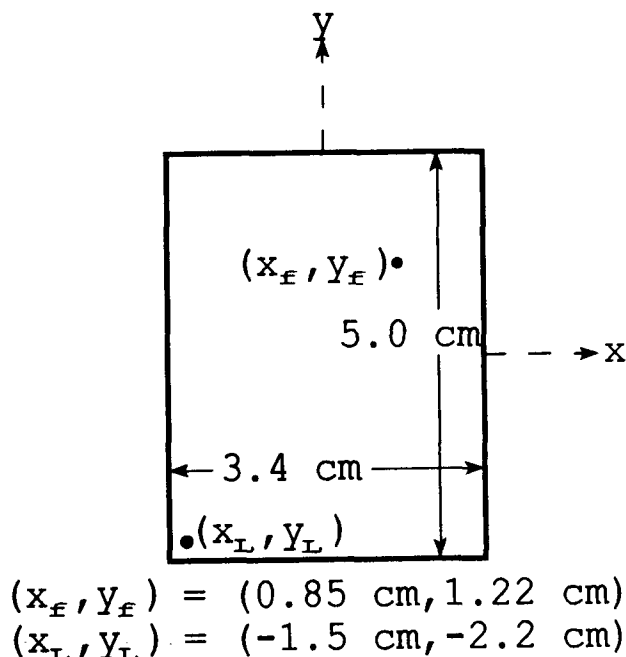for input impedance calculation and measurement.

$$(X_f, Y_f) = (0.85 \text{ cm}, 1.22 \text{ cm})$$
$$(X_L, Y_L) = (-1.5 \text{ cm}, -2.2 \text{ cm})$$

Figure 24: The rectangular microstrip antenna of Figure 22 loaded at the corner for input impedance calculation and measurement.

modes in the range from 1 to 3.5 GHz, using 32 modes from 3.5 to 6.4 GHz and using 72 modes from 6.4 to 8.0 GHz. The curves were virtually the same after the increase in modes. The total CPU time needed to generate the calculated data of Figures 25 and 26 was about 37 minutes on a VAX 8550.

For the calculated narrow band data of Figures 27 - 31, Δf_c was chosen to be 200 MHz and Δf_z was chosen to be 1 MHz. The number of modes used to compute the data of Figures 27 and 28 was 4. For Figure 29, 12 modes were used, for Figure 30, 32 modes were used and for Figure 31, 72 modes were used. The dots on the calculated and measured curves represent the measured frequency closest to resonance, and the frequencies 1% and 2% above and below the closest resonant frequency.

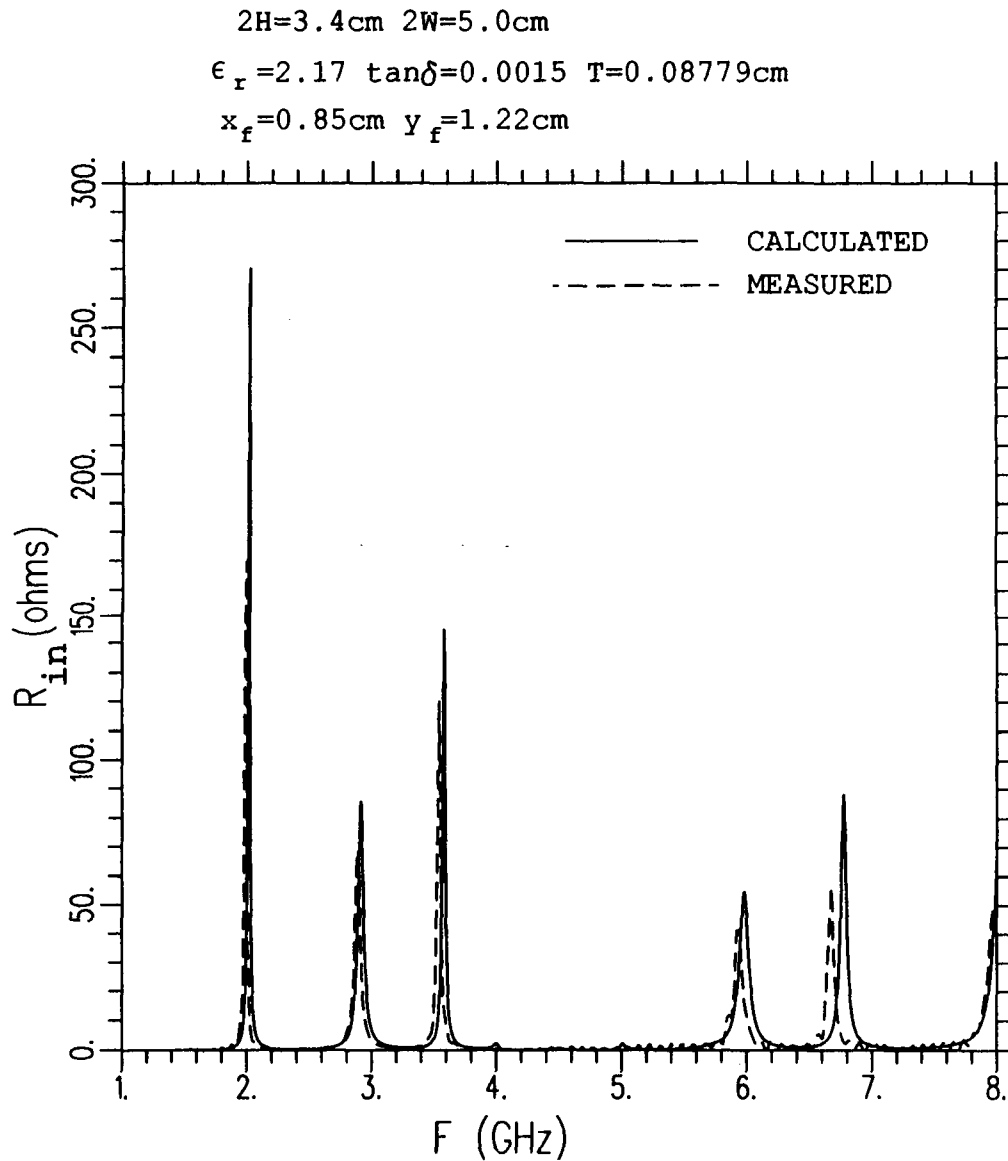The calculation for loaded input impedance of Figures 34 and 35 was made

2H=3.4cm 2W=5.0cm

ϵ_r=2.17 tanδ=0.0015 T=0.08779cm

x_f=0.85cm y_f=1.22cm

Figure 25: A comparison of the computed and measured real part of the input impedance for a microstrip antenna.

2H=3.4cm 2W=5.0cm
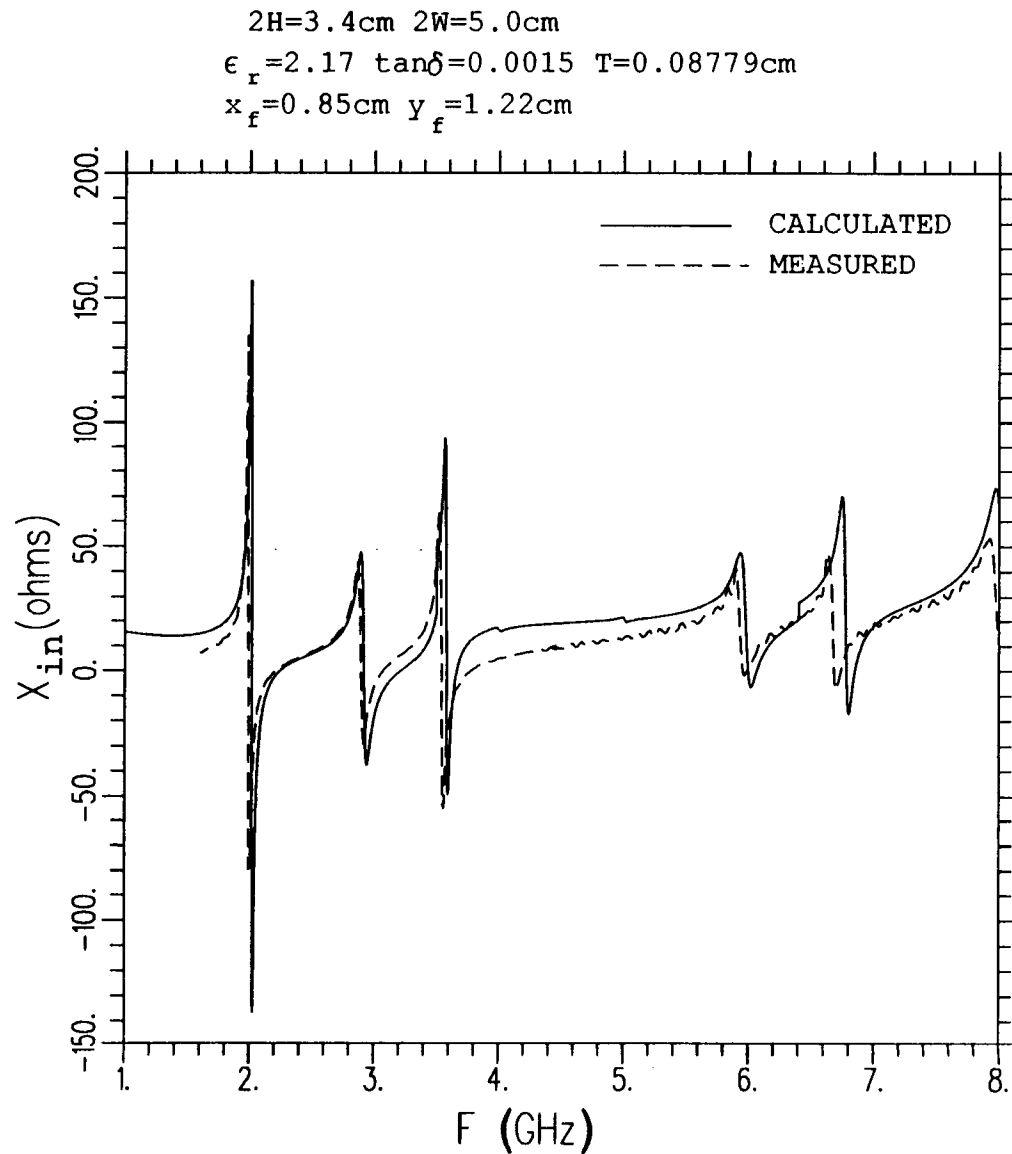ϵ_r=2.17 tanδ=0.0015 T=0.08779cm
x_f=0.85cm y_f=1.22cm

Figure 26: A comparison of the computed and measured imaginary part of the input impedance for a microstrip antenna.

2H=3.4cm 2W=5.0cm
ϵ_r=2.17 tanδ=0.0015 T=0.08779cm
x_f=0.85cm y_f=1.22cm

———— — —— MEASURED

— — — — — — CALCULATED
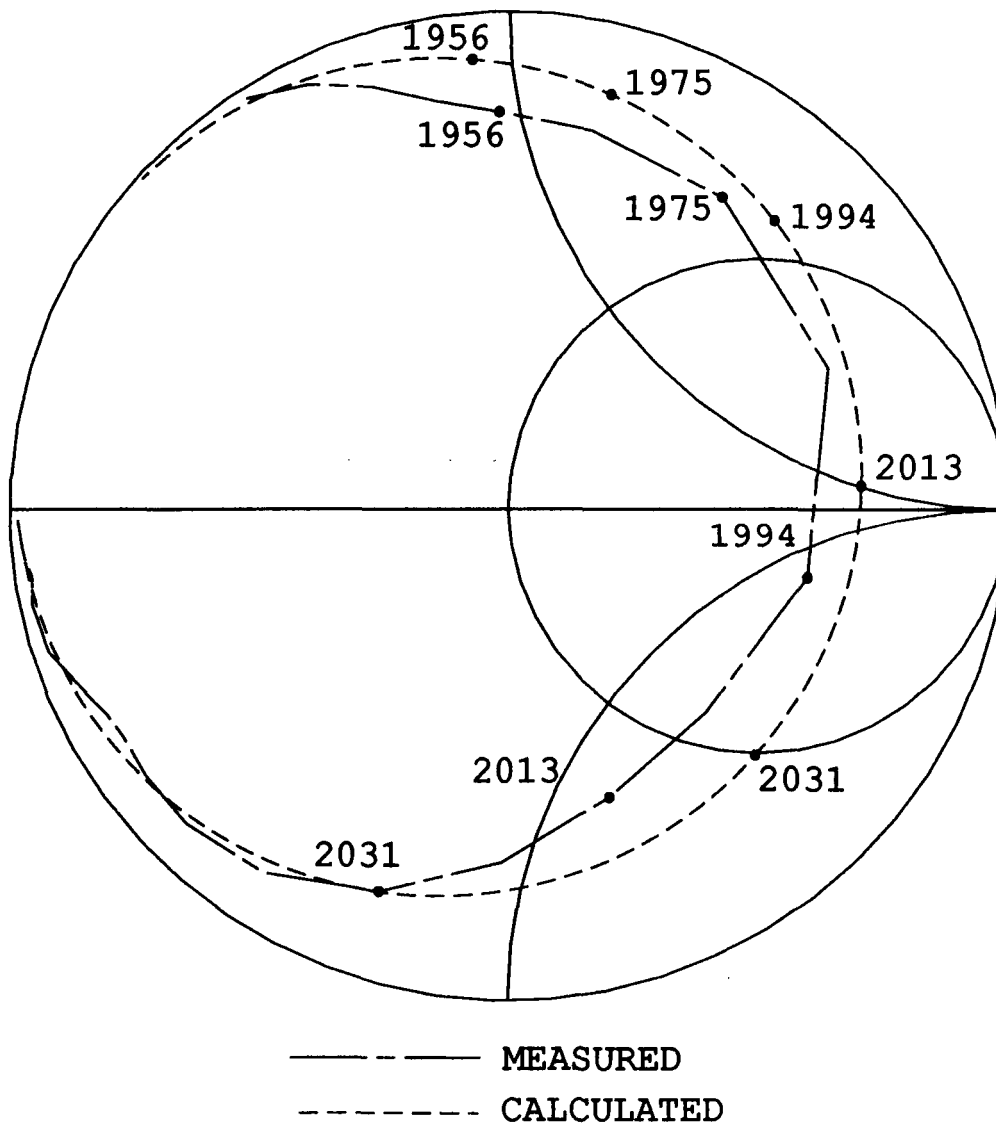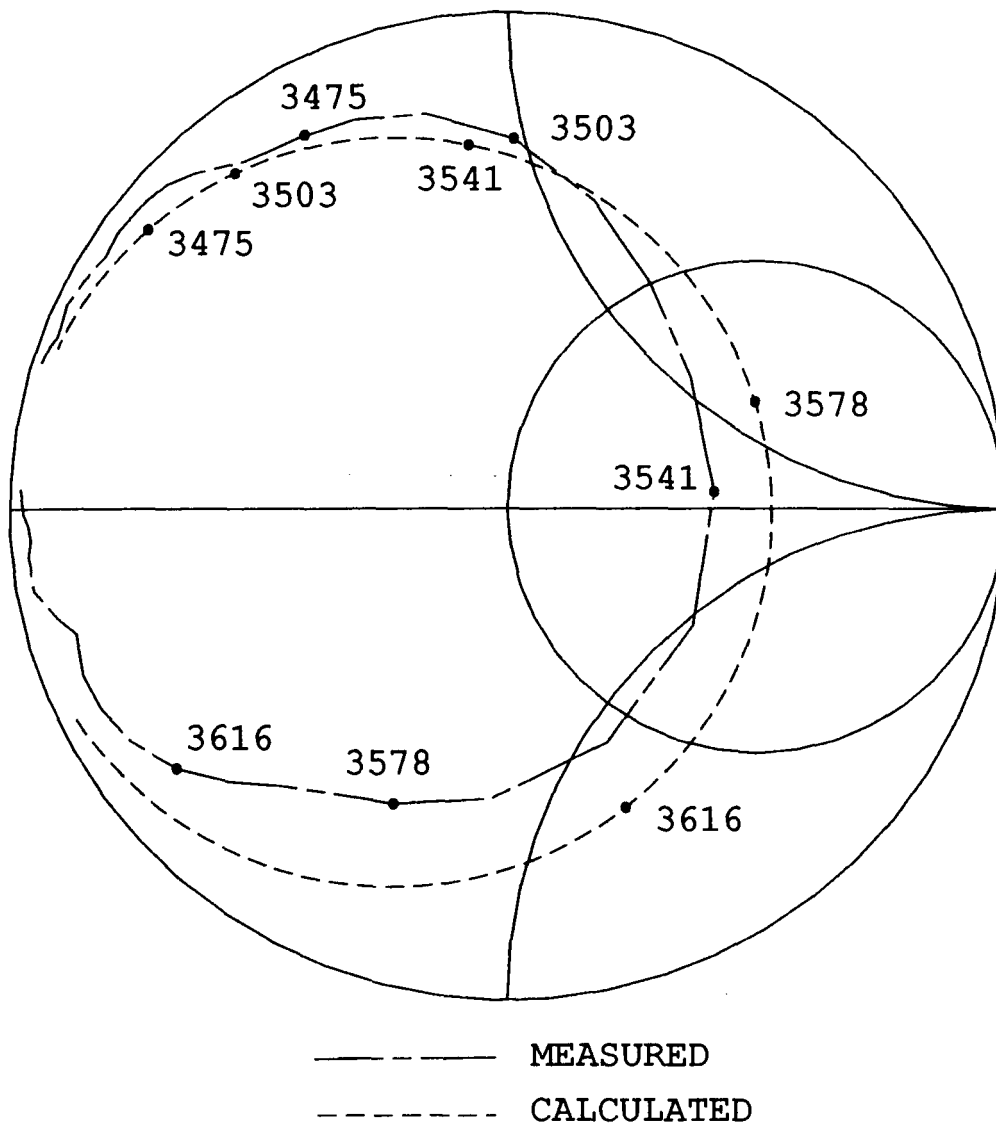
Figure 27: A comparison of the computed and measured input impedance around first resonance plotted on a Smith Chart.

$2H=3.4$cm $2W=5.0$cm

$\epsilon_r=2.17$ $\tan\delta=0.0015$ $T=0.08779$cm

$x_f=0.85$cm $y_f=1.22$cm

————— MEASURED

— — — — — CALCULATED
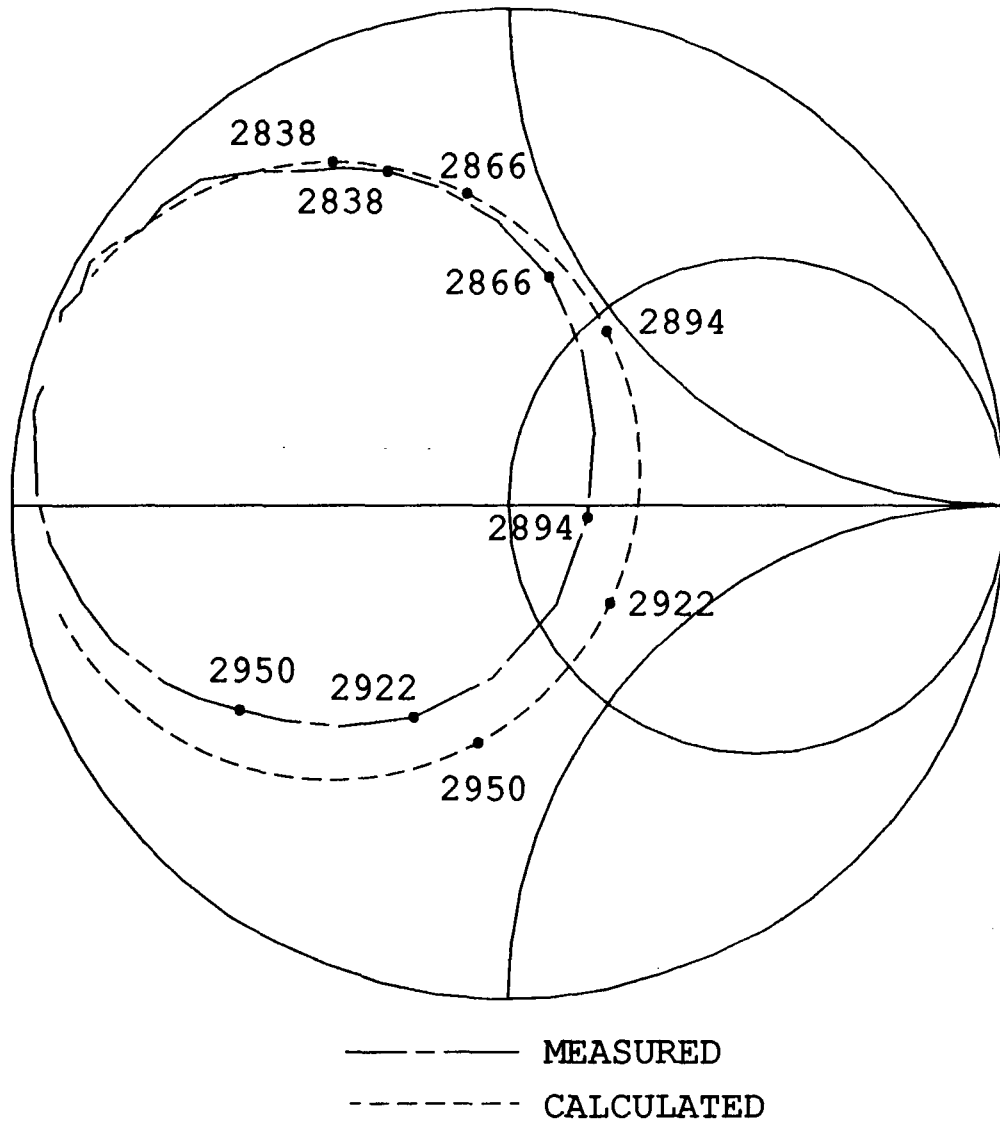
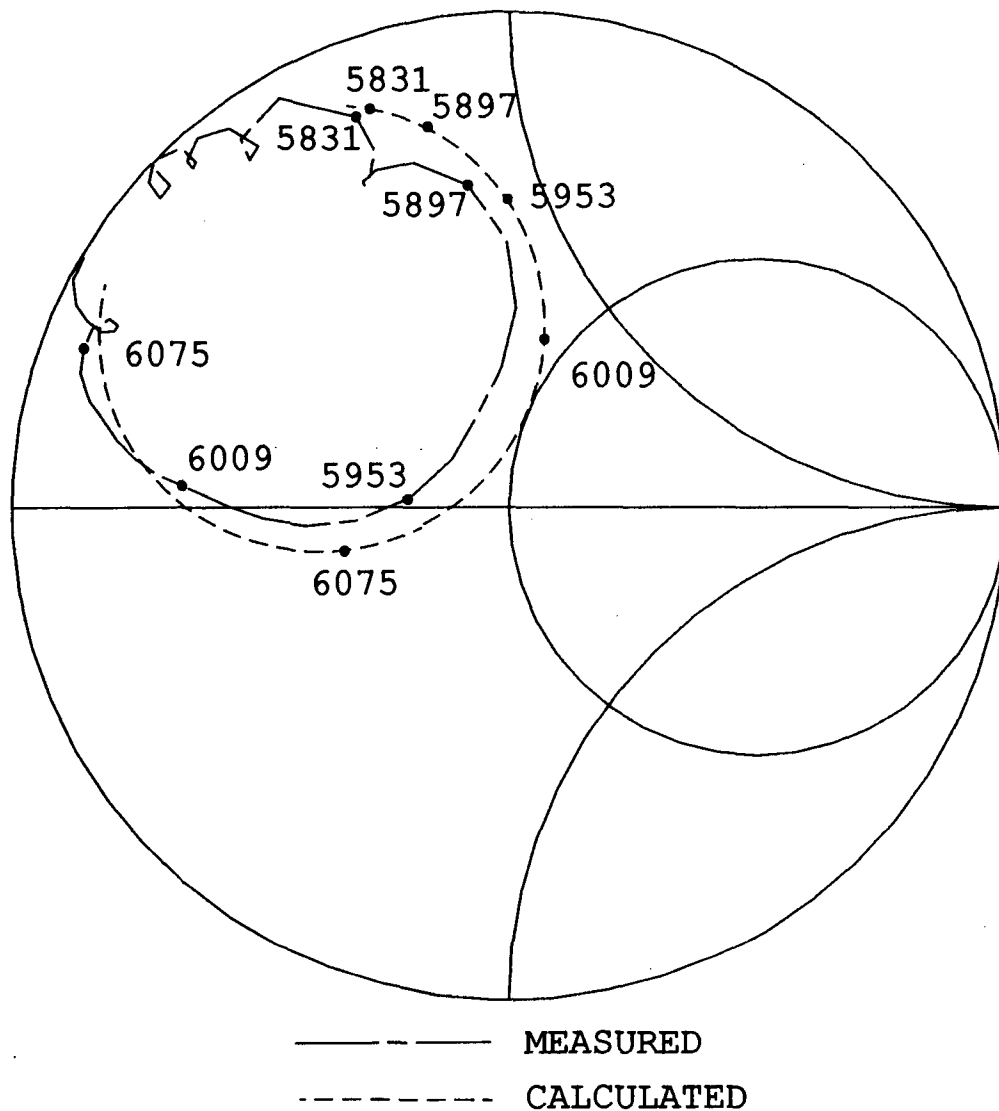Figure 28: A comparison of the computed and measured input impedance around second resonance plotted on a Smith Chart.

71

2H=3.4cm 2W=5.0cm

ϵ_r=2.17 tanδ=0.0015 T=0.08779cm

x_f=0.85cm y_f=1.22cm

———— — ——— MEASURED

— — — — — — CALCULATED

Figure 29: A comparison of the computed and measured input impedance around third resonance plotted on a Smith Chart.

2H=3.4cm 2W=5.0

ϵ_r =2.17 tanδ=0.0015 T=0.08779cm

x_f=0.85cm y_f=1.22cm

Figure 30: A comparison of the computed and measured input impedance around fourth resonance plotted on a Smith Chart.

2H=3.4cm 2W=5.0cm
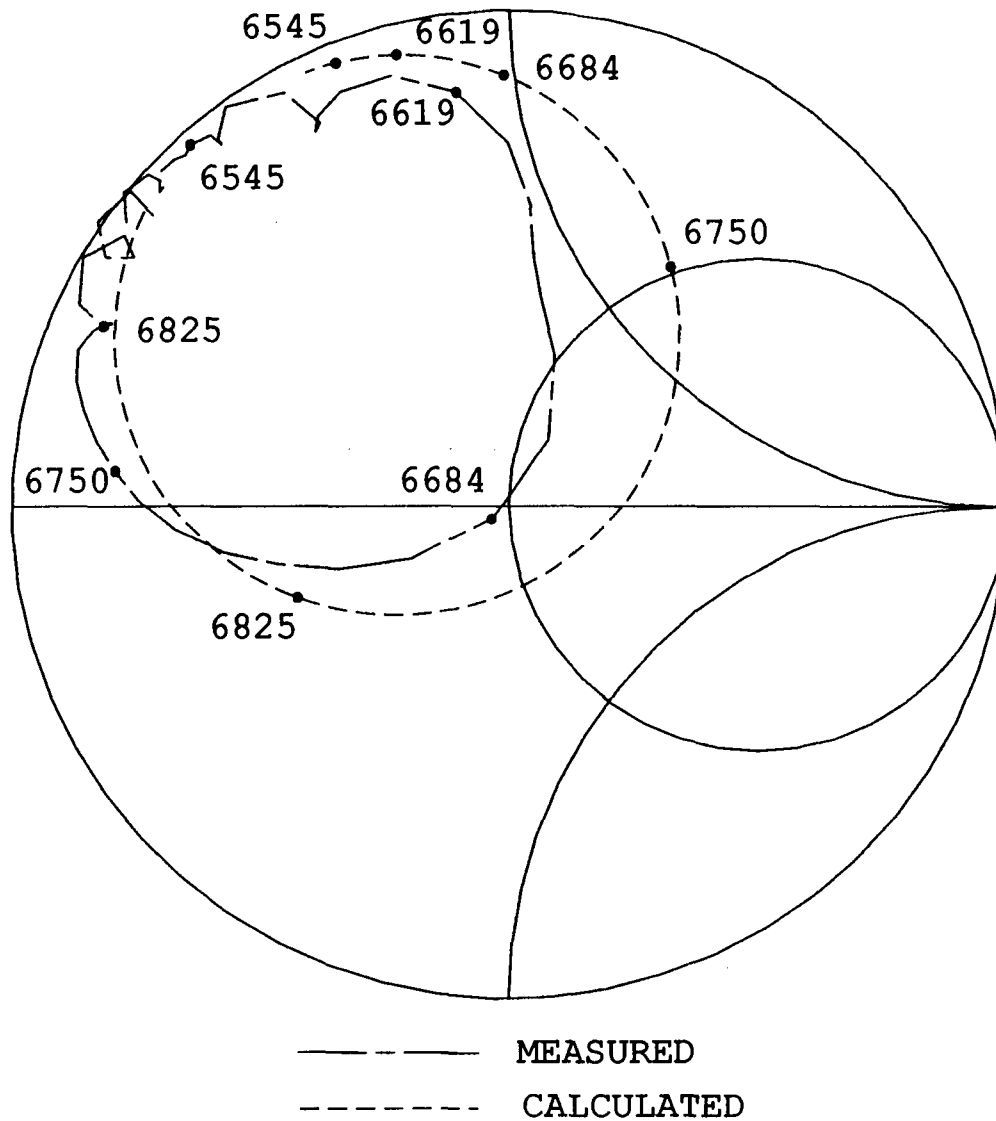
ϵ_r=2.17 tanδ=0.0015 T=0.08779cm

x_f=0.85cm y_f=1.22cm

Figure 31: A comparison of the computed and measured input impedance around fifth resonance plotted on a Smith Chart.

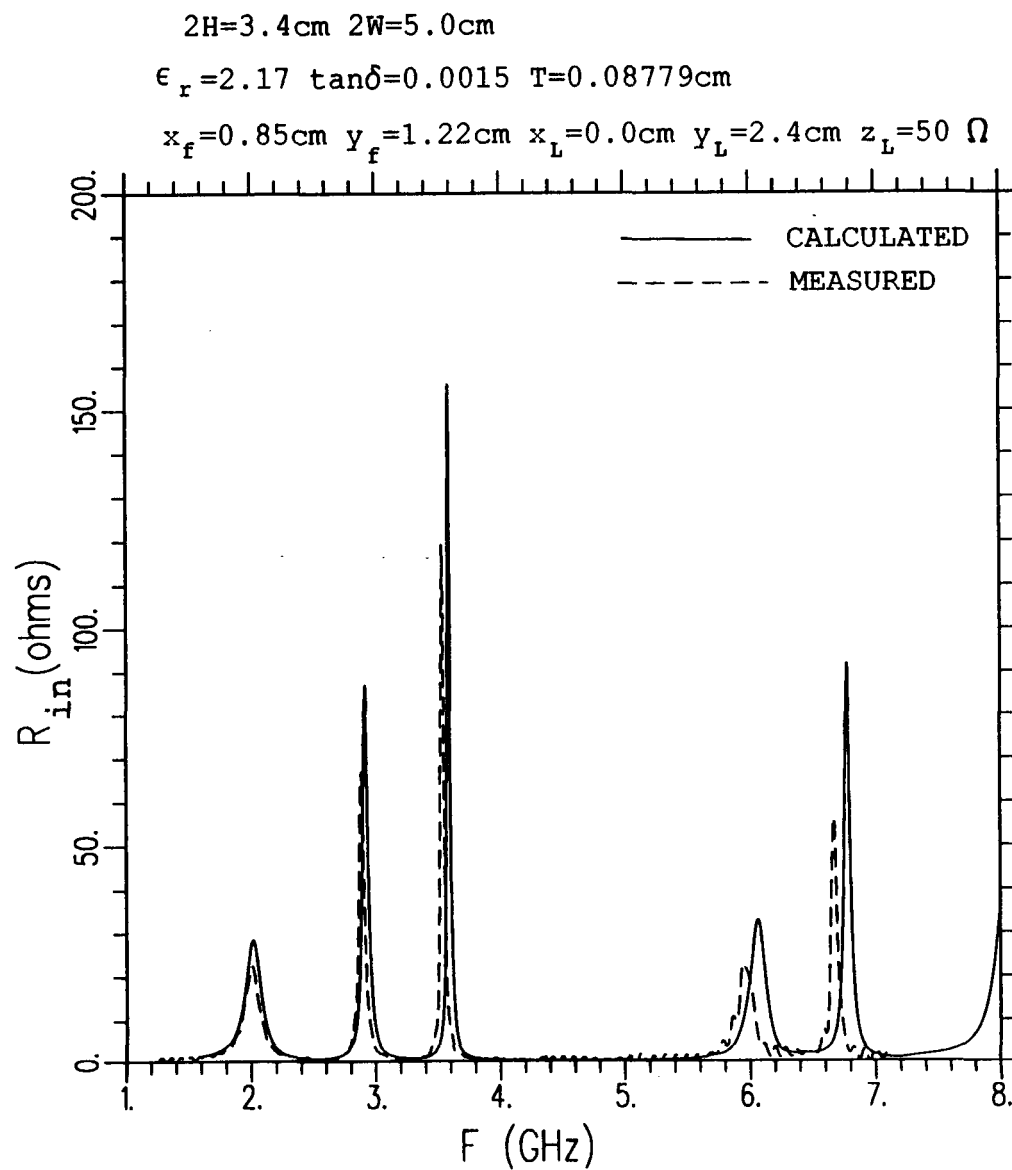$2H=3.4$cm $2W=5.0$cm

$\epsilon_r=2.17$ tan$\delta=0.0015$ $T=0.08779$cm

$x_f=0.85$cm $y_f=1.22$cm $x_L=0.0$cm $y_L=2.4$cm $z_L=50$ Ω

Figure 32: A comparison of the computed and measured real part of the input impedance for an edge loaded microstrip antenna.

2H=3.4cm 2W=5.0cm

ϵ_r=2.17 tanδ=0.0015 T=0.08779cm

X_f=0.85cm y_f=1.22cm x_L=0.0cm y_L=2.4cm Z_L=50 Ω

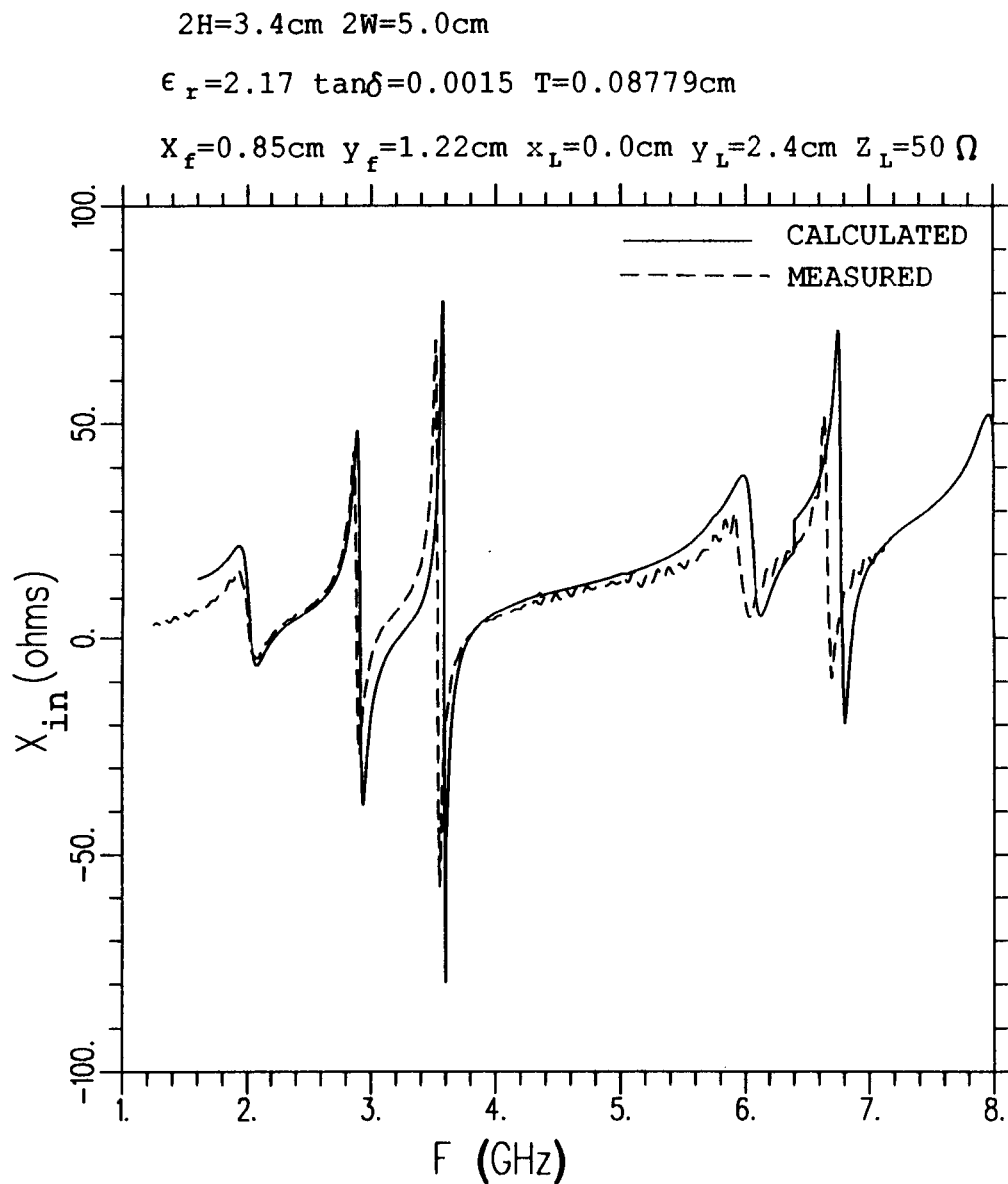Figure 33: A comparison of the computed and measured imaginary part of the input impedance for an edge loaded microstrip antenna.

2H=3.4cm 2W=5.0cm
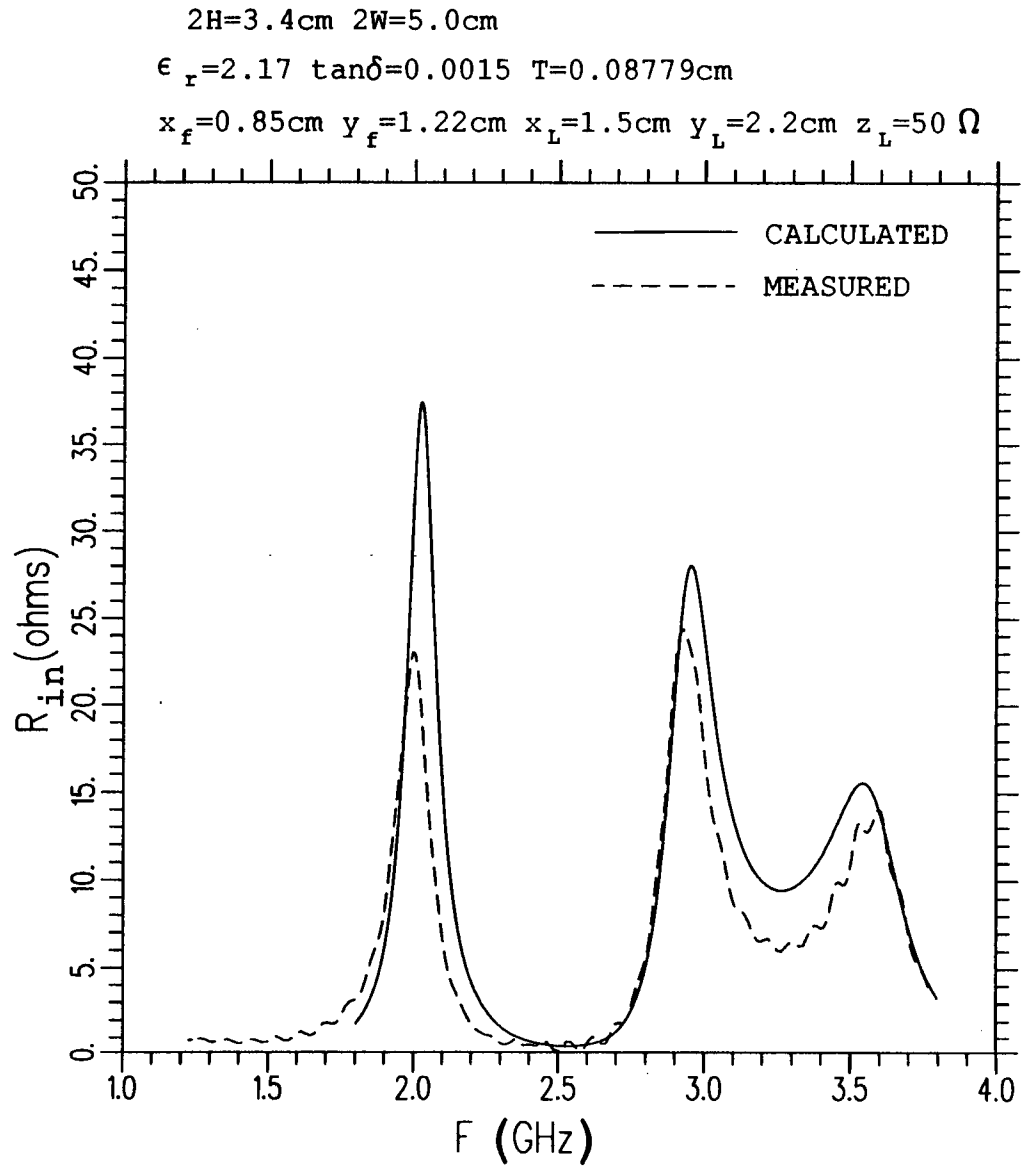
ϵ_r=2.17 tanδ=0.0015 T=0.08779cm

x_f=0.85cm y_f=1.22cm x_L=1.5cm y_L=2.2cm z_L=50 Ω

Figure 34: A comparison of the computed and measured real part of the input impedance for a corner loaded microstrip antenna.

77

2H=3.4cm 2W=5.0cm

ϵ_r=2.17 tanδ=0.0015 T=0.08779cm

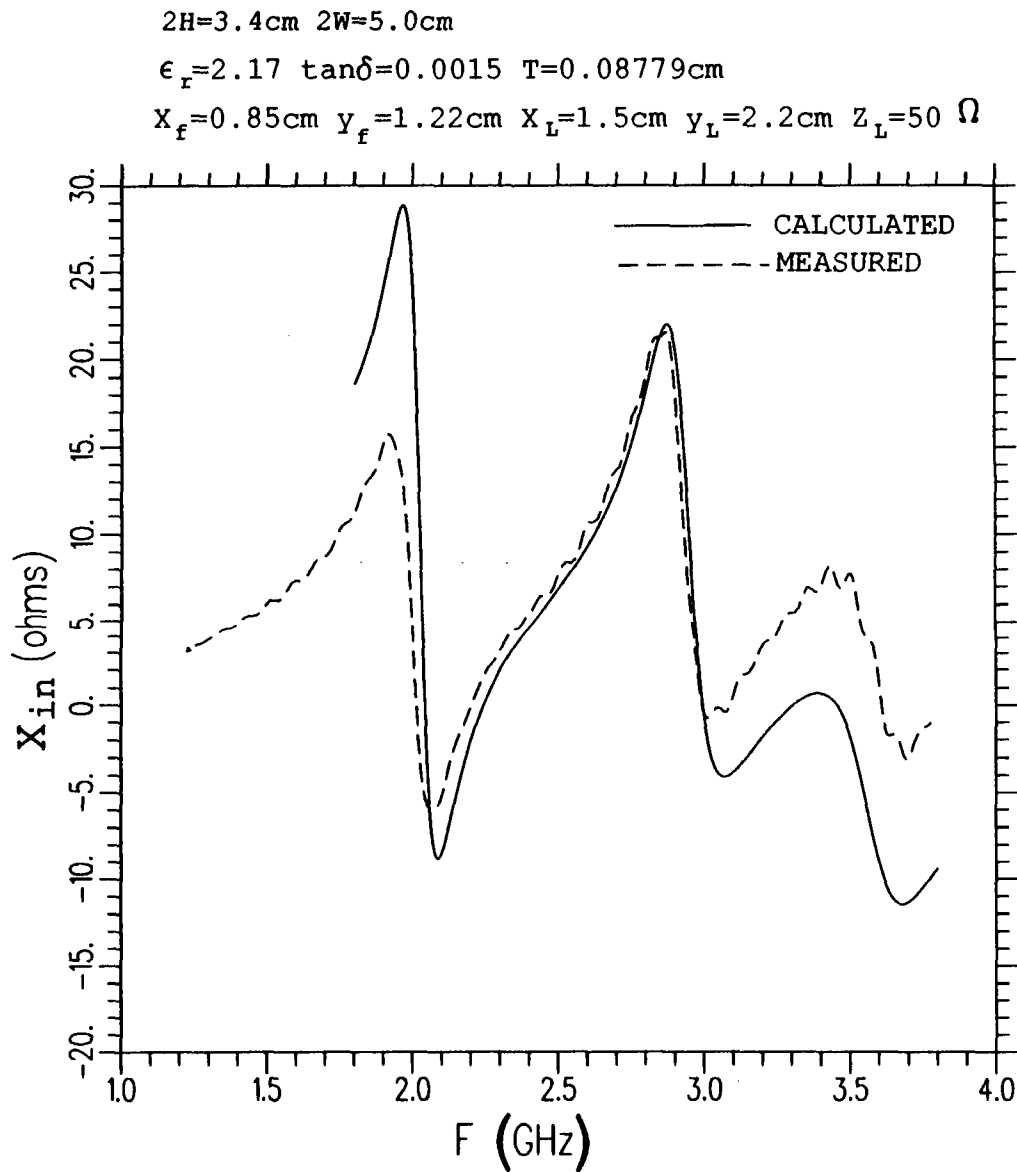X_f=0.85cm y_f=1.22cm X_L=1.5cm y_L=2.2cm Z_L=50 Ω

Figure 35: A comparison of the computed and measured imaginary part of the input impedance for a corner loaded microstrip antenna.

$2H = 3.4cm \quad 2W = 5.0cm$

$\epsilon_r = 2.17 \quad \tan\delta = 0.0015 \quad T = 0.08779cm$

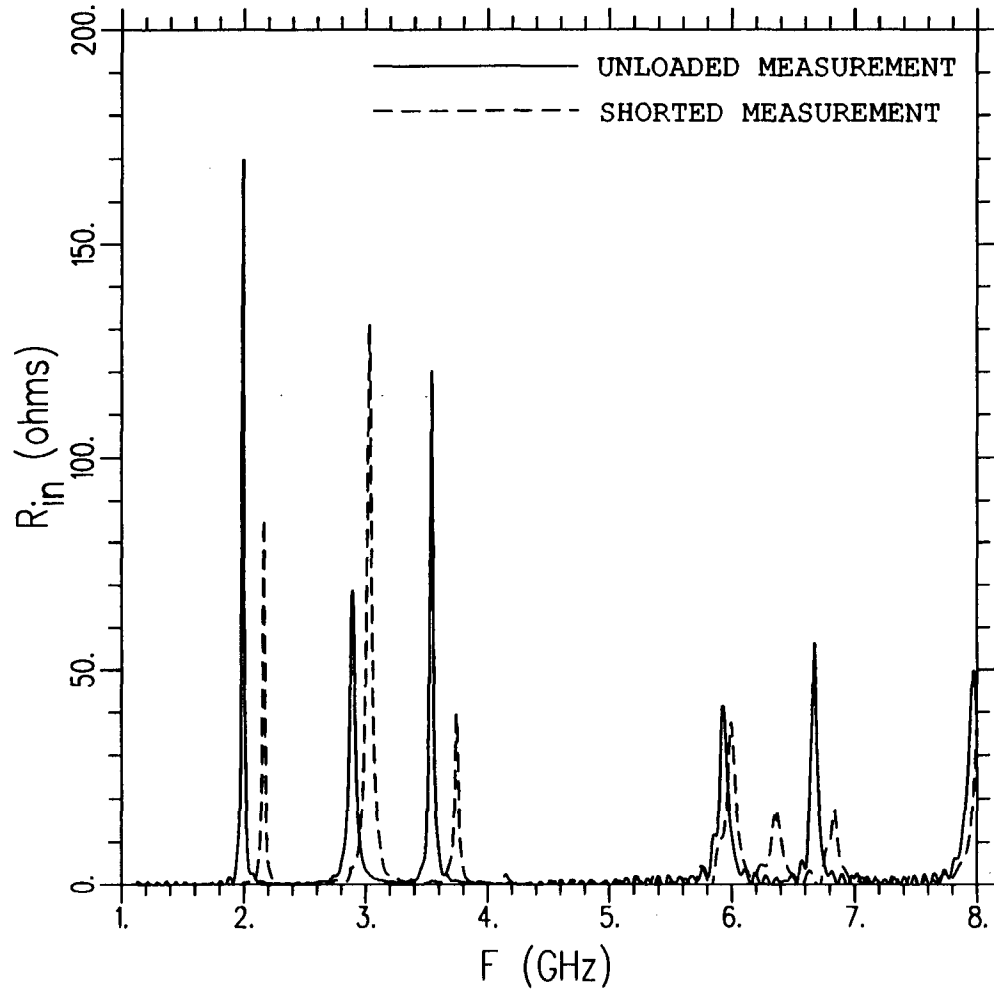$x_f = 0.85cm \quad y_f = 1.22cm \quad x_L = -1.5cm \quad y_L = -2.2cm \quad Z_L = 0\,\Omega$

Figure 36: A comparison of the measured real part of the input impedance for an unloaded and corner shorted microstrip antenna.

$$2H = 3.4\text{cm} \quad 2W = 5.0\text{cm}$$

$$\epsilon_r = 2.17 \quad \tan\delta = 0.0015 \quad T = 0.08779\text{cm}$$

$$x_f = 0.85\text{cm} \quad y_f = 1.22\text{cm} \quad x_L = -1.5\text{cm} \quad y_L = -2.2\text{cm} \quad Z_L = 0 \ \Omega$$
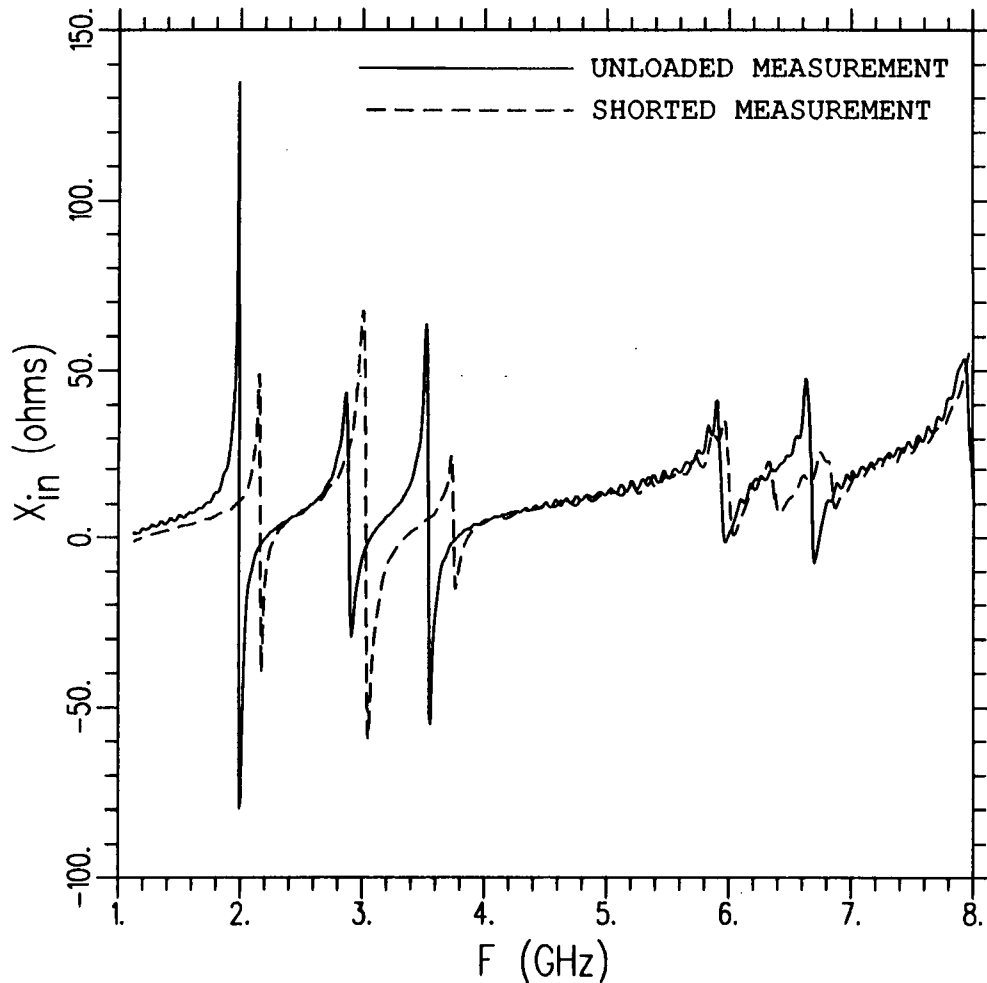

Figure 37: A comparison of the measured imaginary part of the input impedance for an unloaded and corner shorted microstrip antenna.

$2H = 3.4 \text{cm} \quad 2W = 5.0 \text{cm}$

$\epsilon_r = 2.17 \quad \tan\delta = 0.0015 \quad T = 0.008779 \text{cm}$

$x_f = 0.85 \text{cm} \quad y_f = 1.22 \text{cm} \quad x_L = -1.5 \text{cm} \quad y_L = -2.2 \text{cm} \quad Z_L = 0 \, \Omega$
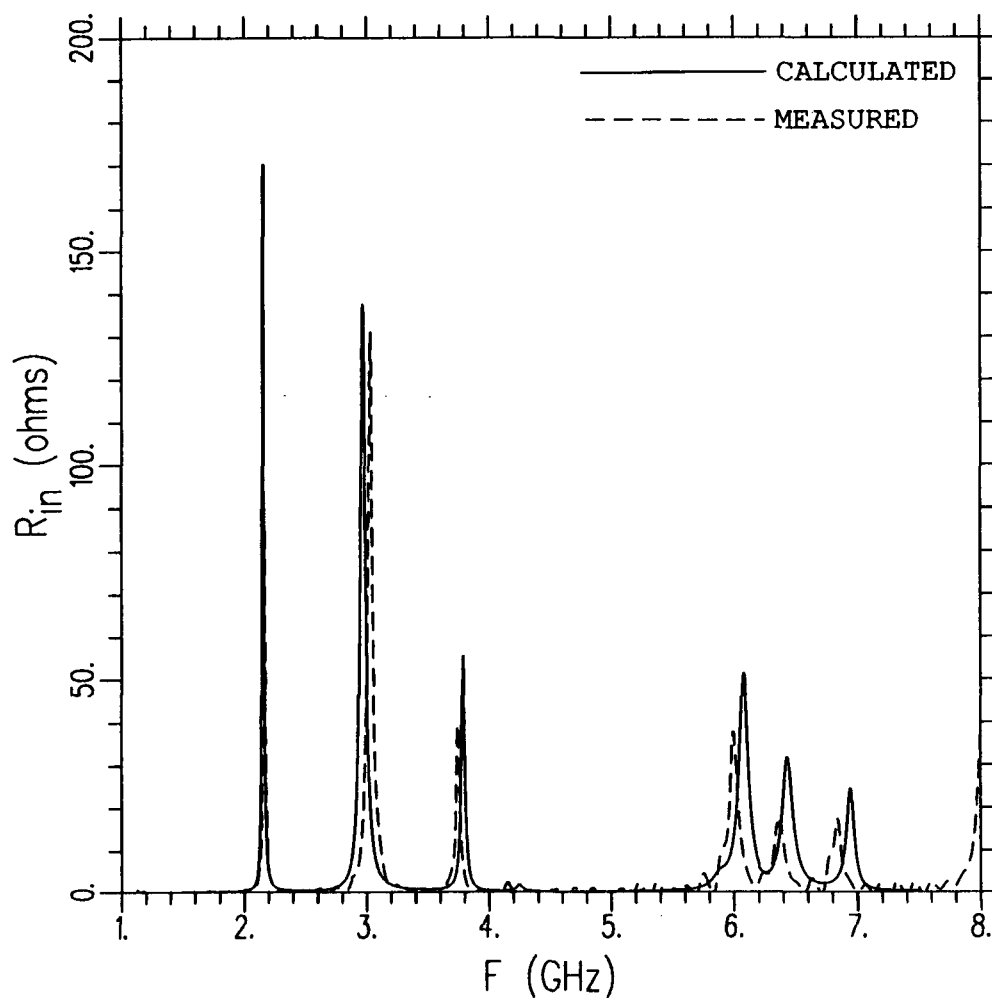

Figure 38: A comparison of the computed and measured real part of the input impedance for a corner shorted microstrip antenna.

$$2H = 3.4cm \quad 2W = 5.0cm$$

$$\epsilon_r = 2.17 \quad \tan\delta = 0.0015 \quad T = 0.08779cm$$

$$x_f = 0.85cm \quad y_f = 1.22cm \quad x_L = -1.5cm \quad y_L = -2.2cm \quad Z_L = 0 \, \Omega$$
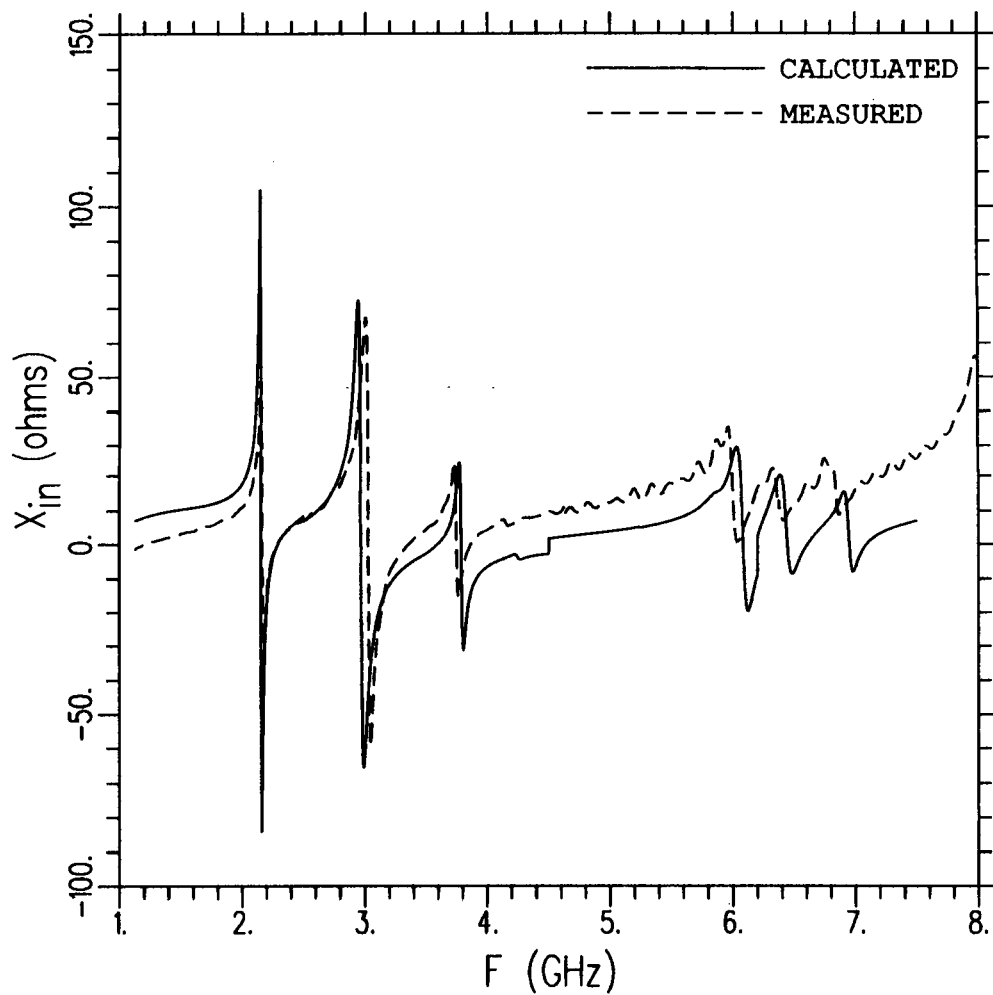

Figure 39: A comparison of the computed and measured imaginary part of the input impedance for a corner shorted microstrip antenna.

82

with $\Delta f_c = 400$ MHz and $\Delta f_z = 5$ MHz. The total number of modes used was 4. The CPU time require to generate this data on a VAX 8550 was about 4 minutes.

Figures 36 and 37 show a comparison of input impedance for the measured unloaded and shorted microstrip antenna. The geometry of this antenna is shown in Figure 24 where the load port is now a vertical wire from the patch to the ground plane. One might expect a short near the corner to eliminate resonances, particularly the first three since they were greatly reduced by the impedance load. Figures 36 and 37 clearly show that this is not the case. Figures 38 and 39 show a comparison of calculated input impedance and measured input impedance for the shorted microstrip antenna. The calculation was made using 4 modes from 1.5 GHz to 2.5 GHz, 12 modes from 2.5 GHz to 4.5 GHz, 17 modes from 4.5 GHz to 6.2 GHz, and 32 modes from 6.2 GHz to 7.5 GHz.

The calculated and measured data shown are close in resonant frequency but usually differ in magnitude. This can be accounted for by the following. First, the excitation for the calculation is not a model for a coaxial feed. Second, the vertical filament of current excitation does not include an attachment mode between the filament and the patch. Third, the microstrip antenna has very high Q resonances and any loss not modeled in the MM solution could result in lower magnitudes for the measurement. When looking at the calculated results, particularly the input reactance data, the discontinuities in the curves are the result of adding more modes to the MM solution. The higher order modes account for the inductive shift of the data as the frequency goes higher.

It is interesting to examine the relationship between the impedance matrix and the input impedance. One might expect an input impedance resonance to directly correlate with a resonance of a particular mode or modes in the impedance matrix. This is the case for three of the five resonances shown in Figures 27 - 31. The other

83

two are caused by the mutual coupling between modes.

For Figure 27, the most strongly excited mode is the 1 0 $\hat{y}$ directed mode and it is resonant. The most strongly excited and resonant mode for Figure 28 is the 1 0 $\hat{x}$ directed mode. The resonance shown in Figure 30 has the 3 0 $\hat{y}$ directed mode most strongly excited and resonant. This is no surprise since it is two octaves above the resonance caused by the 1 0 $\hat{y}$ directed mode. The resonance shown in Figure 29 does not correspond to a resonant mode. The most strongly excited mode is the 1 1 $\hat{x}$ directed mode. By analyzing the input impedance where two modes were used for calculating the impedance matrix, it was found that the 1 1 $\hat{x}$ directed and 1 1 $\hat{y}$ directed modes were needed to create an input impedance resonance at that frequency. Neither of these modes were near resonance. Similarly, for Figure 31, there is no resonant mode in the impedance matrix. The most excited mode is the 3 1 $\hat{y}$ directed mode. The modes that are required to show this resonance in the MM computation were not determined since a large number of modes were needed to generate it for Figures 25, 26, and 31. This resonance was most likely caused by the interaction of the 3 1 $\hat{y}$ directed mode and several other higher order modes.

4.4 Mutual Impedance Between Vertical Thin Wires in a Grounded Dielectric Substrate

The mutual impedance calculation with respect to their separation for two vertical thin wires of equal length inside the dielectric region is compared to previously calculated data [21]. The separation and dimensions have all been normalized to the free space wavelength at the operating frequency. The thickness of the substrate is $0.4152\lambda_0$. The dielectric constant of the substrate is 2.45 and the substrate is considered lossless. The wires extend from the ground plane at $z = -0.4152\lambda_0$ to $z = -0.2636\lambda_0$ and have a radius of $0.001\lambda_0$. The separation of the wires is

varied from $0.03\lambda_0$ to $1.95\lambda_0$. For the published curve, the excitation was a magnetic frill current around the aperture of the coax. Figures 41 and 42 show that the so called delta gap generator yields virtually the same curves for the real and imaginary parts of the mutual impedance. The geometry of this calculation is shown in Figure 40.

For the MM computation, the wires were broken into three equal length segments. This corresponds to three dipole modes on the wires. The data was computed at intervals of $0.01\lambda_0$ separation. The numeric integration had a maximum limit on the κ axis of $200\kappa_0$ but the actual maximum value of κ occurred when the integration converges to within .2%. As the wires moved further apart, the maximum value of κ for convergence decreases but the density of the integration points must increase since the J_0 Bessel function in the impedance matrix integrals oscillate more rapidly with respect to κ as the separation s increases. The total CPU time to compute the data in Figures 41 and 42 was about 9 minutes on a VAX 8550.

The mutual impedance is defined from the two port problem. The excitation ports are at the base of each wire at $z = -0.4152\lambda_0$. The two port linear equation is written as

$$\begin{bmatrix} Z_{11} & Z_{12} \\ Z_{21} & Z_{22} \end{bmatrix} \begin{bmatrix} I_1 \\ I_2 \end{bmatrix} = \begin{bmatrix} V_1 \\ V_2 \end{bmatrix} \tag{4.1}$$

where Z_{11} and Z_{22} are the self impedances of wire 1 and wire 2 respectively, Z_{12} and Z_{21} are the desired mutual impedance, I_1, V_1 are the current, voltage at port 1, respectively, and I_2, V_2 are the current, voltage at port 2, respectively. The two port impedance matrix is developed by solving the MM matrix equations first with the excitation at port 1 and then with the excitation at port 2. When the MM matrix equations are solved with the excitation at port 1, the currents at port 1

85
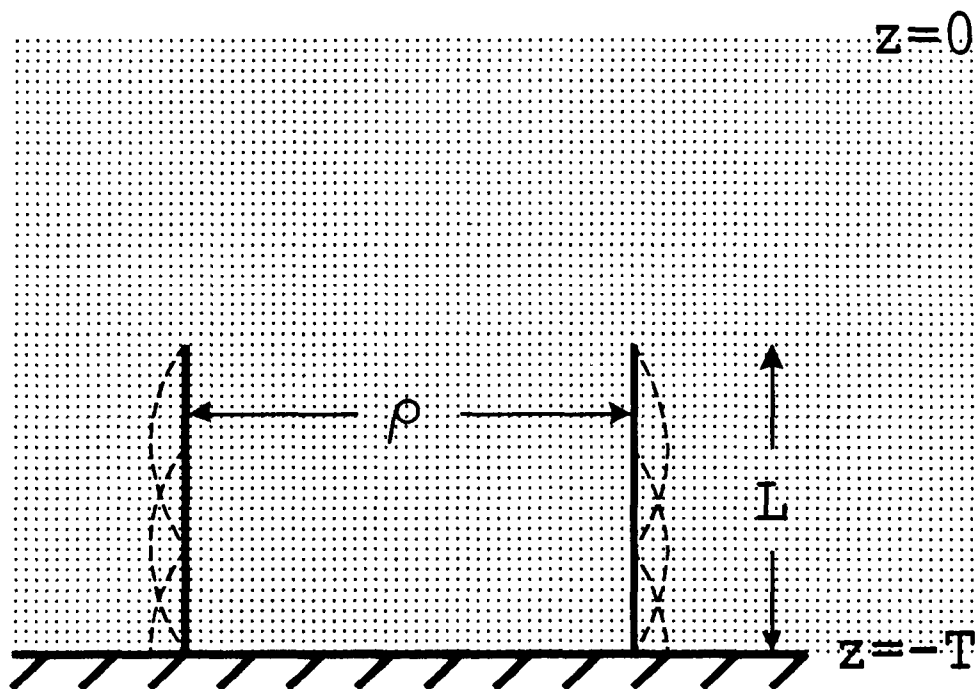
$$L=0.1516\lambda_o$$
$$T=0.4152\lambda_o$$

Figure 40: Two thin wires imbedded in the dielectric of a grounded dielectric substrate. The wires have three dipole MM modes on them.

and port 2 can be determined. Dividing these currents by the voltage exciting port 1, the Y_{11} and Y_{21} elements of the two port admittance matrix are determined. Similarly, the excitation at port 2 will define the Y_{12} and Y_{22} elements of the two port admittance matrix. By inverting this admittance matrix, the two port impedance matrix is obtained.

Figure 43 was constructed to illustrate the effect of the dielectric substrate on the mutual impedance. The dielectric substrate was replaced by free space for the same geometry and the mutual impedance was computed over a wider range of separation. The solid curve is the mutual impedance for the two wires imbedded in the grounded dielectric substrate and the dashed curve is the free space mutual impedance. The mutual impedance magnitude falls off as roughly $\frac{1}{\rho}$ when the the wires are in free space. This is as expected since the magnitude of the mutual impedance is linearly proportional to the electric field and the electric field decreases as $\frac{1}{\rho}$ in free space. When the dielectric is present, there is substantially more coupling between the two wires as the separation increases. The is due to the TM surface waves on the dielectric.

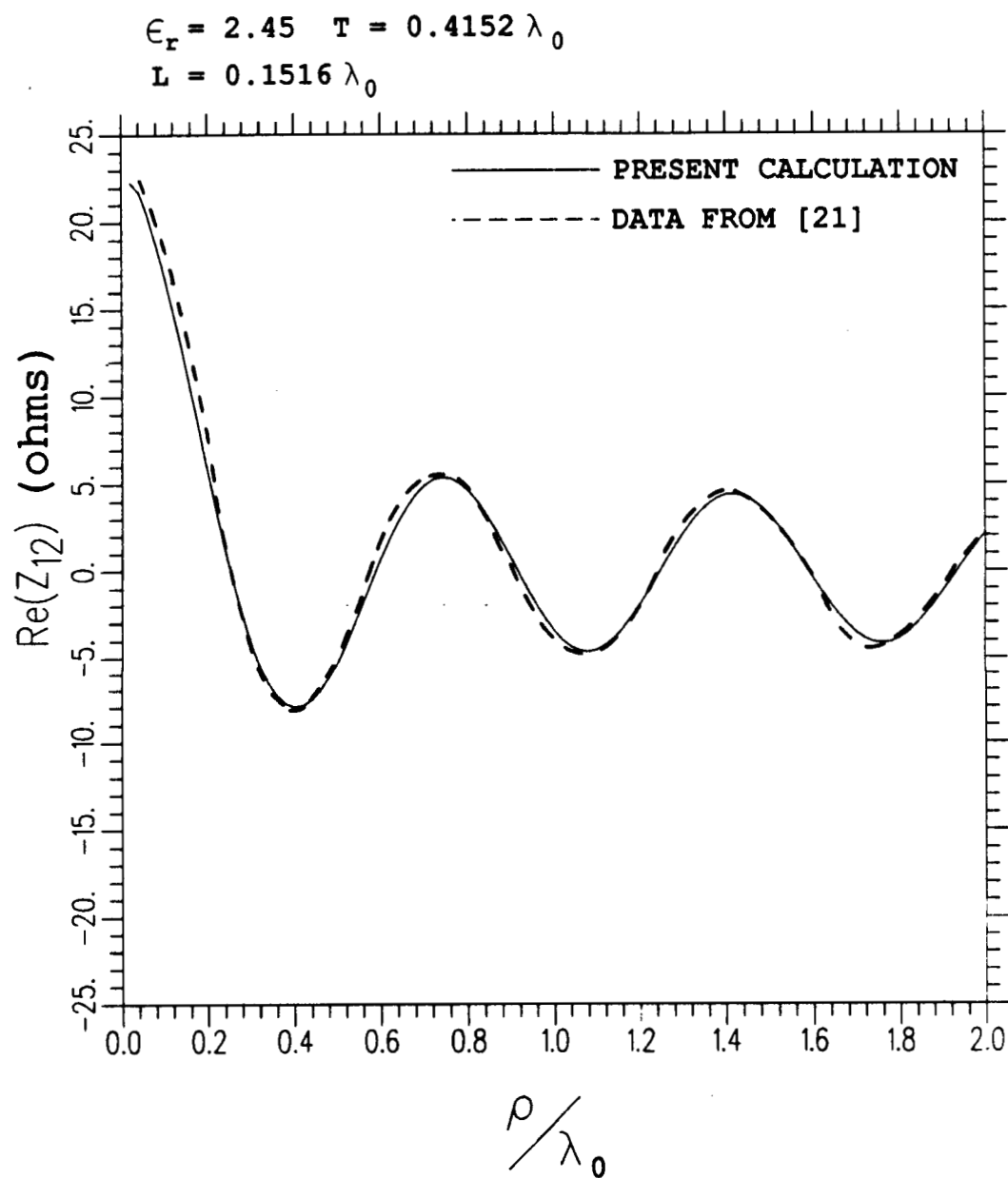$\epsilon_r = 2.45$ $T = 0.4152 \lambda_0$

$L = 0.1516 \lambda_0$

Figure 41: A comparison of present calculation to published data [21] for the real part of the mutual impedance between two thin wires imbedded in a grounded dielectric substrate.

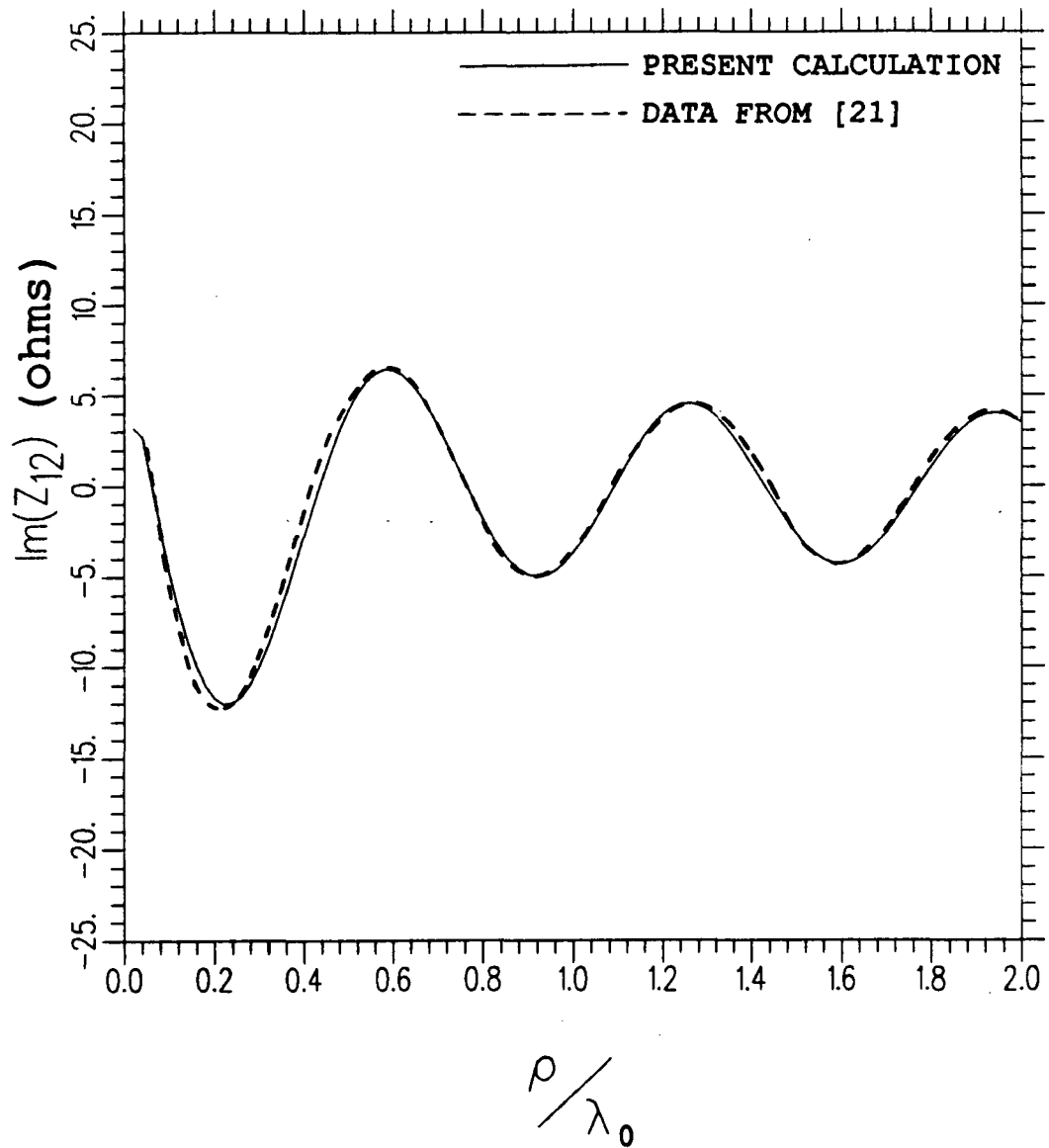$\epsilon_r = 2.45$ $T = 0.4152 \lambda_0$
$L = 0.1516 \lambda_0$

Figure 42: A comparison of present calculation to published data [21] for the imaginary part of the mutual impedance between two thin wires imbedded in a grounded dielectric substrate.
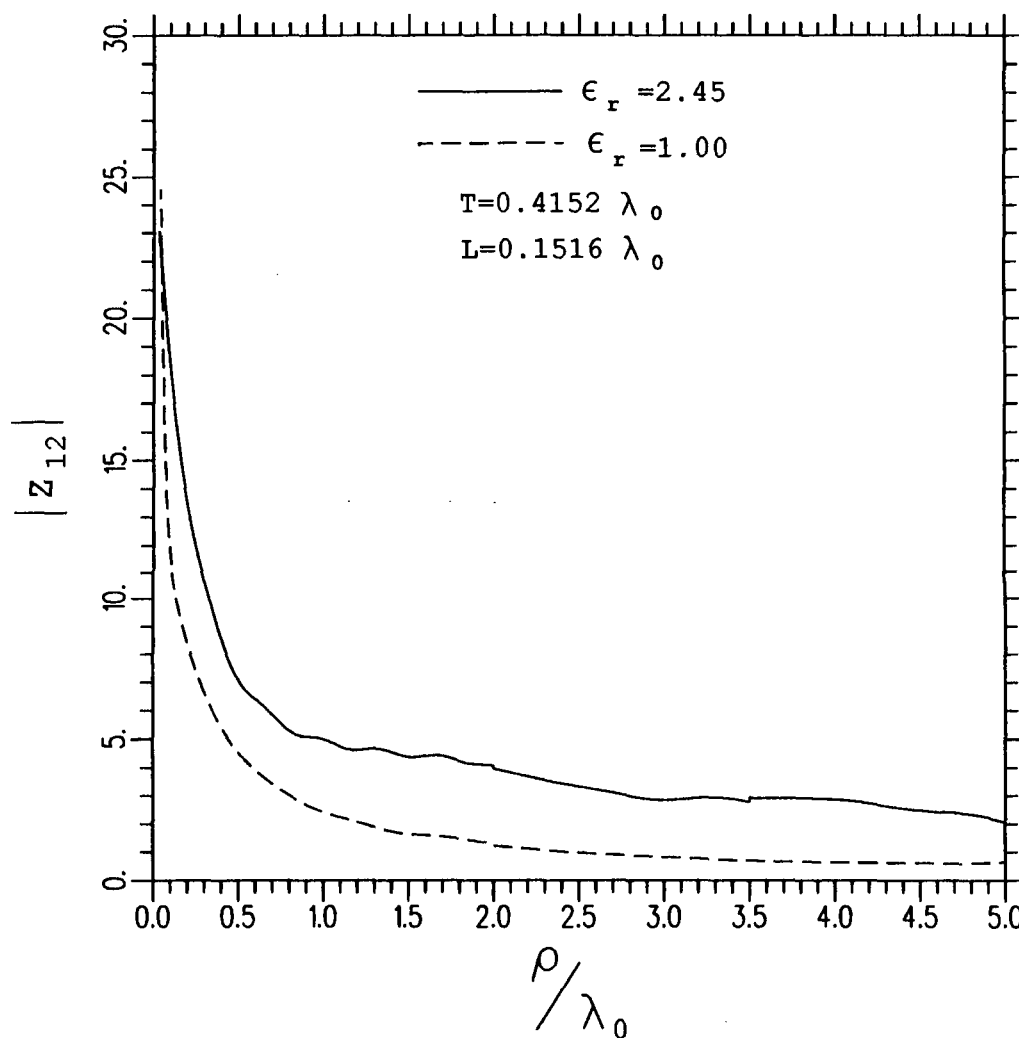
Figure 43: A comparison of the magnitude of the mutual impedance of Figure 40 and the mutual impedance of the same geometry where the dielectric substrate is replaced by free space.

c-2

CHAPTER V

SUMMARY

This report has described an integral equation and MM solutions to the problems of scattering and radiation from an unloaded and loaded rectangular microstrip patch and the self and mutual impedance of vertical thin wires protruding through a grounded dielectric substrate.

For the rectangular microstrip patch, an integral equation was developed for unknown surface currents on the patch. The MM was applied to represent this integral equation as a system of linear equations. A crucial part of the solution was the integral expressions for the impedance matrix elements. The integrands in these expressions were analyzed for even-odd symmetries in order to reduce the time of numeric integration. The voltage vector integral expressions for a uniform vertical current were also analyzed for even-odd symmetries to reduce the time required for their computation. The far field of each mode on the patch was expanded asymptotically so that the voltage vector for an incident plane wave and the scattered or radiated far field could be expressed analytically. Coaxially loading of the patch was modeled by a lumped load in a vertical uniform current filament. The current through the load is determined by a two port analysis.

This report used another technique to improve computational efficiency of the MM solution. The impedance matrix and voltage vector elements were analyzed with respect to their frequency dependance. It was found that they varied slowly

91

and smoothly with frequency so an interpolation scheme was employed to generate impedance matrix and voltage vector data at frequency intervals in between those that were calculated [16]. The result was the ability to generate wide band data from relatively few impedance matrix computations. Calculated and measured data were compared for wide band RCS, wide band input impedance and narrow band input impedance of both unloaded and loaded microstrip antennas. The RCS curve showed good agreement between calculation and measurement. It also showed how the impedance matrix interpolation could discern the narrow band peaks in the RCS that were not obvious from the points where the MM calculated the impedance matrix. The data presented for the wide band input impedance also showed good agreement between calculations and measurement.

For the vertical thin wire in the grounded dielectric substrate, an integral equation was developed for surface currents on the wire. Since a thin wire has a diameter much smaller than a wavelength, this surface current was approximated by a $\hat{z}$ directed filament of current. The current was obtained by the MM. The excitation chosen to determine self and mutual impedance was the so called delta gap generator. The mutual impedance between two thin wires imbedded in the dielectric is compared to a previous calculation [21] which used a magnetic frill current for excitation. The close agreement between the calculated and published curves show that the two types of excitation yield virtually identical results.

LIST OF REFERENCES

[1] Harrington, R.F., Time-Harmonic Electromagnetic Fields, McGraw-Hill, New York, Chapter 4, Section 4-12, 1961.

[2] Harrington, R.F., Field Computation by Moment Methods, Robert E. Krieger Publishing Company, Malabar, Florida, pp. 5-11, 1968.

[3] Munson, R.E., "Conformal Microstrip Antennas and Microstrip Phase Arrays," IEEE trans., Vol. AP-22, pp. 74-78, Jan. 1974.

[4] Derneryd, A.G., "Linearly Polarized Microstrip Antennas," IEEE trans., Vol. AP-24, pp. 846-851, November 1976.

[5] Agrawal, P.K., and Bailey, M.C., "An Analysis Technique for Microstrip Antennas," IEEE trans., Vol AP-25, pp. 756-759, Nov. 1977.

[6] Lo, Y.T., Solomon, D., Richards, W.F., "Theory and Experiment on Microstrip Antennas," IEEE trans., Vol. AP-27, pp. 137-145, Mar. 1979.

[7] Richards, W.F., Lo, Y.T., Harrison, D.D., "An Improved Theory for Microstrip Antennas and Applications," IEEE trans., Vol. AP-29, pp. 38-46, Jan 1981.

[8] Newman, E.H., and Tulyathan, P., "Analysis of Microstrip Antennas Using Moment Methods," IEEE trans., Vol. AP-27, pp. 47-53, Jan. 1981.

[9] Deshpande, M.D. and Bailey, M.C., "Input Impedance of Microstrip Antennas," IEEE trans., Vol. AP-30, pp. 645-650, July 1982.

[10] Bailey, M.C. and Deshpande, M.D., "Integral Equation Formulation of Microstrip Antennas," IEEE trans., Vol. AP-30, pp. 651-656, July 1982.

[11] Pozar, D.M., "Input Impedance and Mutual Coupling of Rectangular Microstrip Antennas,"IEEE trans., Vol. AP-30, pp. 1191-1196, Nov. 1982.

[12] Newman, E.H. and Schrote, M.R., "On the Current Distribution for Open Surfaces," IEEE trans., Vol. AP-31, pp.515-518, May 1983.

[13] Kwan, B.W., "Mutual Coupling Analysis for Conformal Microstrip Antennas," Ph.D dissertation, The Ohio State University Dept. of Elec. Engr., Columbus, Ohio, Dec. 1984.

[14] Newman, E.H. and Forrai, D.,"Scattering from a Microstrip Patch," IEEE trans., Vol. AP-35, No. 3, pp. 245-251, March 1987.

[15] Pozar, D.M., "Radiation and Scattering from a Microstrip Patch on a Uniaxial Substrate," IEEE trans., Vol. AP-35, No. 6, pp. 613-621, June 1987.

[16] Newman, E.H., "Generation of Wideband Data from the Method of Moments by Interpolating the Impedance Matrix," IEEE trans. on Antennas and Propagation, accepted for publication.

[17] Richmond, J.H., "Radiation and Scattering by Thin Wires in the Complex Frequency Domain," Technical Report No. 2902-10, The Ohio State University ElectroScience Laboratory, Columbus, Ohio, Jul. 1973.

[18] Collin, R.E., and Zucker, F.J., Antenna Theory Part 2, McGraw-Hill, New York, pp. 476-482, 1969.

[19] Balanis, C.A., Antenna Theory Analysis and Design, Harper and Row, New York, pp. 316-317, 1982.

[20] Richmond, J.H. and Newman, E.H., "Mutual Impedance Between Vertical Dipoles Over a Flat Earth," Radio Science, Vol. 14, pp. 957-959, November-December 1979.

[21] Chi, C. and Alexópoulos, N.G.,"Radiation by a Probe Through a Substrate," IEEE trans., Vol. AP-34, pp. 1080-1091, September 1986.

[22] Pinhas, S. and Shtrikman, S., "Vertical Currents in Microstrip Antennas," IEEE trans., Vol. AP-35, pp. 1285-1287, Nov. 1987.